



The influence of hybrid reinforcements on Long Fiber Thermoplastic composites

An experimental approach on the production process of
(hybrid) LFT pellets and static/dynamic mechanical testing

Arthur S. Haverkort



Supervisor: Dr. Ir. L. Warnet

Master Mechanical Engineering
Faculty of Engineering Technology
Production Technology chair
University of Twente
12th of July 2023

SUMMARY

In this thesis the research question *'How do hybrid fiber reinforcements affect the mechanical properties of composite parts made of long fiber thermoplastic pellets?'* is answered via an experimental approach. Long Fiber Thermoplastic Pellets (LFTP) are a type of fiber reinforced composite where the fiber length ranges from 10 – 40 mm, those pellets are further processed via a compression molding process to the final product, in this case a flat plate of 125 x 125 mm. The dimensions of the LFTP are a length of 40 mm with a diameter of 3 mm. The material is either glass-polypropylene (G/PP) or glass-aramid-polypropylene (G/A/PP). The pellets are placed in a random orientation in the compression molding die, the fiber direction is measured via image analysis of the surfaces of the plate. Due to boundary effects between the die and the pellets, the fiber angle of 45 – 60 ° was overrepresented in the histogram. Hybridization of the yarns is achieved via a newly designed commingling nozzle, by the help of air pressure a pre-commingled G/PP yarn is commingled with the aramid yarn. The (hybrid) yarns are processed in a pultrusion line to a continuous rod, which consequently is cut into pellets. Important to note is that the fibers run along the full length of the pellet.

The influence of the aramid fibers is researched by performing two types of mechanical testing, static and dynamic, on both G/PP and G/A/PP specimen. A four-point bending test is used to measure the flexural stiffness and stress, while a drop weight impact test is used to test the dynamic behavior of the composite materials. The aramid fibers did have a negative influence in stiffness and maximum stress, however an increased level of work was required to perform the bending tests. The decrease in stiffness over the G/PP specimen can be attributed to the poor aramid-polypropylene bonding, examined by SEM-microscopy. Secondly the aramid fibers have anisotropic mechanical properties, making them less preferable in loading in the off-axis, which is done in a random orientated composite. The increase in work can be explained by the less abrupt failure behavior, after the force peak the force drop-off is much less severe in the hybrid composite. The change in failure behavior was also discovered with the impact tests. For the G/A/PP specimen the impact time is elongated, and thus reducing the peak load, secondly the force reaches a plateau where damage propagation, like fiber debonding, dissipates energy in a more reliable way in comparison to the G/PP composites. This is where the poor aramid-PP bonding is an advantage, where with bigger impacts the glass fibers experience brittle fracture, the aramid fiber de-bond and deform ductile. Energy is dissipated in that process as well as a bigger residual stiffness because of the non-broken aramid fibers. Concluding the hybridization: with the materials used in this thesis the hybridization of G/PP with aramid resulted in a tougher composite with a less brittle fracture behavior. The downside is the reduced stiffness.

Finally the real-world applicability is tested by producing a demonstrator part. This is a flat plate with more complex features like ribs and thicker sections added to it. With the relatively simple die the void content is higher than in the earlier produced flat plates, however with more fillet-features the flow during the pressing process can be increased. Overall speaking the LFTP as a base material for compression molding is a feasible method for creating thermoplastic composite parts for (semi-)structural purposes. With a G/PP material most likely automotive parts.

CONTENTS

Summary	i
Acronyms	iv
1 Introduction	1
1.1 Background	2
1.1.1 Hybrid fiber reinforcements	3
1.2 Research question	4
1.3 Outline of the report	4
2 Theoretical background	5
2.1 Long fiber thermoplastic pellets	5
2.1.1 Production process	5
2.1.2 Modelling the stiffness	6
2.2 Hybrid yarns	6
2.2.1 Hybrid reinforcements	7
2.2.2 Commingling processes	9
3 Material production	10
3.1 Base materials	10
3.2 Pultrusion process	11
3.2.1 Commingling	12
3.2.2 Pellet production	13
4 Experimental methods	16
4.1 Specimen production	16
4.2 Four point bending test	18
4.2.1 4PBT procedure	19
4.3 Impact test	19
4.3.1 Pre-testing	20
4.3.2 Test procedure & machine setup	22
4.4 Data management & post processing	22
5 Results	24
5.1 Compression molding results	24
5.2 Theoretical approach mechanical properties	26
5.3 Bending tests	27
5.4 Impact tests	31
5.5 Failure analysis	36

6 Demonstrator	40
6.1 Demonstrator design	40
6.2 Compression molding	41
6.3 Results	41
7 Discussion	45
8 Conclusion and Recommendations	48
8.1 Recommendations	49
References	49
A Commingling machine	53
A.1 Machine information	54
A.2 Nozzle analysis	56
A.2.1 CFD Analysis nozzles	56
A.2.2 Test improved nozzle	58
A.3 Parametric optimization process	59
B Microscopy images	60
B.1 Glass Polypropylene samples	61
B.2 Glass Aramid Polypropylene samples	64
B.3 Samples compression molded composites	67
B.4 Fiber angle analysis	71
C Test specimen	73
C.1 Test report 4 point bending test	74
D Demonstrator part	77
E Plagiarism report	78

Acronyms

3-PBT Three-point bending test

4-PBT Four-point bending test

CFD Computational Fluid Dynamics

CLT Classical Laminate Theory

CM Compression Molding

CTE Coefficient of Thermal Expansion

FRPC Fiber Reinforced Polymer Composite

G/A/PP Glass fiber, polypropylene and aramid commingled yarn

G/PP Glass fiber Polypropylene commingled yarn

G/PP/PA6 G/PP pellets with a wrong Pa6 yarn included

LFTP Long Fiber Thermoplastic Pellet. Cylindrical pellets with a length range of 10-40 mm with continuous fibers along its length.

M.R.Z. Matrix-rich zone

PA6 Nylon 6

PLA Polylactic acid

PP Polypropylene

QI Quasi-isotropic fiber layup, fibers evenly distributed in all directions of 1-2 plane.

ROM Rule of Mixture

SEM Scanning Electron Microscope, Thermofisher Phenom XL TableTop

TKE Turbulent Kinetic Energy

Twaron Aramid yarns made by Teijin Aramid

UD Uni-Directional (fiber alignment)

V_f Fiber volume fraction [%]

1 INTRODUCTION

The overall subject of this thesis is composite materials, albeit a quite general term. Reinforced concrete, wood and fiber polymer material are all examples of composite materials. The definition states: "A composite material is a material that consists of two or more materials, while the combined (mechanical) properties are better than that of the individual materials alone." For this thesis the fiber polymer composites are considered, to be more specific; glass fiber, aramid fiber and PP (Polypropylene) are used.

The working principle for fiber reinforced polymer composites is that the load is transferred from fiber to fiber by the polymer matrix. The mechanical properties are a combination of the two materials, depending on fiber volume fraction, fiber direction and the production process.

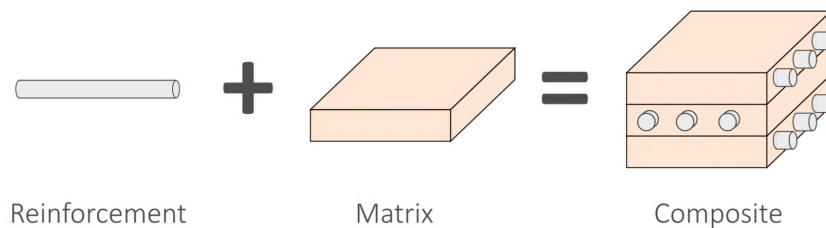


Figure 1.1: Principle sketch of fiber reinforced polymer composites [1]

Before a deeper dive in the world of these composites is taken, let us answer the question: Why should you use them? The key in this answer is the word 'specific'. Specific stiffness and specific strength. A glass fiber or carbon fiber composite (can) have a lower stiffness than steel or aluminium, however the density is also much lower. To give an example: the specific stiffness of a stainless steel (316L) is 24.8 MNm/kg (Young's modulus/density), a commonly used aluminium (6061 T6) 25.1 MNm/kg and a carbon/PEEK composite has a specific stiffness up to 95 MNm/kg. [2]

Next to this advantage, production process freedom and the ability to add strength and stiffness in specific areas (directions) gives a significant advantages over other (isotropic) engineering materials.

A lot of different production processes can be used to produce FRPC (Fiber Reinforced Polymer Composite), an important point is to know if the matrix polymer is a thermoset or thermoplastic. Thermoplastic polymers can be remelted and reshaped, enlarging the production methods to stamp forming, compression molding, while enabling assembly methods like welding. The matrix material used for this project is Polypropylene, which is a thermoplast. More advantages of thermoplastics are shorter production times, recycling possibilities and properties like chemical resistance, impact toughness are better over thermoset matrices like epoxy or polyester. As mentioned earlier, the mechanical properties are greatly dependent on the fiber orientation. Along with the fiber orientation there is a difference between continuous fibers and discontinuous fibers. Continuous fiber composites are used to achieve the highest stiffness and strength. A downside of these products is a more complex production process, since all the layers have to be placed manually (or automatically) within strict fiber angle tolerances. On the other hand, discontinuous fiber composites

can have advantages in more automated production processes like compression molding of bulk material. A general plot to illustrate the difference in mechanical properties between short, long and continuous fiber composites is given in Figure 1.2 . The green area is drawn into the figure, this is the area where LFTP (Long Fiber Thermoplastic Pellet. Cylindrical pellets with a length range of 10-40 mm with continuous fibers along it's length.) should sit in. The pellets differ not only by the physical size from short fiber pellets, a more important difference is the actual fiber length. Short fiber thermoplastics usually have a fiber length of less than 1 mm [3], and are usually processed with injection molding. LFTP have fiber along the length of the pellet, up to 40 mm. An important note to Figure 1.2 is that with the same trend that the material properties follow, the price of the products also increases. The strongest/stiffest material is also the most expensive and is the most labour intensive in the production process. All these factors are relevant for choosing a specific material and process.

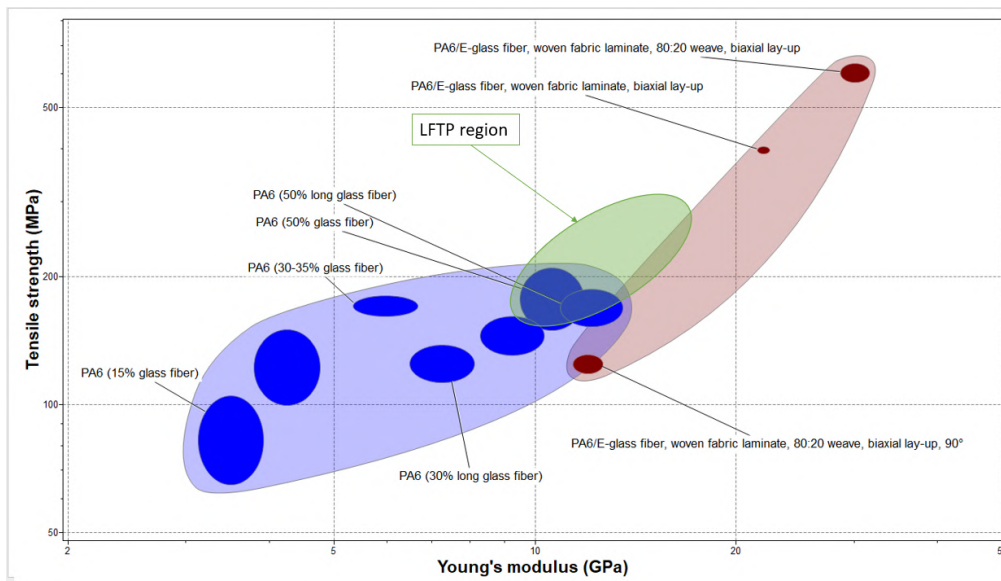


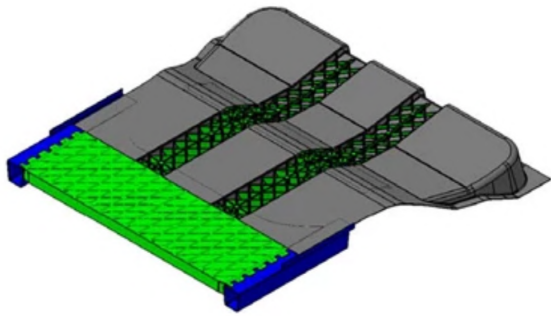
Figure 1.2: Short, long, LFTP and woven fibers [2]

A short background on the topic is given in Section 1.1. A more in-depth background can be found in Chapter 2. The introduction chapter finishes with the Research Objectives (Section 1.2) and the outline of the report (Section 1.3).

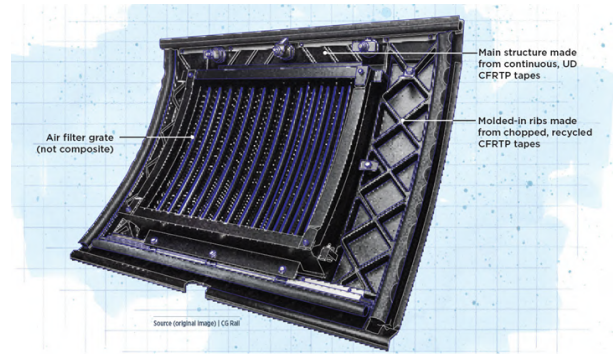
1.1 Background

As already mentioned in the first section of the Introduction, continuous fiber composites are used to achieve the highest strengths in the composite. In this section the state of art of LFTP products and processes is given.

Two production processes are commonly used in the industry for the processing of LFTP, namely injection molding and CM (Compression Molding). The main difference between these processes is the length of the fibers in the final product. During the injection process the longer fibers are damaged by the flow process in the extruder, resulting in significantly shorter fibers after the process [3]. With compression molding the fiber length is not compromised during the process. However, CM products have in general less complex features in comparison to injection molded parts.



(a) SMiLE rear load floor, green parts are glass/PA6 LFTP [4]



(b) Compression molded side panel for a high speed train made of long fiber tapes and continuous tapes [5]

Figure 1.3: Two products made with LFTP

An example of LFTP used in the industry can be found in the publication of the SMiLE project by the Fraunhofer Institute [4], Figure 1.3a. In this project an automotive rear load floor of a battery electric vehicle is redesigned in thermoplastic composites instead of the 'normal' metallic variant. To achieve sufficient crash-worthiness a relatively simple shape is made with UD tapes. The stiffeners of the part are made of LFTP, both the stiffeners and the UD structure are processed in a single Compression Molding step.

Another project [5] that utilizes the compression molding process in combination with long fiber thermoplastic composites is the prototype production of a side panel of a high speed train, pictured in Figure 1.3b. The part is made of continuous UD-tapes on the outside, the stiffeners are molded from scrap UD-tapes and all together compression molded into the panel. The composite part achieved a 30% weight reduction over the original aluminium panel.

1.1.1 Hybrid fiber reinforcements

FRPC (Fiber Reinforced Polymer Composite) usually have one type of reinforcement fiber and one type of matrix polymer. However, it is possible to use two (or more) different reinforcement fibers. Reasons to do this can be improving certain mechanical performances [6][7][8], adding electrical conductivity and adjusting the damping properties of the composite part.

In this research changes in mechanical properties are investigated when aramid fibers are added to the G/PP composite. Starting with the question: Why would this combination work? And what is the limitation of G/PP composites (or FRPC in general)?

The failure behavior of FRPC is brittle and abrupt. Carbon and glass fibers are both brittle fibers and the ultimate tensile strength is mainly dependent on the reinforcement fibers. When the first fiber fails in tension the load is transferred to the neighboring fibers by the shear stress of the matrix. With the increased load on those fibers they are more likely to fracture. Due to these stress concentrations the fracture will propagate and will form a critical size, at this point the composite will reach global failure.

By combining a brittle fiber with a lower maximum tensile strain with a ductile fiber with a higher tensile strain, the fracture propagation can be stopped or delayed. The global effect is that the ultimate tensile strain of the composite is increased.

1.2 Research question

In the previous paragraphs the topic of LFTP and composite materials is general introduced. This forms the basis for the problem statement.

The research question is:

Investigation of mechanical properties of hybrid long fiber thermoplastic pellets composite parts for structural applications.

With the following sub-questions that aid in answering the research questions:

1. How can a hybrid reinforcement thermoplastic yarn be manufactured consisting of two types of reinforcement fiber and a thermoplastic fiber?
2. Which reinforcement fibers can be combined as a hybrid setup and how are the mechanical properties changed?
3. What is the level of commingling of the produced pre-pultruded yarns?
4. What pultrusion parameters result in a good quality pultruded rod? Good is defined as a constant cross-section and well impregnated fibers.
5. What mechanical tests are relevant to evaluate the mechanical properties like stiffness, tensile strength and impact?
6. How do the mechanical properties of a LFTP part compare to other Fiber Reinforced Composites (FRC) production methods, produced with the same fiber/matrix materials? Verify by the Classical Laminate Theory or micromechanics.
7. Investigate the ability of the pellets to be pressed into a plate with a rib, to validate the pellets' real-world use case and processability.

1.3 Outline of the report

In Chapter 2 a review of relevant topics is given. More information on the materials that are being used during the research can be found in Chapter 3. Starting with information on the base materials and followed by the explanation of the production process of the LFTP. After that all the experiments including the specimen production and test procedure are explained in Chapter 4. Followed by the Results (Chapter 5). The producibility of LFTP for composite parts with more complex shapes is evaluated in Chapter 6. The final two chapters of the report are the Discussion (Chapter 7) and Conclusion (Chapter 8). Extra information and test results can be found in the Appendices.

2 THEORETICAL BACKGROUND

In this chapter a theoretical background is given. More information, previous research and real-world use-cases of LFTP can be read in this chapter.

2.1 Long fiber thermoplastic pellets

As already touched upon in Chapter 1, LFTP are used in as a 'base material' for (semi)-structural parts in for example the automotive industry. The two production methods that are suitable are injection moulding, for shorter pellets (<10 mm) and compression moulding (all length of pellets). In Figure 2.1 both a long and a short fiber pellet are pictured, the obvious difference is that with long fiber pellets the fibers are aligned with the main axis while at the short pellet the orientation is random.

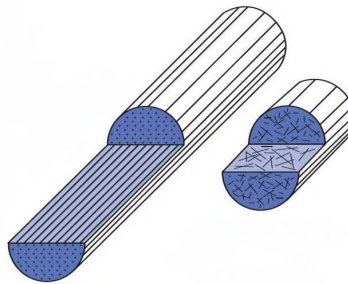


Figure 2.1: Long fiber (left) vs short fiber (right) [9]

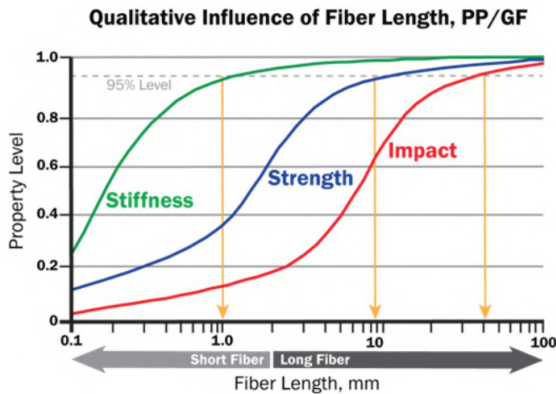
2.1.1 Production process

As is in the name of LFTP, the fibers are long but discontinuous, usually in the range 10-40 mm. Consequently the pellets do have the same length. This fact combined with the constant cross section of the pellet, the pultrusion process is perfectly suitable. Next to those arguments for pultrusion, the process itself is considered a clean and efficient way of production composite materials. Every fiber that enters the pultrusion die is converted to pellets, without cutting losses.

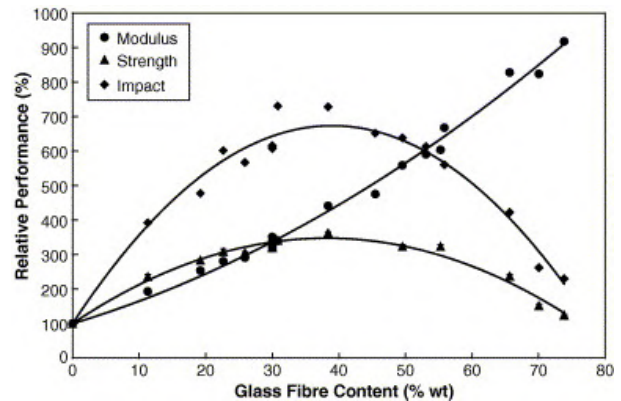
The effect of pellet length is researched in multiple papers [10][11]. One of the findings in these papers is the influence of fiber length to three mechanical properties, namely stiffness, strength and impact as shown in Figure 2.2a (Note the logarithmic x-axis). The graph shows what fiber length is required to get 95% of that specific mechanical property. Linking those fiber lengths to the pellet production, 10 and 40 mm pellets can be produced with relative ease by using a cut-off saw or shear cutter.

Besides the pellet length, the fiber volume fraction is an important measure of composites. Research by Thomason [12] found the relation between the fiber weight content and mechanical properties of G/PP by injection moulding, see Figure 2.2b. Interesting to see is that despite the increase in modulus with a higher fiber fraction, the strength and impact properties (rapidly) decrease. This decrease is explained by an increase of fiber interactions, which reduces the fiber orientations (more tangled, less in flow directions). Also stress can be introduced due to the lower

matrix content. Noting that injection moulding is not the same process as compression moulding, the effects of too many fibers and pile ups are still present in compression molding.



(a) Influence of fiber length in LFTP for different properties [13][11].



(b) Influence of fiber weight content on mechanical properties of G/PP injection moulded parts [12].

Figure 2.2: Influence of pellet length on mechanical properties

2.1.2 Modelling the stiffness

Many theoretical models have been developed over the years to approximate the stiffness of FRPC, the most used one for laminates being the CLT (Classical Laminate Theory). The basis of most models is the ROM (Rule of Mixture), with additions on that like the Halpin-Tsai model. For discontinuous fiber reinforced composites a shear lag model by Cox [14] can be used.

With mechanism that stiffens fiber reinforced composites is the load transfer by the fiber to the matrix via a shear load, this is modelled in the Cox model [14]. Another important dimension in the critical fiber length, the fibers should be longer than this length to make full use off the load carrying capabilities of the fiber-matrix combination. It can be calculated by the following equation:

$$L_c = \frac{\sigma_f \cdot d}{2 \cdot \tau_c} \quad (2.1)$$

The σ_f is the maximum fiber stress, d is the diameter of the fiber and finally τ_c is the shear yield strength of the matrix (this can also be the interface strength). More information and calculations are given in Paragraph 5.2, including the comparison with test results.

2.2 Hybrid yarns

Hybrid yarns are designed to combine the properties of two or more materials into one strand. This can be done to fulfill requirements on mechanical properties or production techniques. But also to gain electrical conductivity. For example, in 3D printed cube satellite modules, carbon is added to the PEEK filament to gain electrical conductivity and so replacing (a part of the) wiring [15]. For our research only the mechanical properties and production techniques are considered.

A well known example of a hybrid yarn in composites is combining a reinforcement fiber with a thermoplastic fiber. This type of strand can be directly used in production methods for thermoplastic composites like hot pressing or pultrusion. A well known G/PP variant is Twintex [16], this is a woven fabric where the yarns are a combination of glass fiber and PP yarns. These fabrics are used in compression molding or stamp forming. For pultrusion with thermoplastic materials the polymer matrix is usually added via a commingled yarn. The reinforcement fiber and polymer fiber are intermingled, due to the generated friction between them the polymer is pulled through the die even in a molten state.

2.2.1 Hybrid reinforcements

Producing hybrid composites with two types of reinforcement fibers is done to increase certain properties like abrasion resistance or impact resistance.

High stiffness modulus fibers like carbon fibers can be mixed with a lower modulus fiber to increase the impact properties. Generally, the lower modulus fibers have a higher ultimate tensile strain, aiding in the better impact properties. In Kedar [17], the mechanical properties of carbon-glass composites are investigated. They found that the increase of ultimate tensile strain is significantly higher than the loss in ultimate tensile strength for the hybrid composites. The tensile test results can be seen in Figure 2.3. In the stress-strain curve the results of the hybrid specimen (H1 and H2) display an interesting result. With H1 the high strain fibers (glass) are placed on the outside, this limits the damage propagation of the low strain carbon fibers.

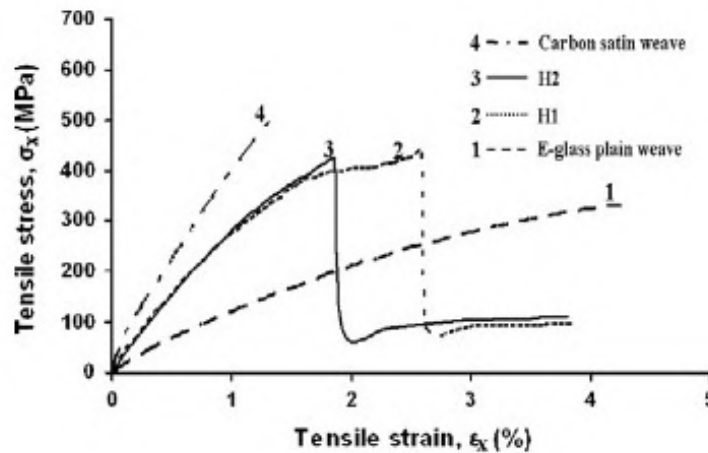


Figure 2.3: Tensile test for hybrid composites [17].

H1: $[G_3C_2]_s$, H2: $[C_2G_3]_s$

Another paper [18] described that intraply composites made of glass and aramid showed a significant improvement of the impact resistance of laminates. Rajpurohit et al. [6] found that interply glass/carbon hybrid composites (unidirectional glass and carbon layers stacked) achieved higher failure strain than the intraply (glass and carbon mix within one layer) counterpart. On the other hand the intraply composites resulted in higher tensile- and flexural strength.

Next to the improved impact properties, the residual flexural stiffness after impact is also greatly improved. Wagih et al [19] researched the change in flexural properties after impact with a hybrid composite. Two laminates were produced with fourteen layers, with the middle eight consisting of a plain woven aramid. The outer layers are plain woven carbon fiber. This is compared to a full carbon fiber laminate. Where the full carbon fiber sample had a reduced flexural strength loss of 60 % after a 15 J impact. The carbon-aramid sample only had a reduced strength of 20 %. Even at an impact energy of 25 J, the reduction was only 30 %. This is the result of the lower stiffness aramid fibers, due to their lower E-modulus and higher elongation to break the aramid fibers can absorb more energy. So it can be concluded that hybrid composites can be advantageous in certain situation in comparison to a composite with only one type reinforcement fiber. The impact properties of high modulus fiber composites can be increased as well as the fatigue properties [20].

Swolfs et al. [7] made a comprehensive review of hybridization of polymer composites, aiming at two reinforcement fibers. They categorize 'the hybrid effect' in three categories; residual stresses, changes in damage development and dynamic stress concentrations.

Starting with the residual stresses. These stresses are occurring due to the different CTE (Coefficient of Thermal Expansion) of the two different fibers. When the composites solidifies and the

temperature lowers the stresses are created. The fibers with the lowest CTE will face a compressive load, counteracting a physical tensile load. This enlarges the maximum tensile load of that fiber. The opposite is valid for the other fiber.

The second point is stress due to damage development. In Figure 2.4 this is illustrated schematically. In the case of hybridization with a higher breakage strain fiber, the fracture propagation can be stopped, whereas with a normal composite this can rapidly grow to a catastrophic failure.

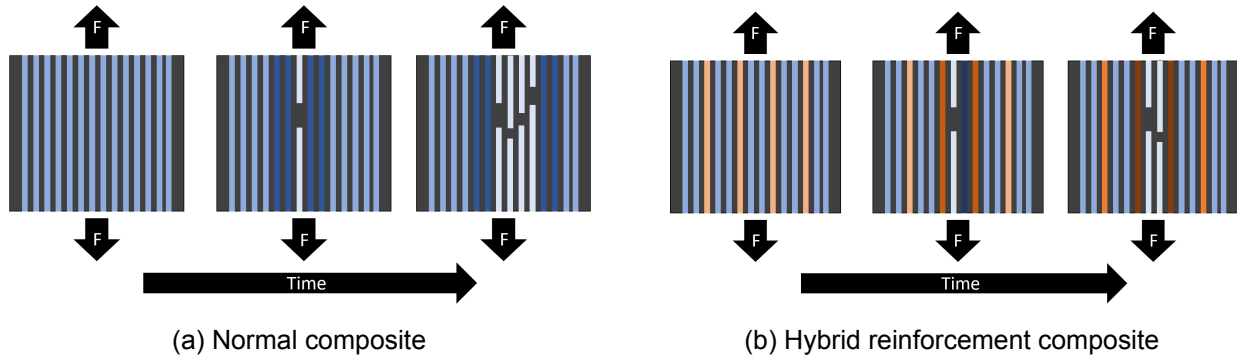


Figure 2.4: Fracture propagation of hybrid and non-hybrid composite (darker color is a higher stress, white is a broken fiber)

Finally the dynamic stress concentrations, the stress wave caused by the relaxing of the broken fibers. The hypothesis is that the stress waves are out-of-phase of each other and partly cancel. This topic is not widely researched and more research is needed to make this relevant.

An interesting topic in hybridization is pseudo-ductility. By combining different types and dispersion of fibers the ductile failure of (most) metals is approached. In the paper [7] multiple examples are listed, however most have a very specific layup/fiber configuration. The topic of pseudo-ductility is an interesting topic, since FRPC usually have a brittle and abrupt failure point with a big drop of load carrying capacity. Czel and Wisnom [21] researched the pseudo-ductility with a glass-carbon hybrid and found that the thickness of the middle carbon layer in a 3-layer glass-carbon-glass composite significantly influences the hybrid effect and failure mode. A layer thickness of $62\mu m$ was found to be the optimum for a stable pull-out, and thus flatten the stress-strain curve's peak to create pseudo-ductility. This is much more than a UD prepreg, but this thickness is achievable with mixing on yarn level. To illustrate the behavior a sketch is displayed in Figure 2.5. The blue line is a general curve for an UD composite, with the orange line and even more with the green line the failure points are less abrupt. A common conclusion of these papers is that a finer distribution of both fibers results in a more noticeable 'hybrid effect'.

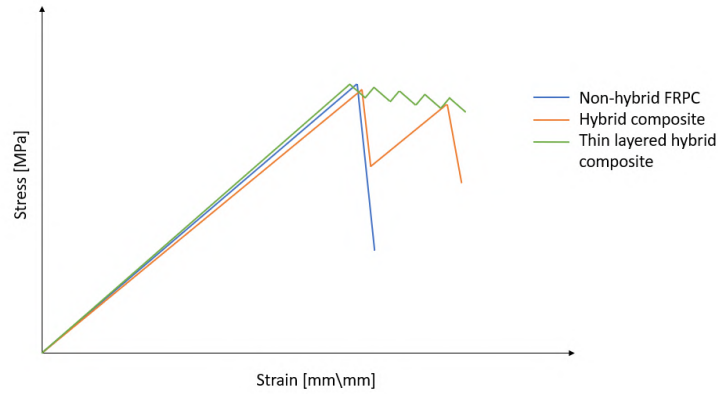
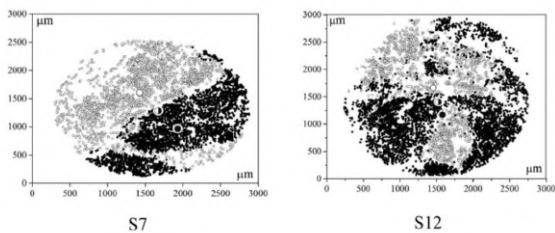


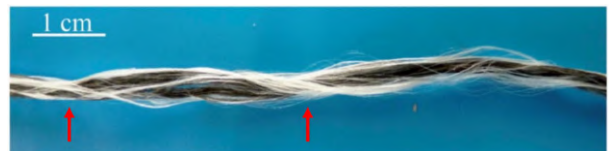
Figure 2.5: Sketch of the different Stress-Strain curves for a non-hybrid, hybrid and fine layered hybrid composites.

2.2.2 Commingling processes

A production method for a thermoplastic hybrid yarn, meaning a reinforcement fiber and thermoplastic fiber, is the commingling process. Other methods rely on spinning processes, like ring core-spun yarns, rotor core spun yarns and wrap yarns. The common factor in these processes is that one yarn is longitudinal while the second yarn is wrapped around. The commingling process uses compressed air to intermingle the two (or more) different yarns, creating a non-repeating structure of multiple yarns. Yarns are fed into a tube-shaped nozzle where air streams blow onto the yarns to open and intermingle them. Important parameters of the nozzle design are the angle of the air nozzles in relation to the yarns, the number of air nozzles, air pressure and yarn feed rate. Multiple nozzle configurations are evaluated in [22], they found that a single air inlet nozzle at a 90° was less effective than multiple air inlets. With more inlets a bigger volume of turbulent air is created aiding in more interlacing of the yarns. Important to note is that with the commingling process the yarns are not knotted or braided, due to friction in between the yarns they stay together. Research on this topic is done by Kravaev et al. [23], they found that an increase in air pressure resulted in more nips and higher mingling level. Nips are the locations where the yarns form a tighter section which holds the yarns together. Looser and thinner fibers also have a positive influence on the commingling process, see the more homogeneous distribution of the glass fibers in Figure 2.6a.



(a) Distribution of glass fiber and PP with one thick (left) filament or three thinner filaments (right) [23]



(b) Commingled hybrid yarn of carbon/PPS [24]

Figure 2.6: Commingling yarns

3 MATERIAL PRODUCTION

In this chapter the topics concerning the materials used are involved are discussed here. From the raw base materials to the pellet productions and finishing with the compression molding. The goal of the LFTP is using them in the compression molding process to make parts with more complex features like stiffeners. The chapter will start with section 3.1 on base materials and how these are converted into the pellets via the pultrusion process. Besides the production process, also the quality of the pellets is checked. The pellets are considered the end of the Materials chapter, further processing for specimen is the topic of section 4.1. To give an overview of the process steps all the phases can be found in Figure 3.1. The pre-commingled glass/PP yarns can be seen in Figure 3.1a, after the pultrusion and cutting process the cylindrical pellets as can be seen in Figure 3.1b are made. The final step is CM (Compression Molding) of those pellets into a flat plate, of which a front view is pictured in Figure 3.1c.



(a) Pre-commingled glass/PP yarn 2000 TEX



(b) LFTP Glass PP 3x40 mm



(c) Front view of compression molded plate

Figure 3.1: The materials during the process steps

3.1 Base materials

In this project all the composites are made of a PP (Polypropylene) matrix material. Two different reinforcement fibers are being used during the project, glass fiber and aramid (Twaron [25]). It can be just glass fiber - PP or a mixture of glass fiber, aramid fiber and PP. The glass fiber and PP are a pre-commingled yarn, available in two different linear densities, made by Comfil [26]. The commingling of the glass fibers and PP yarns is necessary for the pultrusion process. When the PP is melting in the die, sufficient friction is generated such that the glass fibers pull the PP matrix in the die. If both materials would be arranged side-by-side the glass fibers would not be impregnated well. The specifications of the G/PP yarns are given in Table 3.1. These different weights are combined to get the desired fill ratio of the pultrusion die, this will be explained in section 3.2.

Name	Total linear density [TEX]	Vf [%]	Linear density matrix [TEX]	Linear density fibers [TEX]
G/PP	2000	34	800	1200
G/PP	500	34	200	300

Table 3.1: G/PP commingled yarn types [26]

In order to produce the hybrid composites, a second reinforcement fiber is required. For this research an aramid fiber is chosen. The specific type is Twaron Standard [25] with a linear density of 161 TEX. The Young's modulus is similar to that of glass fiber, the elongation to break is 3 %. Next to that, the failure will be mostly ductile, in contrast glass fiber has a brittle fracture.

3.2 Pultrusion process

All rods are produced with the pultrusion setup using a die with a circular 3 mm diameter. An overview of the most important components is given in Figure 3.2. The bobbins with commingled yarns are located at (1), (2) is the alignment frame before the die entrance. The die is located at (3), including the linear bearings and the load cell (4). Finishing with the pulling unit at the end of the machine (5).

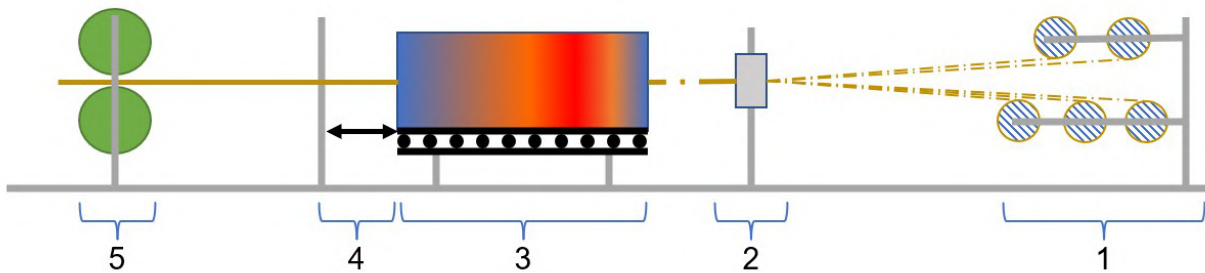


Figure 3.2: Schematic of pultrusion machine

In total six heating cartridges are placed inside the die, three per side. The temperature is controlled via a thermostat and a thermocouple. The thermostat is set at 210 °C. The pulling speed is set at 250 mm/min. These values are based on previous research[27], the quality of the composite is checked via optical microscopy (Section 3.2.2).

The configuration of the yarn has a direct relation with the cross-sectional area of the die. For the pultrusion process a slightly overfilled die produces a better quality composite e.g. with less voids. Due to the tapered section in the die and the overfilling, the reinforced fibers are impregnated with more pressure, the excess polymer exits the die at the front as a back flow. Research by [28] and previous use of this pultrusion line found that a filling ratio of 100 – 105% results in a stable process with a low void content. Different configurations are listed in Table 3.2, the configurations in bold-face have been chosen. The fill ratio is in the desired range, with the hybrid yarn the configuration is tested in the commingling machine with acceptable results. The same settings for the pultrusion machine are being used for G/PP and G/A/PP.

Fiber combination	Configuration	Ratio of fill	V_f	V_f per fiber
Glass/PP	6x 2000 TEX	1.22	0.34	G: 0.34
	5x 2000 TEX	0.92	0.34	G: 0.34
	5x 2000 TEX + 2x 500 TEX	1.06	0.34	G: 0.34
Glass/PP and Twaron hybrid	5x G/PP 2000 TEX + 5x A 161 TEX	1.04	0.38	G: 0.32 A: 0.078
	4x G/PP 2000 TEX + 16x A 161 TEX	1.02	0.48	G: 0.26 A: 0.26

Table 3.2: Pultrusion fiber configuration for the 3 mm diameter die

3.2.1 Commingling

The glass fiber yarns are already pre-commingled with the PP yarns. This is not the case for the Twaron® yarns, these are available as a standalone yarn. In order to produce the hybrid composite in the pultrusion line a commingled yarn with all the components is required. To solve this problem a commingling nozzle has been designed and tested. In Appendix A the full design process is elaborated, in this section the headlines are given.

The concept of a commingling nozzle is that with the help of air pressure/flow the individual yarns are opened and intermingled. Due to friction between the yarns they will stay at the intermingled position, creating a commingled yarn. The nozzle is 3D-printed (PLA, Ultimaker S5 printer, engineering preset), this method is the most time- and cost-efficient for the prototype. And as it turns out, this product works perfectly fine on a lab-scale project. The printed nozzle is displayed in Figure 3.3.

With a CFD parametric optimization analysis in SOLIDWORKS an optimal design within borders set by literature research [29] is made. Optimization parameters like air channel diameter, commingling channel diameter and air channel angle are optimized to maximize the TKE (Turbulent Kinetic Energy), a higher TKE in the commingling channel results in a better mix [29].

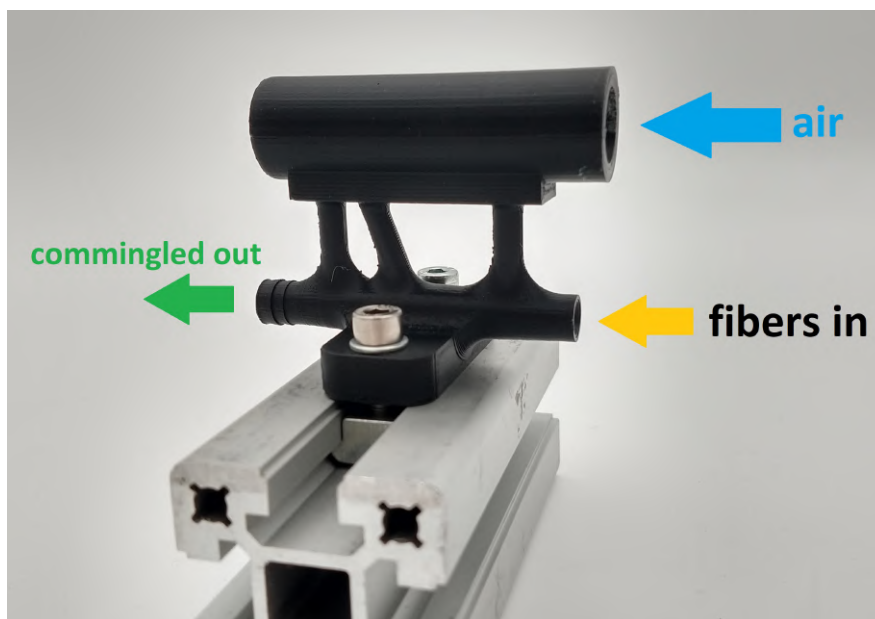


Figure 3.3: 3D printed commingling nozzle (40x40 mm t-slot profile for reference)

3.2.2 Pellet production

After producing the bars via the pultrusion process, the next step is making them into pellets. Bundles of ± 10 pultruded rods are attached to each other with general purpose tape, forming a flat 'mat' of rods. The bundle is sawed into pellets with a water cooled diamond circular saw. A consistent length of the pellets is guaranteed by the end-stop on the saw table.

The majority of the cooling water is dried absorbed by shop towels, followed by a drying cycle in a convection oven at 60 °C for 4 hours.

To ensure a 'good' quality of the composite pellets, samples are taken from different section of the production run. The pellets are considered good when there are few voids percent (order of magnitude of 2 %) and the reinforcement fibers are well impregnated with the PP.

A cross-section of a G/PP pellet is shown in Figure 3.4. In this Figure it can be seen that the void percentage is relatively low and the pellet has the desired round shape. In Appendix B all the microscopy images can be found. In Figure 3.5 the same procedure is done on a pellet containing Twaron and glass reinforcement fibers (G/A/PP). As with the G/PP material the void percentage is low, albeit slightly higher. The distribution of the Twaron yarns is good, however the five yarns can be clearly identified.

Void analysis of cross section
sample3_1.jpg

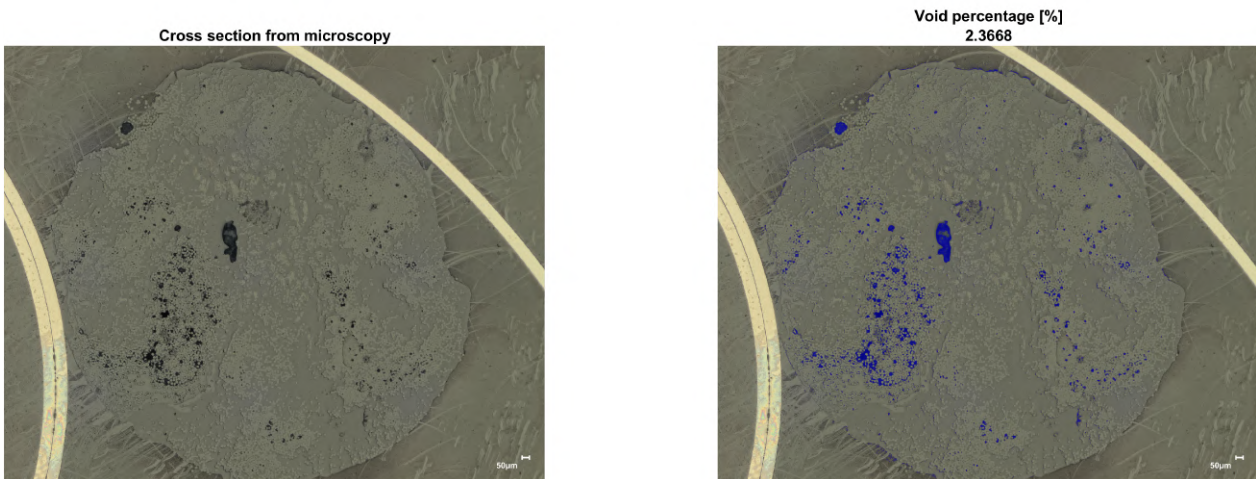


Figure 3.4: GPP sample 1, 3rd meter batch 1

Void analysis of cross section
GAPPSample16_2.jpg

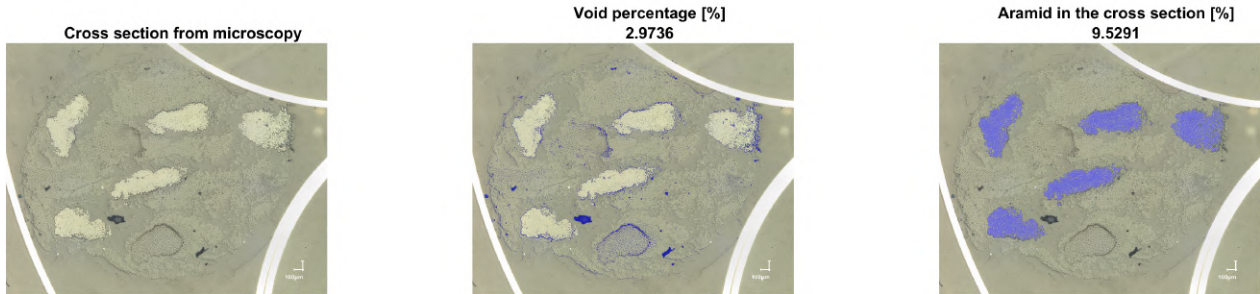


Figure 3.5: GAPP 16th produced meter, 2nd sample

During the analysis of the micrographs of the G/PP pellets a slightly concerning discovery is made, two different diameters fibers are present in the cross-section of the G/PP pellet, as shown in Figure 3.6. At first it was assumed that not all the PP yarns are completely molted. However the fibers were also discovered in later produced pellets. After checking all the steps in the production process the cause of this problem was found: an unmarked roll glass fiber / PA6 that was stored in the same box as the G/PP rolls. The bigger fibers are indeed unmelted fibers, but made from PA6 instead of PP. This was discovered after producing the first test specimen, in Chapter 5 the difference between the pure G/PP (new pure G/PP pellets have been made, batch 3) and G/PP/PA6 specimen can be found.

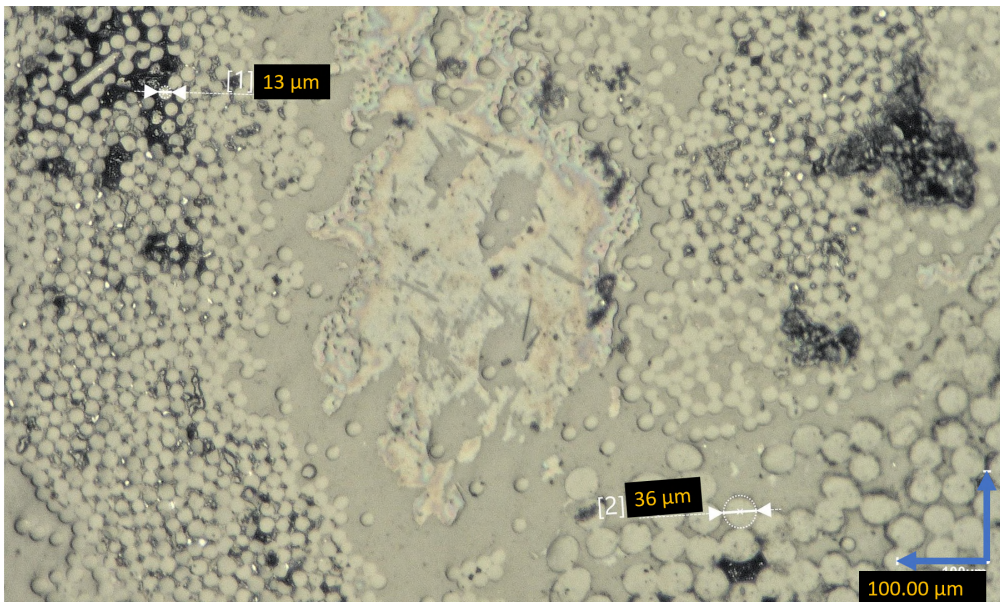


Figure 3.6: Different diameter fibers in G/PP pellet (Batch 1)

To determine if the production process is robust and the quality consistent, more samples have been taken from different sections and batches. The same image analysis is performed and the results are plotted in Figure 3.7. Multiple observations can be made from these plots. Starting with the voids at the steady-state pultrusion. After the initial meters the void percentage drops and stabilizes, as can be seen that the samples from the first or second meter (red values) usually have a higher void content. Secondly is the difference between G/PP and G/A/PP. The samples with the

hybrid reinforcement do have a higher void content. It has to be noted that during the production the cooling block was slightly misaligned, resulting in less cooling power. This is the cause of the slightly higher void content in comparison to the G/PP samples, the same has been found in a previous master project [27].

The fiber volume fraction is theoretically determined by the fibers that enter the pultrusion die, however due to the backflow of the polymer the V_f will increase slightly. The same image analysis script in Matlab is used to measure the fiber content. The measured fiber volume fraction for the G/PP pellets is 38.0% and for the G/A/PP pellets the aramid fibers add 10.6% fiber volume fraction, resulting in 48.6% V_f .

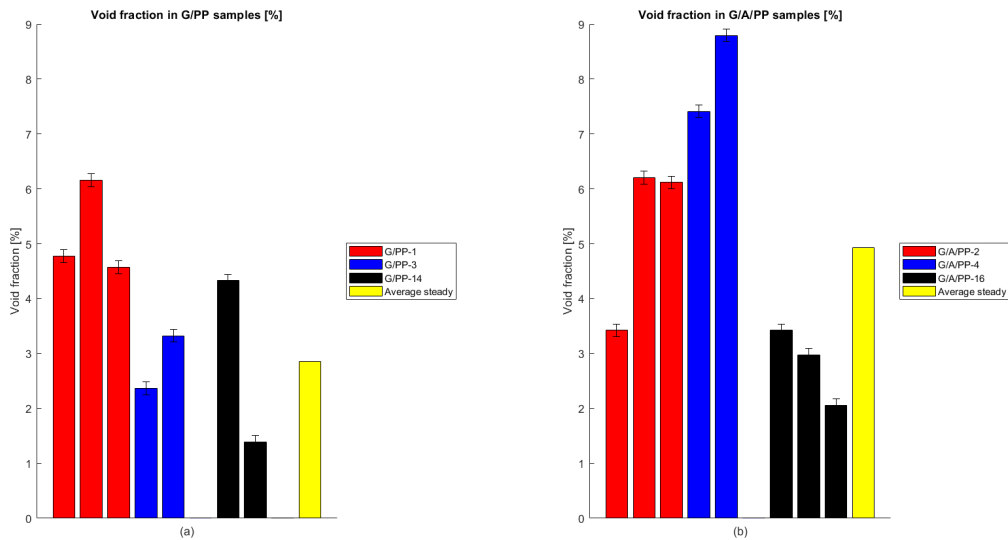


Figure 3.7: Void fraction of G/PP and G/A/PP pellets

The error bar is determined with a calibration image. The image consist of pie-charts with known fractions in different colours. It is processed multiple times and the standard error is calculated. With this method the precision error is determined.

4 EXPERIMENTAL METHODS

This chapter describes the experimental methods of the research. We start with specimen production, followed by the two experiments that are performed in Section 4.2 and 4.3. The chapter's last paragraph includes information for the data management and post-processing of the data. The results of the experiments is presented in Chapter 5.

4.1 Specimen production

The final product discussed in the previous chapter, the pellets, is the base material for the specimen production. To produce the specimen, for both the 4-PBT (Four-point bending test) and impact test, the CM (Compression Molding) process is used. The machine used is a Fontijne Lab press with metal molds that can compress the material to a flat plate.

The processing parameters are derived of hot pressing parameters for Twintex [16]. In Figure 4.1 the production cycle is given. A processing temperature of 210 °C with a force of 31 kN is used. During the heating stage a lower pressing force is applied to increase the contact area and so the thermal conductivity. A dwell time of 15 minutes is taken to ensure that there is enough time to flow in the die with the random orientated pellets.

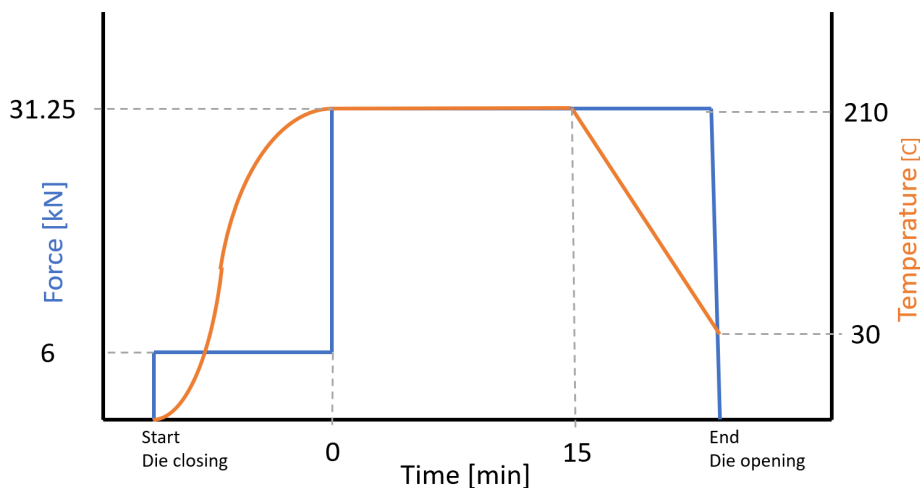


Figure 4.1: Compression moulding program

To determine the mechanical properties of the composite, two different type of plates have to be compression molded. To test the unidirectional properties, the pellets are aligned inside the die. Other plates are made with a random orientation, in which the pellets are not placed in a specific order. In the Figures 4.2 and 4.3 the two options are displayed before and after compression moulding.

In Figure 4.3a the squeeze flow is visible on the left side of the plate, the fibers are slightly buckled and resin-rich areas can be seen on about one-third side from the right. The randomness of the

other plate is considered good. The fiber directions on both sides of the plate do not match and no big clusters of pellets in the same directions are visible on the surface.



(a) Aligned brick stacking



(b) Random alignment

Figure 4.2: Different die (125 x 125 mm) filling configurations. In this case both GPP 40 mm pellets.



(a) Aligned pellet configuration after pressing



(b) Random pellet configuration after pressing

Figure 4.3: Photographs of aligned and random pressed plates (125 x 125 mm). Images edited to make the fibers better visible.

An interesting property to investigate is the pellet alignment. For all the molded plates images are taken of both sides and analyzed with the Directionality plugin of ImageJ [30]. The plugin recognizes lines in an image and gives a histogram of their appearance as an output.

In Figure 4.4 the histograms and an average of all the plates is plotted. In order to cancel some of the edge effects the photos are cropped, removing ± 1 cm from the edges. Judging the histogram (Figure 4.4, left), the software clearly recognizes the pellets in the aligned plate. The histogram for the random pellet orientation is ideally a horizontal line, simply an equal amount of fibers in all directions. However after multiple plates a pellet angle of 45-60 degree pellet angle is clearly more present than other directions.

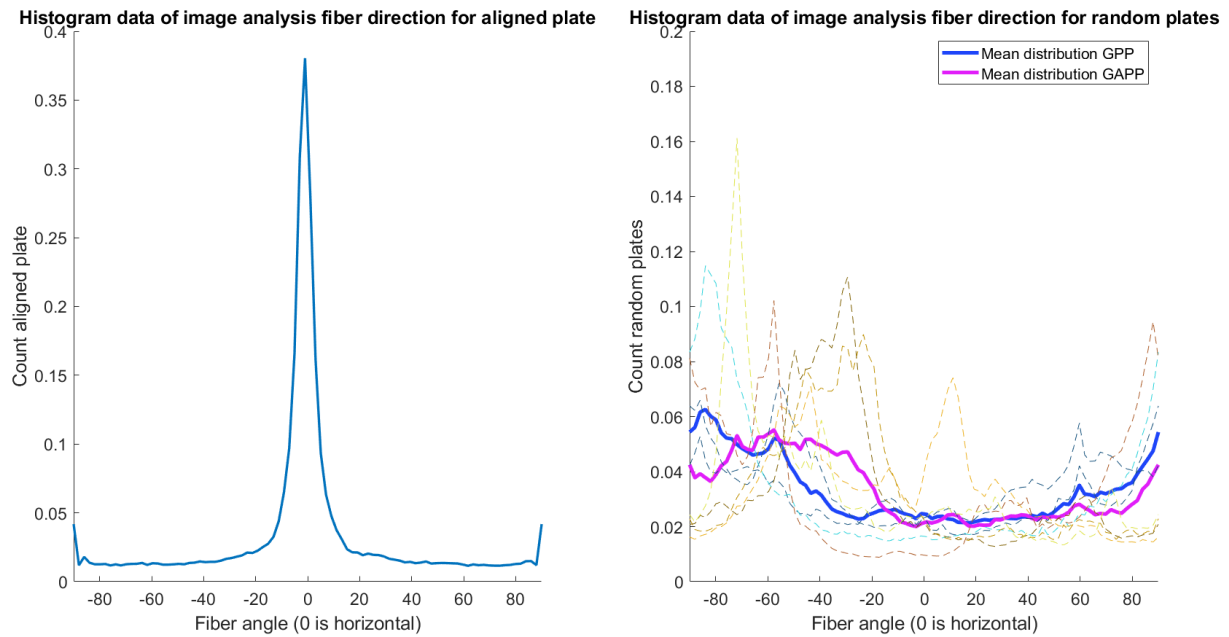


Figure 4.4: Fiber angle distribution in the compression molded plates. Aligned plate (left) and random orientated pellets (right).

4.2 Four point bending test

One of the main goals of the project is to determine the mechanical properties of the LFTP composite materials. Can this material be used for semi-structural applications? And how wide is the spread in the mechanical properties?

The 4-PBT (Four-point bending test) is used to determine the bending stiffness (Flexural modulus), bending stress and strain. This test is chosen over a 3-PBT (Three-point bending test) because of the constant bending moment in-between the indenters. For composite materials, especially random fibers, it is important that a wide section is subjected to a load. This ensures that the failure will be on the weakest link. With a 3-PBT the maximum load is a line load underneath the indenter, resulting in a stress concentration on the specimen. Tensile tests are not chosen for different reasons; it requires much larger specimen, the shape of the specimen is more complex to manufacture and PP matrices have a low surface tension limiting the ability to bond reinforcement tabs on the specimen.

As a guideline in the testing ISO 14125-1998 [31] is used. The type of material classifies as 'Class I, discontinuous fiber reinforced thermoplast', see Table 4.1. The specimen dimensions can be found in Table 4.1 and the test fixture dimension is displayed in Figure 4.5.

	Specimen length (l)	Outer span (L)	Inner span (L')	Width (b)	Thickness (h)
Dimensions [mm]	80	66	22	10	4
Tolerances [mm]	-0,+10	± 1	± 1	± 0.5	± 0.2
Other dimensions	L/h	l/h			
	16.5	20			

Table 4.1: Preferred dimensions test specimen according ISO 14125

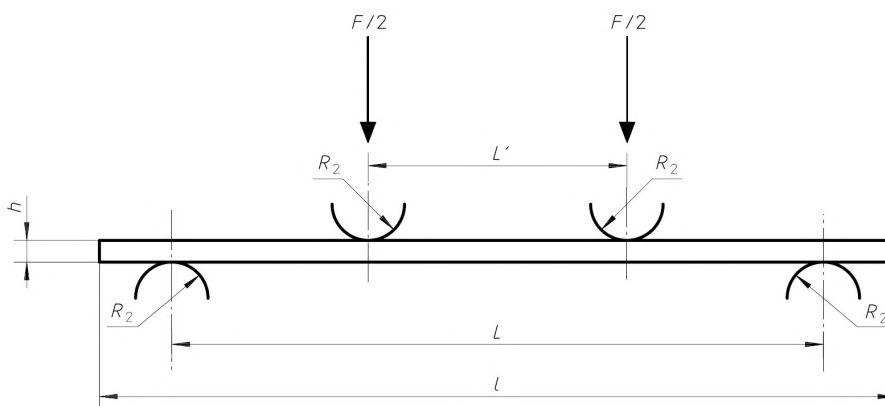


Figure 4.5: Specimen and setup dimensions 4-PBT [31]

4.2.1 4PBT procedure

As mentioned in the previous paragraph, ISO 14125 is used as a guideline for the test. This standard also includes a test procedure, as follows:

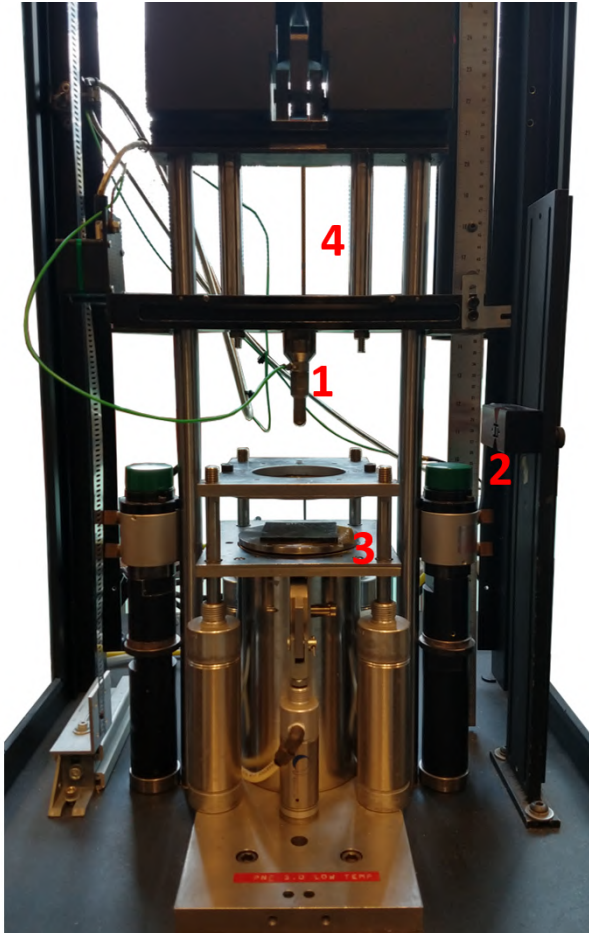
1. Cut specimen to size and number them.
2. Measure the width and thickness with calipers and micrometer.
3. Assemble the Zwick i-line Z5.0 universal test machine with the required supports and indenter. Calibrate the crosshead displacement.
4. For the random fiber orientation specimen: 2 mm/min crosshead velocity. The aligned specimen: 1 mm/min crosshead velocity.
5. Start test. Test ends when either 10 mm crosshead displacement is reached or 20 % peak force reduction is reached.
6. Take photo of specimen in final position.

4.3 Impact test

The goal of the impact tests is to investigate the influence of the aramid fibers in the G/PP composite in dynamics loading. The tests are performed with the Dynatup 8250 drop weight impact test machine. ISO 6603-2 [32] is used as a guideline. The test setup, pictured in Figure 4.6, consists of the frame, hemispherical striker, pneumatic clamping device and specimen.

The impact tests are performed to investigate the difference in impact resistance of the G/PP and G/A/PP composite materials. With these tests the influence of the addition of aramid to the G/PP

composites can be found. For both materials the specimen and test environment are kept identical. Hence with this setup it is possible to see the difference in damage and energy absorption behavior. The impact energy should be determined so that the damage is visible for the human eye. The indent, if not completely through, can be measured. To gain knowledge on the topic, impact tests with pure PP plate and Twintex [0/90]₂ are performed. With the data sets of these experiments the starting point for the LFTP plates is set.



(a) 1: Striker and piezo load cell. 2: Second impact stops. 3: Pneumatic clamp. 4: Strike guide and mass.



(b) Specimen (60x60 mm) on clamping surfaces. The $\varnothing 40$ mm impact zone on the lower image.

Figure 4.6: Dynatup 8250 impact machine with close-up of the specimen in the clamp

4.3.1 Pre-testing

As mentioned in the the introduction of this section, the goal of the test is to see the difference in behaviour with and without the presence of aramid fibers. To determine the required impact energy for visible damage on the composite plates the plate and shell theory of Timoshenko [33] is used. The maximum force of a cylindrical plate loaded in the center can be calculated with Equation (4.1). In which σ_{max} is the maximum stress [MPa], found with the 4-PBT. ν is the poisson's ratio, taken from literature [2], a and h are the radius of the plate and the thickness in mm.

$$P = \frac{\sigma_{max}}{(1 + \nu) \cdot (0.485 \cdot \log \frac{a}{h} + 0.52)} \cdot h^2 = \frac{148}{(1 + 0.35) \cdot (0.458 \cdot \log \frac{20}{3.7} + 0.52)} \cdot 3.7^2 = 1714N \quad (4.1)$$

The maximum displacement is calculated with the maximum force as an input, Equation (4.2). D is the bending stiffness in MPa, also a result of the 4-PBT. r the radius of the loaded area, taken at 1

mm.

$$w = \frac{P^2}{8\pi} \cdot \log \frac{r}{a} + \frac{P}{16\pi} \cdot (a^2 - r^2) = \frac{1714 \cdot 1^2}{8\pi \cdot 12281} \cdot \log \frac{1}{20} + \frac{1714}{16\pi \cdot 12281} \cdot (20^2 - 1^2) = 1.1mm \quad (4.2)$$

With the assumption that the force-displacement relation is linear, the area of the triangle is the work [J], Equation (4.3). This impact energy should result in a maximum tensile stress at the bottom of the specimen.

$$energy = e = \frac{1}{2} \cdot P \cdot w = \frac{1}{2} \cdot 1714 \cdot 1.1 = 0.94J. \quad (4.3)$$

Next the impact velocity is calculated (4.4):

$$E_{kinetic} = \frac{1}{2} \cdot m \cdot v^2 \rightarrow v = \sqrt{\frac{e}{0.5 \cdot m}} = \sqrt{\frac{0.94}{0.5 \cdot 1.142}} \quad (4.4)$$

And finally in the height of the falling weight is calculated:

$$v = \sqrt{2 \cdot g \cdot h} \rightarrow h = \frac{v^2}{2 \cdot g} = \frac{1.283^2}{2 \cdot 9.81} = 8.9cm \quad (4.5)$$

With these settings the Twintex plates are tested, the damage is determined with a depth gauge and optical microscope. As a final pre-test a few cut-offs of the random pellet plates are subjected to the impacts. In Table 4.2 the results are summarized.

Impact energy [J]	Material	Damage top	Damage bottom
0.8	Twintex	Almost none on exterior	tiny crack in matrix along the fiber bundle
1.9	Twintex	Visible indentation, roughly 0.12 mm	more matrix cracks visible and some glass fibers sticking out
2.8	Twintex	Visible indentation, roughly 0.15 mm	Clear fiber bundle break
3.3	Twintex	Visible indentation, roughly 0.15 mm	Fiber bundle broken, matrix cracked, whole bundle sticks out
4.5	Twintex	Visible indentation, roughly 0.16 mm	Fiber bundle broken, matrix cracked
4.3	G/PP	Visible indentation, roughly 0.30 mm	Matrix cranking on pellet borders, slight pellet tear-out.
4.3	G/PP	Visible indentation, roughly 0.32 mm	Matrix cranking on pellet borders, slight pellet tear-out. Damage not under impact location.

Table 4.2: Pre-testing Twintex plates ([0/90] with a 2 mm thickness) and G/PP random fiber pressed plate

The conclusion from the pre-testing is that the calculated impact energy to get damage is correct. Even with 0.8J some matrix damage is visible with a microscope. However, the force-time graph does not show force peaks that would indicate damage. Conclusion: more energy is required. At the impact energy of 4.3J both the Twintex and the G/PP LFTP plates experience a good amount of damage, also visible in the data plots. This impact energy is used for the testing of the G/PP and G/A/PP LFTP plates.

The post-processing of the tests with an impact energy of 4.3J showed damage in the force-time graph, however it could be better visible. The remaining G/A/PP LFTP plates are tested with an impact energy of 13.2J. This value is experimentally chosen with the requirement that on the impact side of the specimen glass fiber breakage was visible but the aramid fibers should remain intact.

4.3.2 Test procedure & machine setup

As mentioned in the introduction of the chapter, the tests are performed on a Dynatup 8250. This is a drop weight impact machine, capable of impact velocities up to 6 m/s by gravity or 13 m/s with pneumatic assistance. The specimen is held in place by a pneumatic clamping device and the dart can be swapped for different sizes/weights. The test setup is summarized in Table 4.3 .

Component	Information	
Dart	10 mm hemispherical cap	
Load cell	15 kN piezo electric ring load cell, Kistler 9011A	
Impact energy	4.3 J	13.2 J
Impact weight	1286 gram	2280 gram
Impact height	105.5 cm	78 cm
Impact velocity	2.6 m/s	3.6 m/s

Table 4.3: Impact test machine setup

The list below should be followed to assure the repeatability of the experiments.

1. Assemble the machine, set pre-tension on the load cell and input the correct sensitivity in the amplifier.
2. Input the mass of the indenter, sensitivity in the LABView IAFImpactlogger for the datalogging.
3. Insert the specimen in the pneumatic clamp. Position marked with tape.
4. Start new specimen on the PC in the IAFImpactlogger, start amplifier by pressing the red 'start' button.
5. Arm machine (clamp engages), Fire machine, turn off automatic clamp (to prevent hitting the load cell wire in this configuration).
6. Machine retrieves indenter, release clamp by enabling the automatic clamp and get specimen out of the machine.
7. Measure the indent on the measurement table and do an optical damage assessment with the microscope.
8. Save data in the logging software and start over at step 3.

4.4 Data management & post processing

The collection of the raw test data and converting that to readable data is very important. For two reasons: to analyse the data and secondly to make the data is readable for use at a later point in time. The data from the 4-PBT is exported as a Microsoft Excel file, the impact tester exports a text file. For the bending tests an Excel workbook is made and the impact tests are analysed in Matlab. The first sheet in the Excel workbook is an export sheet for Matlab, the 2nd sheet contains information about the experiment, the 3rd sheet contains the information of the test specimen. All the other slides are data-slides with raw and processed test data. Considering the impact tests, the .txt files are read into Matlab and saved as a .mat file. After that all the data sets are loaded and plotted. A figure is made with four plots, namely force-time, force-displacement, displacement-time and velocity-time. A table is generated with the maximum force, the time and displacement of that peak and the total energy dissipated.

The equations for the flexural stiffness and stress are taken from the ISO 14125 [31]. To determine the maximum stress/load/strain is more difficult since the failure point is not always a clearly defined point. In some cases the load increases after the first drop in the force-displacement graph. The maximum point is set at the first peak (orange dot), see Figure 4.7. This point is chosen because after that point visible damage occurs. However the full measurement curve is of interest, namely to determine the total work of the test.

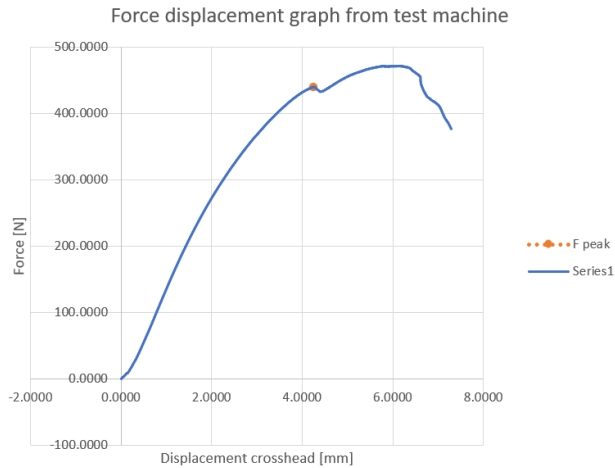


Figure 4.7: Example of force-displacement graph

For both the 4-PBT and impact tests the specimen are named, an overview of all the specimen can be found in Table 4.4.

Test type	Name	Fibers	Information
4-PBT	G/PP plate 1	9K TEX G/PP, 1x 1.8k TEX G/Pa6	Set of specimen made of G/PP, with the PA6 contamination.
4-PBT	G/PP plate 2	9K TEX G/PP, 1x 1.8k TEX G/Pa6	Set of specimen made of G/PP, with the PA6 contamination.
4-PBT	G/PP plate 3	11K TEX G/PP G/PP	Set of specimen made of G/PP, without the PA6 contamination.
4-PBT	G/A/PP plate 1	10K TEX G/PP + 805 TEX Twaron	Set of specimen made of G/A/PP
4-PBT	G/A/PP plate 2	10K TEX G/PP + 805 TEX Twaron	Set of specimen made of G/A/PP
Impact	G/PP-1x	11K TEX G/PP G/PP	x = 1-4, impact specimen made of G/PP. 4.3J impact energy
Impact	G/A/PP-1x	10K TEX G/PP + 805 TEX Twaron	x = 1-4, impact specimen made of G/A/PP. 4.3J impact energy
Impact	G/A/PP-2x	10K TEX G/PP + 805 TEX Twaron	x = 1-4, impact specimen made of G/A/PP. 13.2J impact energy

Table 4.4: All specimen with names and information summarized

5 RESULTS

This chapter presents the results of the mechanical tests, the Four-point bending test and impact tests. Before the results of the mechanical tests are given, the quality of the compression molding process is evaluated, this is covered in Section 5.1. Section 5.3 is about the Four-point bending test results, the impact tests are described in Section 5.4. Section 5.5 includes the damage evaluation of the specimen with optical and SEM microscopy.

5.1 Compression molding results

Multiple questions arise when the compression molding of LFTP in a random fiber orientation is considered. Does the random pellet stacking introduce voids? How random is the pellet alignment? And in the case of the hybrid composite, how well is the distribution of the Twaron yarns?

Multiple samples are made from the pressed plates. The samples have a thickness of ± 3.5 mm and a width of roughly 20 mm. One of the samples is displayed in Figure 5.1. In the blue ovals some matrix rich regions are located, especially the right region is critical since this one spans over the full thickness of the sample. This region is locally significantly less stiff, so upon loading this can be a failure initiation point.

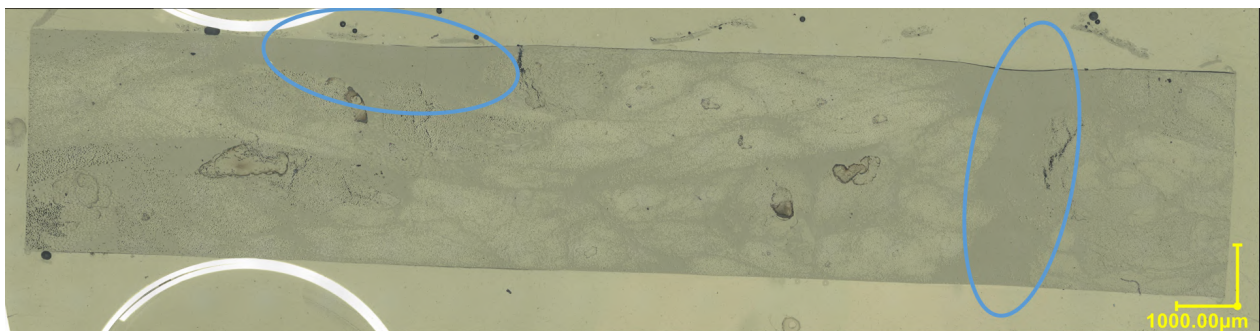
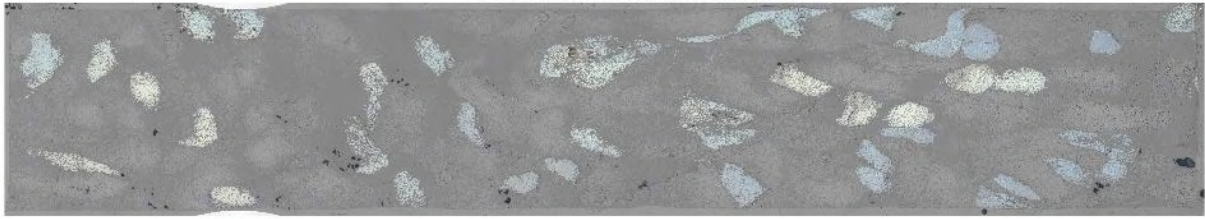


Figure 5.1: Cross section of G/PP random pellet plate

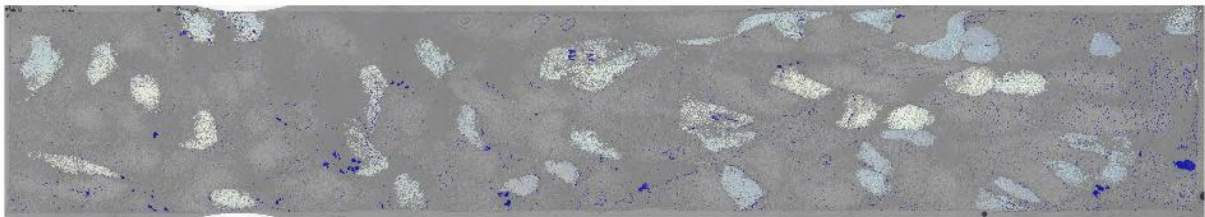
A cross section of a G/A/PP sample can be found in Figure 5.2. The aramid bundles are clearly visible, both the yellow/white and blue tinted bundles are aramid (discolouring is due to the polishing procedure). The glass fibers have a light grey tint. The void percentage with 1.47% (Appendix B.3) is low and the distribution of the aramid bundles is good. The percentage of aramid in the cross section is 11%.

Analysis of cross section GAPP1random

Cross section from microscopy



Void percentage [%]
1.4222



Aramid in the cross section [%]
11.0229

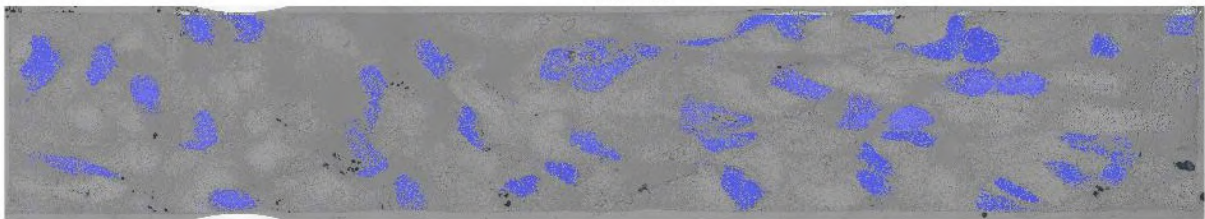


Figure 5.2: Cross section of G/A/PP random pellet plate with analysis

An interesting defect in the microscopy image of the G/A/PP sample of the pressed plate (Figure 5.3) is the matrix cracking inside the Twaron bundle. This crack is most probably formed during the cooling phase of the CM process. Aramid has a negative CTE (Coefficient of Thermal Expansion) ($-3.5\mu/^\circ C$), meaning that the fibers will shrink when heated, whereas glass fiber ($4.9 - 5.1\mu/^\circ C$) and the PP matrix both have a positive CTE ($37.5 - 115\mu/^\circ C$, exact value not known based on [2]). In a worst case situation this could reach the yield stress of the PP.



Figure 5.3: Matrix cracking inside a Twaron fiber bundle

5.2 Theoretical approach mechanical properties

Besides the experimental approach to gain knowledge on the mechanical properties of the LFTP composites it is interesting to know how theoretical approaches like the CLT (Classical Laminate Theory) and other methods compare to the measurements. In Figure 5.4 the results of the 4-PBT (Four-point bending test) are given, as well as some theoretical values. The basis for calculation on composite materials is micro mechanics and the CLT.

With micro mechanics (Equations 5.1-5.3) the Young's modulus is calculated on basis of the V_f and respectively the stiffness of the matrix and fiber. This method assumes perfect fiber-matrix bonding, equal strain in matrix and fiber.

$$E_1 = E_m * V_m + E_{f11} * V_f \quad (5.1)$$

$$E_2 = \frac{(1 - \sqrt{V_f}) * E_m + (\text{sqrt}(V_f) * E_m * E_{f12})}{V_f * E_m + \text{sqrt}(V_f) * (1 - \text{sqrt}(V_f)) * E_{f12}} \quad (5.2)$$

$$G_{12} = \frac{1}{\frac{V_m}{G_m} + \frac{V_f}{G_{f1}}} \quad (5.3)$$

The gained stiffness values are then used as input for the CLT. In Equation 5.4 the main equation for the CLT given. With a strain-curvature vector, the stiffness matrix and the resulting force-moment vector.

$$\begin{Bmatrix} \varepsilon^0 \\ \kappa \end{Bmatrix} = \begin{bmatrix} a & b \\ b & d \end{bmatrix} \begin{Bmatrix} N \\ M \end{Bmatrix} \quad (5.4)$$

The engineering properties can be extracted from the abd -matrix. For a glass-polypropylene laminate with a V_f of 0.38 the mechanical engineering properties can be found in Table 5.1, as well as in Figure 5.4.

$$E_x = \frac{1}{abd(1,1) * h} \quad E_y = \frac{1}{abd(2,2) * h} \quad G_{xy} = \frac{1}{abd(3,3) * h} \quad \nu_{12} = -\frac{abd(2,1)}{abd(1,1) * h} \quad (5.5)$$

$$E_{flex-x} = \frac{12}{abd(4,4) * h^3} \quad E_{flex-y} = \frac{12}{abd(5,5) * h^3} \quad (5.6)$$

Previous research on short fiber reinforced composites [34] have found that a good approximation of the stiffness of a composite with random orientated fibers is as follows:

$$E_{composite} = \frac{1}{5} * E_1 + \frac{4}{5} * E_2 \quad (5.7)$$

Property	Fiber lay-up	Value	Line spec in Fig. 5.4
UD flexural stiffness x	$[0\ 0\ 0\ 0]_s$	32.80 GPa	Red coarse stripes
UD flexural stiffness y	$[0\ 0\ 0\ 0]_s$	5.37 GPa	Red dotted line
QI Flexural stiffness lowest stiffness	$[90\ -45\ 45\ 0]_s$	9.73 GPa	Lower boundary magenta area
QI Flexural stiffness highest stiffness	$[0\ -45\ 45\ 90]_s$	17.44 GPa	Higher boundary magenta area
Random orientated fiber composite [34]	Random	10.85 GPa	Yellow dotted line

Table 5.1: Engineering constants for a glass-polypropylene laminate

5.3 Bending tests

In Figure 5.4 is given where the flexural stress over the flexural stiffness is plotted for all the specimen, added to that are the theoretical stiffness values. The raw test data can be found in Appendix C.1.

The graph displays the measurements of the 4-PBT with a 'plus', 'cross' and 'circle', depending on the type. The horizontal lines describe the theoretical stiffness values, all explained in Section 5.2. The lowest and highest stiffness via the CLT are described with the magenta area.

The measurements of the UD-specimen (red markers) do agree very well with the theoretical values found by micro mechanics. For the G/PP from plate 3 (magenta markers) series four out of the six specimen fall in the range that is derived from the CLT, the mean value is firmly in the range, close to the theoretical value by Lavengood [34]. The section is continued with more detailed graphs on the G/PP-G/PP/PA6 and G/PP-G/A/PP specimen.

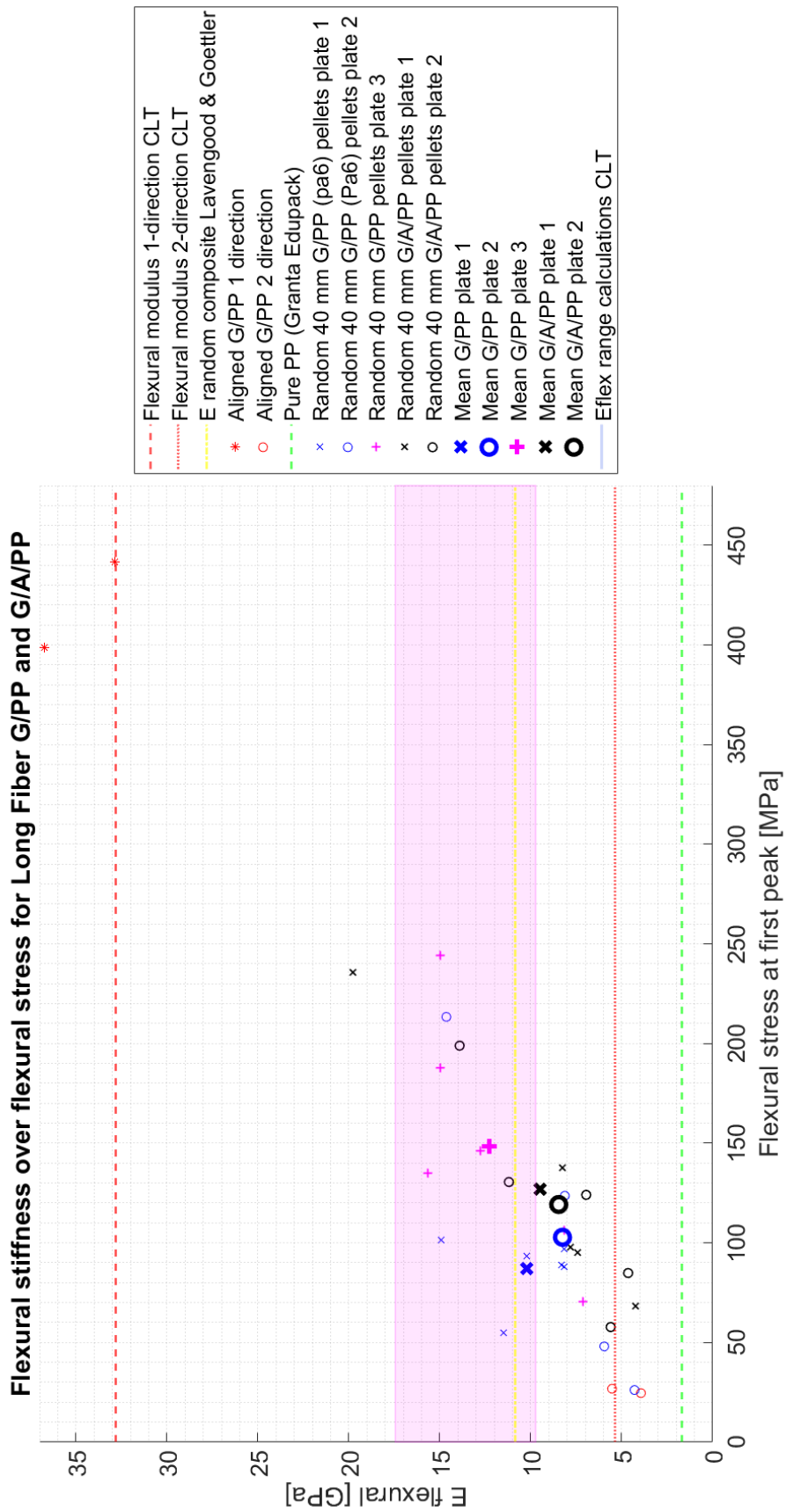


Figure 5.4: Overview of the 4PBT results

In Section 3.2.2 the issue with the bigger PA6 fibers was already introduced. Since the PA6 fibers were found after performing the tests, results can be compared with the specimen with pure G/PP specimen (batch 3). This comparison is plotted in two graphs, stress over strain (left) and stiffness over strain (right), displayed in Figure 5.5. The blue markers indicate the two specimen sets with the PA6 yarn included and the purple crosses represent the batch with the pure PP matrix. The individual values of each tests are marked with the markers, the average of a set is displayed by the dot with the standard deviation added to it. The big spread in the results is present in both data sets which is explained by the random fiber orientation. More important in this graph is the different between the matrix materials. It can be clearly seen that the specimen with the pure PP matrix perform better in all the plotted properties.

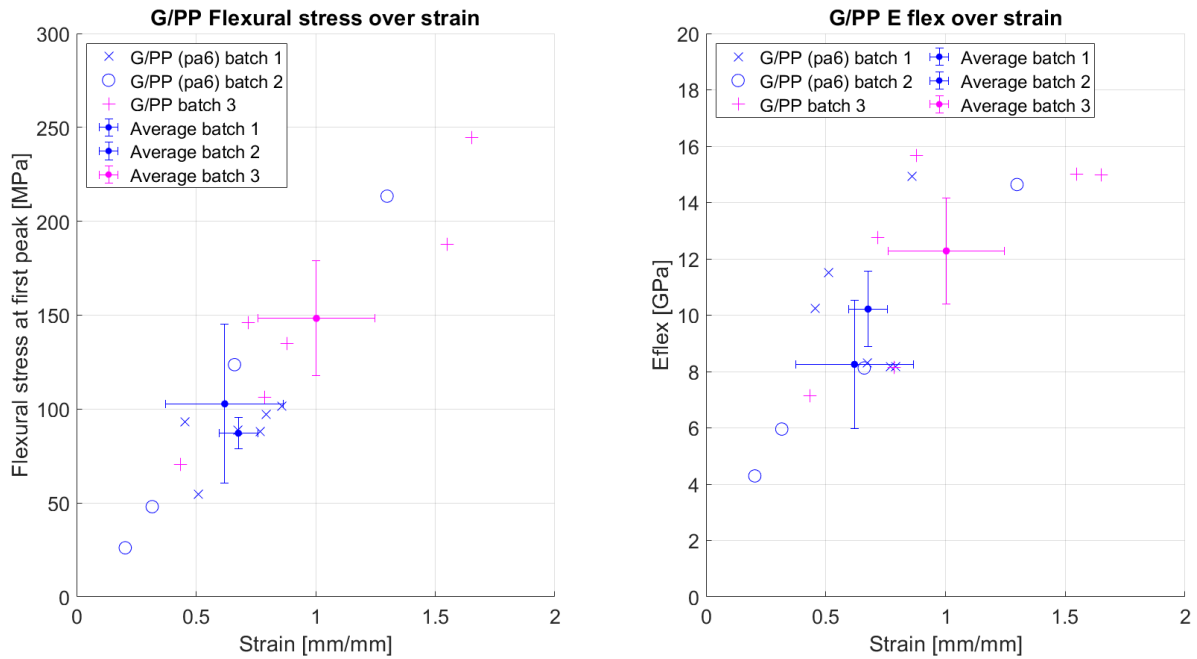


Figure 5.5: G/PP specimen versus the G/PP with PA6 yarn. Errorbar is the standard deviation of the set.

The stiffness and flexural stress for the G/PP and G/A/PP specimen are plotted in Figure 5.6. The same axis and marker structure used as in Figure 5.5. Interestingly the G/A/PP specimen perform worse in bending stiffness or stress by a significant margin, despite having a slightly higher fiber volume fraction. A possible reason for these results is poor fiber-matrix bonding, this will be further investigated with a SEM (Scanning Electron Microscope, Thermofisher Phenom XL TableTop). Poor fiber-matrix bonding can reduce the stiffness in 2-direction to only the stiffness of the matrix material, with a random fiber orientation this will have an influence on the measured result. Besides the strength and stiffness properties, the work during the bending test is an interesting property. In many instances hybrid composites are not designed to increase just the stiffness of the composites, but rather to increase the toughness. The work of the bending tests is calculated and displayed in Table 5.3. The capability of the G/A/PP specimen to continuing carrying load after the first failure point is the main contribution to the increased work. This effect is clearly visible in the raw data where the Force-Displacement curves stay flatter for much longer, plotted in Appendix C.1.

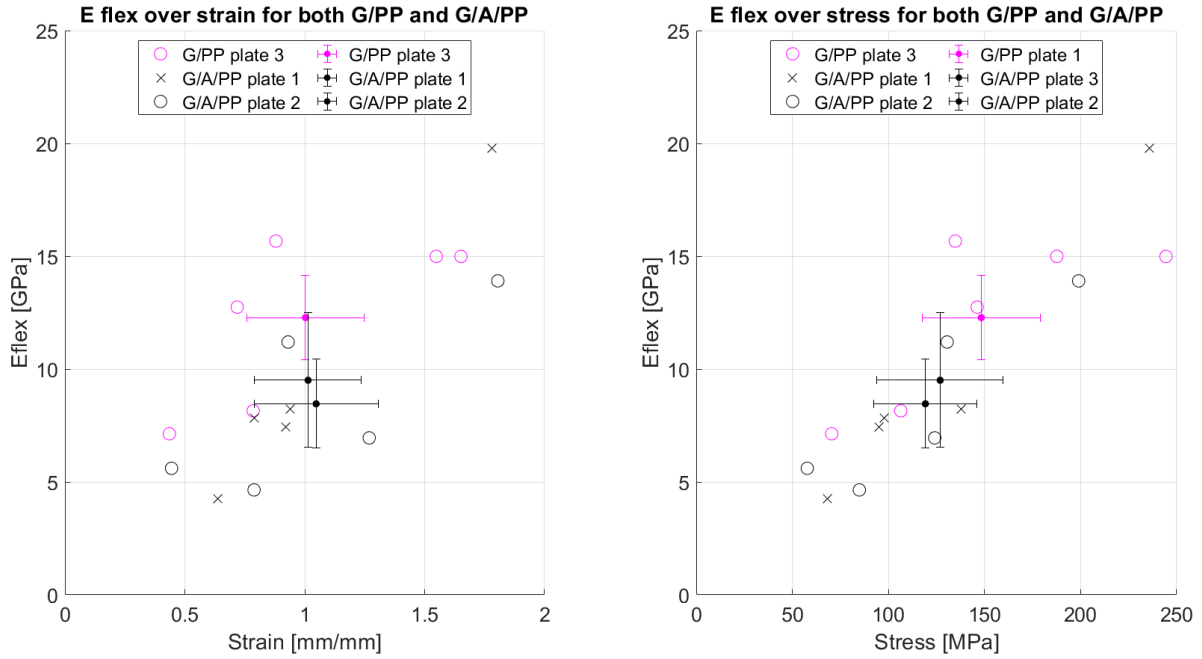


Figure 5.6: G/PP specimen versus G/A/PP specimen

Material	$\bar{E} \pm \sigma$ [GPa]	$\Delta\%$	$\bar{\sigma}_{flex} \pm \sigma$ [MPa]	$\Delta\%$	$\bar{\epsilon} [-]$	Δ
G/PP plate 3	12.28 ± 3.74	-	148.3 ± 61.3	-	1.003 ± 0.48	-
G/A/PP plate 1	9.51 ± 5.96	-22.6%	126.9 ± 65.7	-14.4%	1.031 ± 0.44	+2.8%
G/A/PP plate 2	8.46 ± 3.94	-31.1%	119.2 ± 53.5	-19.6%	1.048 ± 0.51	+4.5%

Table 5.2: Flexural tests results

Material	$\bar{W}_{peak} \pm \sigma$ [J]	$\bar{W}_{total} \pm \sigma$ [J]	$\Delta\%$ with G/PP
G/PP plate 3	0.672 ± 0.43	1.462 ± 0.72	-
G/A/PP plate 1	0.758 ± 0.47	1.665 ± 0.36	+14%
G/A/PP plate 2	0.642 ± 0.54	1.663 ± 0.33	+14%

Table 5.3: Average work bending tests

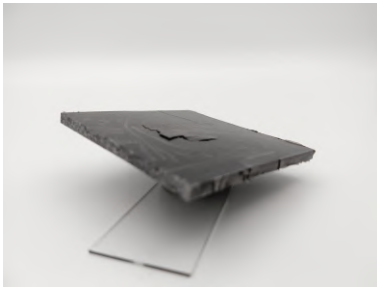
5.4 Impact tests

This section covers the results of the impact tests. The measurements done by the impact machine data logging are supplemented with an optical assessment and the indentions are measured after the tests. These results can be found in Table 5.4. In the Figures 5.8-5.11 the plots from the data logging are given and commented upon.

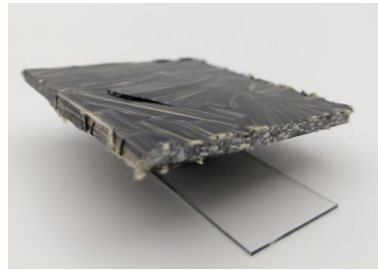
Specimen	Energy [J]	Thickness [mm]	Indent top side [mm]	Note on damage (optical)
G/PP-1	4.3	3.36	0.162	Little optical damage
G/PP-2	4.3	3.44	0.266	Tear-out of 3 pellets on their boundaries on the back.
G/PP-3	4.3	3.58	0.25	Crank in between pellets on the back.
G/PP-4	4.3	3.58	0.23	Front side pellet/fiber breakage, rear side crank around pellet.
G/A/PP-1.1	4.3	3.61	0.25	Not a lot optical damage.
G/A/PP-1.2	4.3	3.82	0.31	Some tear-out of pellets on backside.
G/A/PP-1.3	4.3	3.70	0.32	On the rear the pellet seams to be split (crack along pellet).
G/A/PP-1.4	4.3	3.81	0.30	Wide tear-out, multiple pellet width on the backside.
G/A/PP-2.1	13.2	3.82	2.26	Big tear-out, glass fiber break on impact side
G/A/PP-2.2	13.2	3.73	2.44	Glass fiber broken, big crater.
G/A/PP-2.3	13.2	3.82	1.83	Matrix crack on top, small cracks in the glass fiber.
G/A/PP-2.4	13.2	3.76	0.47	Small tear-out on the bottom, impact precisely on aramid bundle.

Table 5.4: Manual measurements on impact test specimen

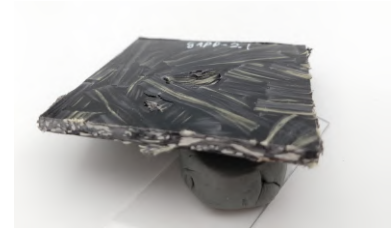
As an addition to Table 5.4, images of three specimen can be found in Figure 5.7. These include a G/PP, G/A/PP specimen with the smaller impact and an image of a G/A/PP specimen with the bigger impact. Images 5.7a-5.7c are a generic photo of the damage, images 5.7d-5.7f have the crack highlighted in red and a circle that represents the boundary of the clamps highlighted in blue, all on the bottom side of the specimen. With the lower impact energy of 4.3J the damage on the underside of the specimen is similar for all specimen. The pellets tear out and the fracture happens at the borders of a pellet. This is clearly visible in 5.7e, the red line (crack) follows the border of the pellet, the crack is stopped due to the pellet that has an angle of roughly 45 degrees. The effect of pellet debonding was already visible with the 4-PBT, fiber breakage is not yet visible on a large scale with the lower impact energy. Fiber breakage occurs with the larger impact, in Section 5.5 the failure mechanisms are researched in more detail.



(a) Specimen G/PP-2 bottom side



(b) Specimen G/A/PP-1.4 bottom side



(c) Specimen G/A/PP-2.1 impact side



(d) Specimen G/PP-2 fracture on bottom



(e) Specimen G/A/PP-1.4 fracture on bottom side



(f) Specimen G/A/PP-2.1 fracture on bottom

Figure 5.7: Damage on the bottom side of the specimen

The force-time graphs are displayed in Figure 5.8, the left and middle graph are respectively G/PP and G/A/PP at 4.3J and the graph on the right is G/A/PP with an impact energy of 13.2J. While comparing the smaller impact tests, it is directly visible that the magnitude of the force is different between the two materials. On average the G/PP plates peak at 2090N whereas the G/A/PP plates have an average peak force of 1727N. The spread in the peak forces is small, especially in comparison to the results of the 4-PBT. This can be the result of the increase in specimen size. Although for the bigger 13.2J impact the comparison with G/PP cannot be made, the force-time graph does show that more plastic deformation is present. This is visible by a bigger spread in peak forces and a less smooth data.

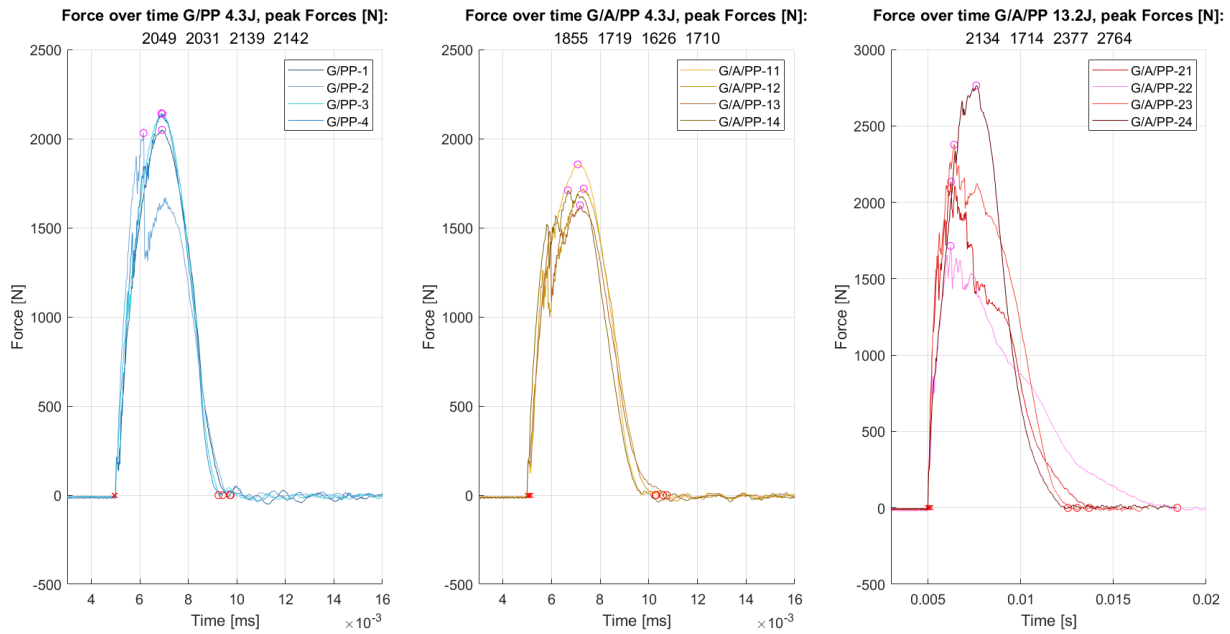


Figure 5.8: Force-Time graph for G/PP and G/A/PP

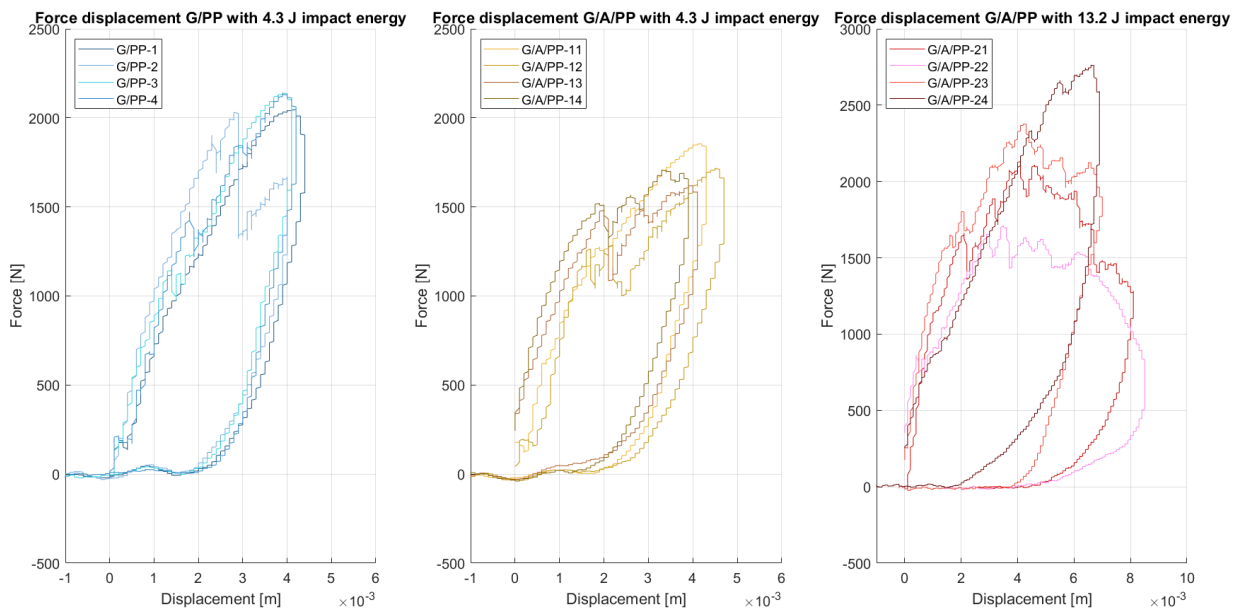


Figure 5.9: Force-displacement graph for G/PP and G/A/PP

The displacement over time graphs are displayed in Figure 5.9. The difference between the G/PP and G/A/PP in the smaller impact tests seems that the path to the maximum force is different. In the case of the G/PP specimen the force-displacement curve is relatively smooth up to to maximum. On the other hand the G/A/PP specimen (middle graph) have a less direct path to the maximum force. A plateau-like path can be seen with a more defined saw tooth profile in the measurement signal. This effect is even better visible in the graph on the right with the 13.2J impact on the G/A/PP specimen. The difference in behaviour of specimen GAPP-24 is explained via the optical assessment (Table 5.4), relatively little damage was found after testing. The other three specimen in the GAPP-2x series all experienced major damage. The damage modes included pellet debonding, plastic deformations and glass fiber fracture. The peaks of the saw tooth profile in the

force-displacement graph are points where the composite is damaged.

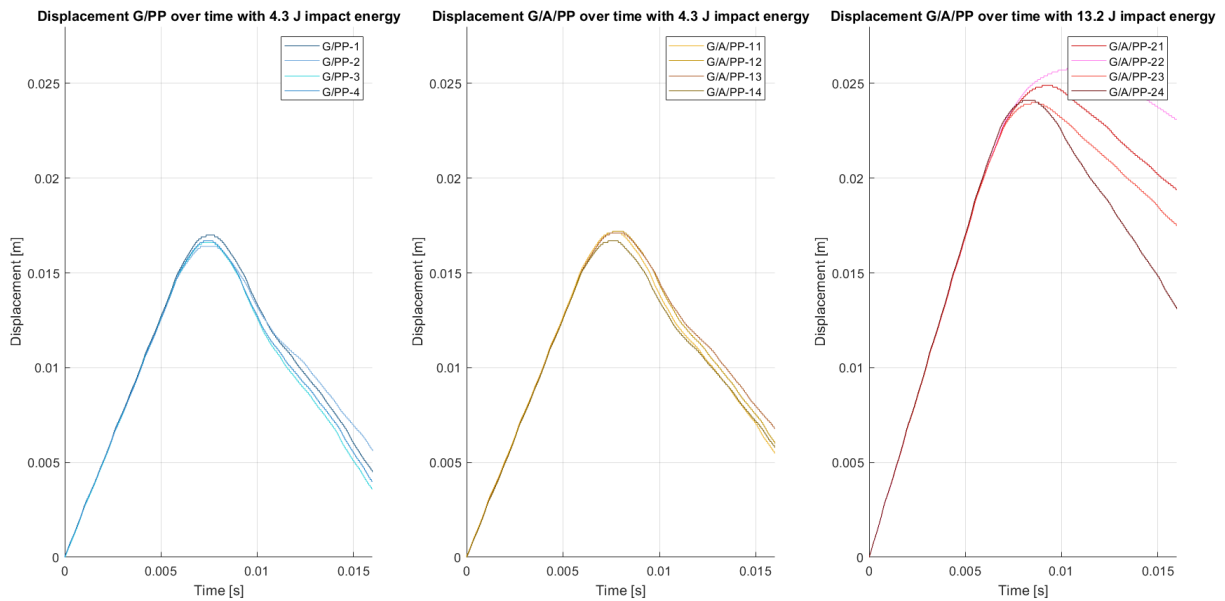


Figure 5.10: Displacement-Time graph for G/PP and G/A/PP

With the displacement-time graphs we can conclude that for a 4.3J impact a relatively linear response is acquired. All four specimen of each material have a very similar response, indicating that the rebound is mostly linear. The second set of G/A/PP specimen, with 13.2J impact energy, have a much wider spread in the return phase of the displacement-time graph. The velocity-time graphs (Figure 5.11 display the same behaviour. These graphs display the measured velocity of the striker over the time. At the 4.3J impact tests the entry and rebound velocity are relatively constant over the specimens. With the larger 13.2J impact the rebound velocity differs much more. In agreement with the optical assessment of specimen GAPP-24 the rebound velocity is the highest, indicating an elastic effect with less energy dissipation due to damage. The other three specimen in the series, with more optical damage visible, have a significant lower rebound velocity. This effect is made visual in the bar plot in Figure 5.12. In this bar plot the input- and return energy based on the striker velocity is plotted. For the low energy impact (4.3J) the input energy is consistent for all the specimen, however there is a difference in energy return considering the G/PP and G/A/PP specimen. The G/PP specimen have an average energy return of 34% while the G/A/PP specimen returns 30% of the input energy on average. For the bigger 13.2J impact the energy return is only 9.6%, this is in line with the expectations since much more plastic deformation is visible on the specimen.

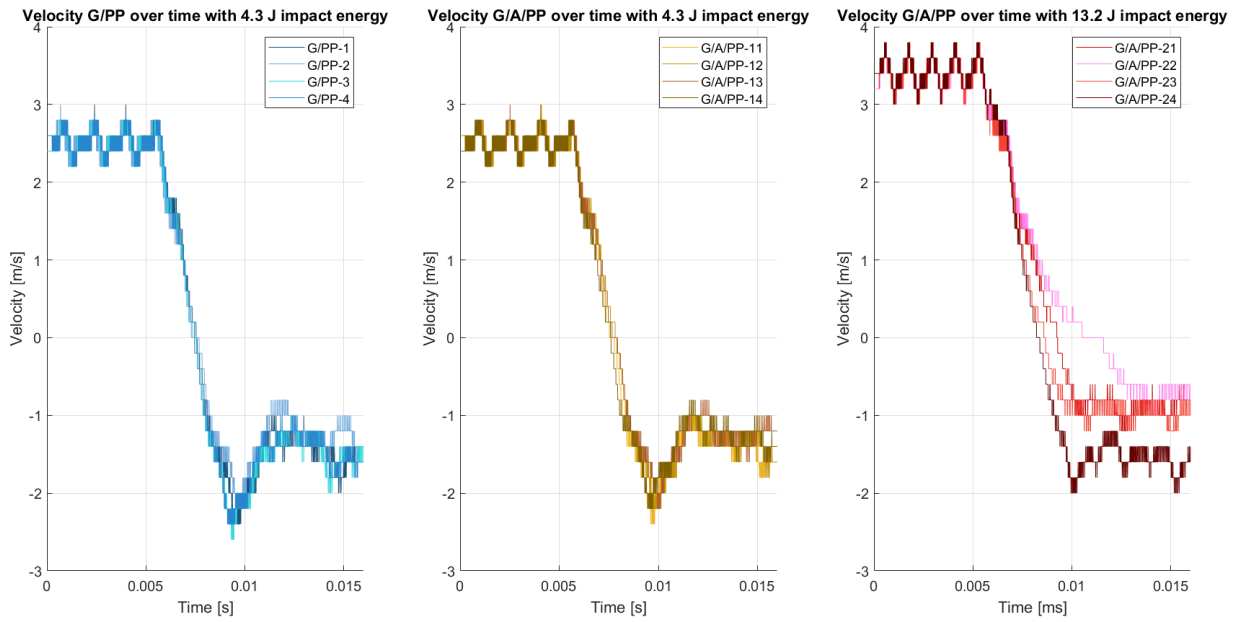


Figure 5.11: Velocity-Time graph for G/PP and G/A/PP

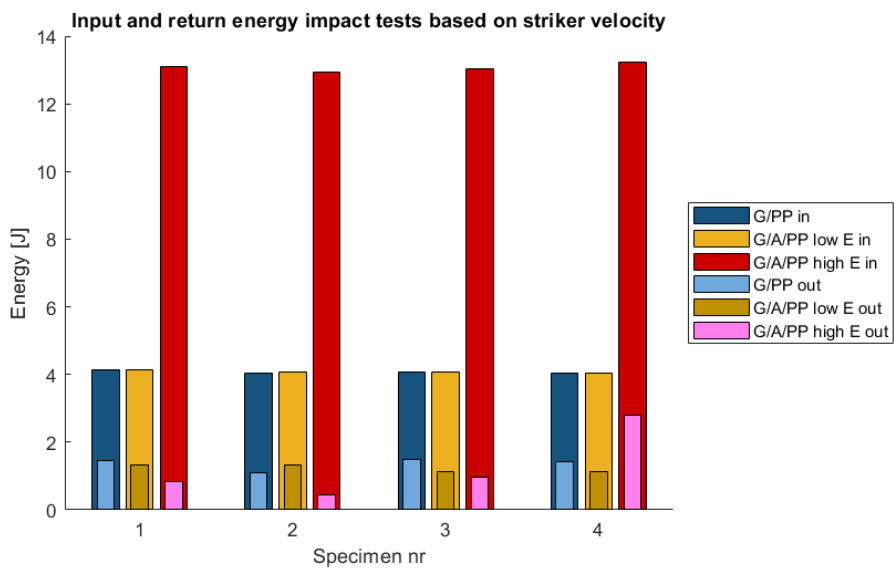


Figure 5.12: Energy input (wide bar) and return energy (smaller bar) based on striker velocity

5.5 Failure analysis

The SEM (Scanning Electron Microscope, Thermofisher Phenom XL TableTop) is used to inspect the fractured surfaces of the specimen which are subjected to the bending or impact tests. The SEM offers a higher magnification than the optical light microscope and offers an increased depth of field, aiding in obtaining sharper images.

The specimen of the 4-PBT are folded/broken to get the fractured surface in vision. Only the original crack formed by the mechanical testing is inspected. The goal is to see if there is a difference between the bonding of the PP and glass fibers or Twaron fibers. Figure 5.13 displays a part of the fracture edge of a G/A/PP specimen. On the top of the image the outer surface of the specimen is visible, at that point it is matrix dominated. Slightly below the outer surface the white fibers are visible, these are the glass fibers. It can be concluded that those fibers stick well to the PP matrix and that the matrix has a ductile failure mode. Bundles of darker fibers are visible at the left bottom of the image, those are the Twaron fibers. It can be clearly seen that the matrix materials is not sticking well to the Twaron fibers. This effect can be seen even better in Figure 5.14, the white fibers at the top of the image are glass fibers with PP sticking to it. The darker gray fibers at the bottom of the images are clean aramid fibers.

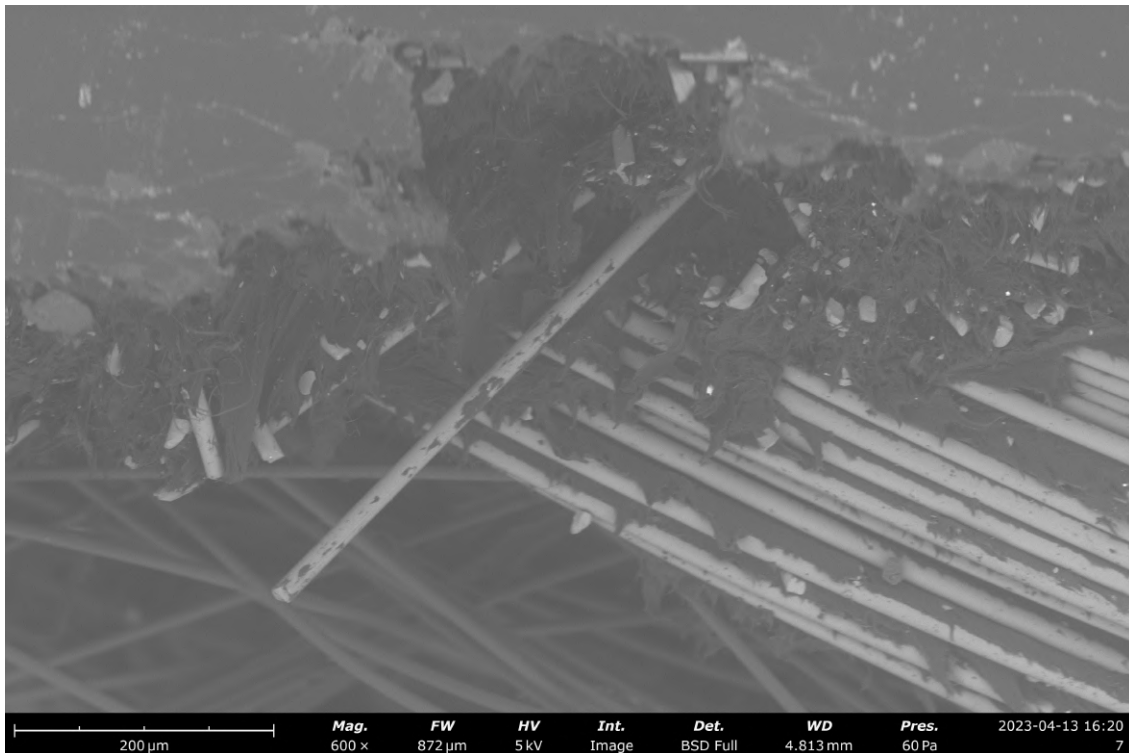


Figure 5.13: SEM image of G/A/PP specimen on the fracture surface of the 4 point bending test

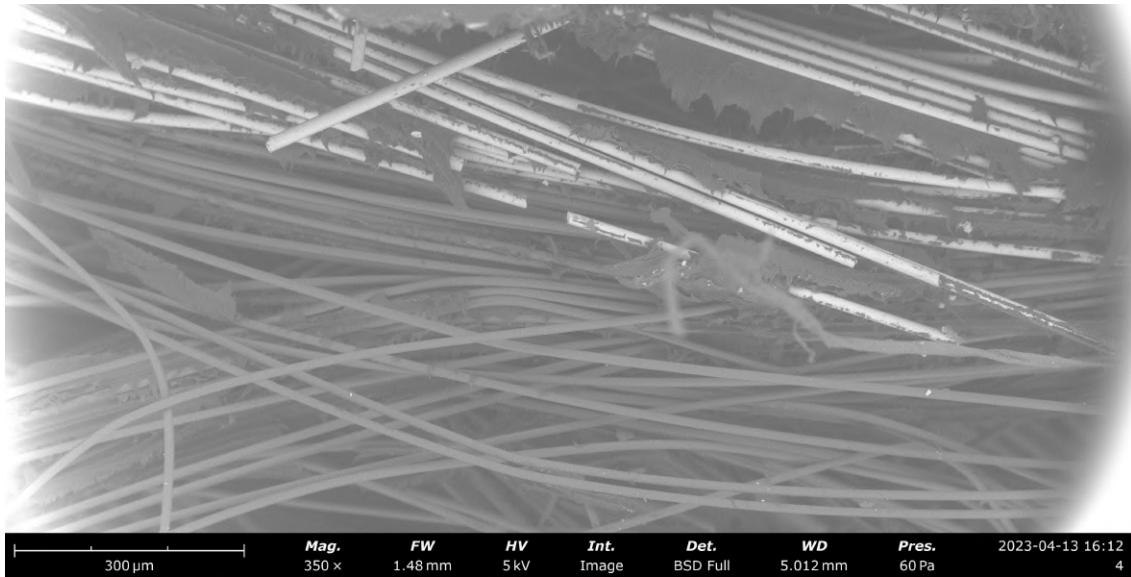


Figure 5.14: SEM crop on the same G/A/PP specimen

Another point of interest is to determine what causes the failure of the composite plates. This is investigated for both the bending tests as well as for the impact tests. Starting with the 4-PBT specimen. One thing that was in common with all the specimen is that the fracture cracks initiated from matrix cracks on the bottom surface. The matrix failed in tension in these cases. Another interesting phenomena is that the crack propagation is at the boundaries of the pellets. In Figure 5.15, specimen R1-6 is displayed with three different lighting conditions. With the concentric light (5.15(b)) the surface is visible, with the ring light (5.15(c)) the structure and fiber angles become more visible. Finally in Figure 5.15(a) a normal image is given to indicate the scale and position of the fracture. Although the side of the specimen is not polished prior to testing and microscopy, it can be seen that the crack initiates at the point where the fibers are not in the 1-direction. In Figure 5.15(c) the red bracket indicates a part of a pellet which is positioned in the 1-direction, indicating a local high material stiffness. The blue bracket is where the crack starts, and in this region the fibers are more at 90 degrees. Hence this region is the strength and stiffness is mainly dominated by the matrix. It seems that the crack follows the path of least resistance in between the pellets.

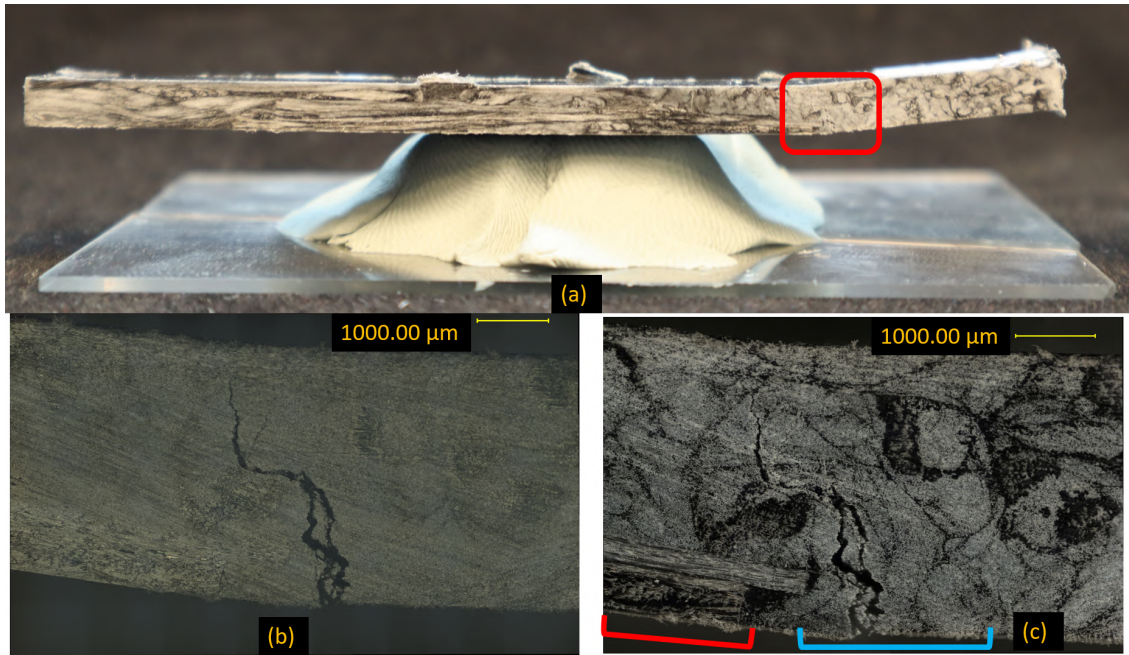
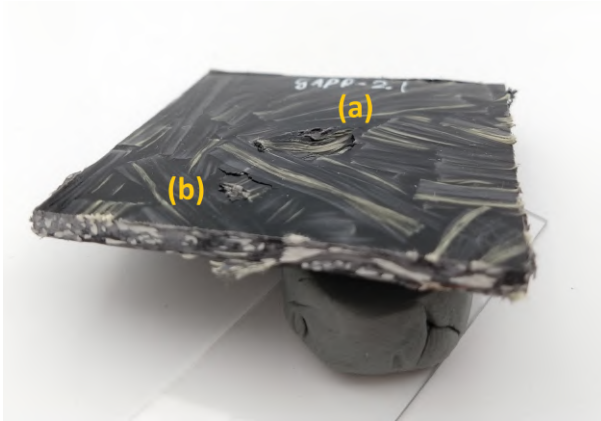


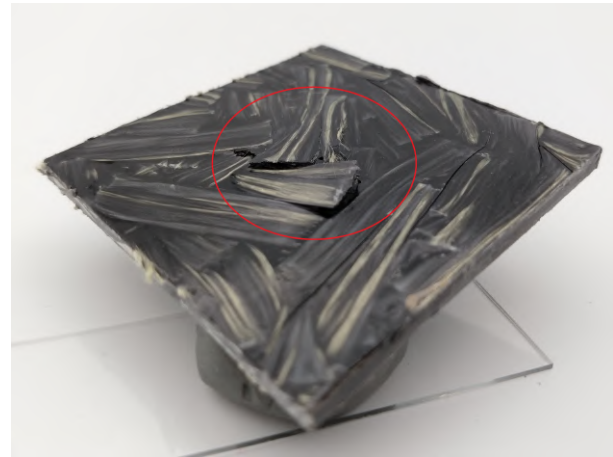
Figure 5.15: Crack in Specimen R1-6 of the 4-point bending test. Looking from the side. (a): normal photograph (b): Optical microscope concentric lighting (c): Optical microscope ring lighting

The phenomena of pellet tear-out is also visible with the impact specimen (Figure 5.16). At the top-side some minor fiber breakage occurs with the low energy impacts, however, severe fiber breakage is present with the high energy impact. On the bottom side the pellets do tear out, but they remain their shape. The position of cracks on the bottom side are usually not directly under the impact location. The impact-side of a specimen can be seen in Figure 5.16a: at (a) the striker hit the specimen, on this location fiber breakage is present and a big crater is formed. At position (b) the end of the pellet that the striker hit has debonded, the aramid fibers do not break and deform the pellet over its full length. The tear-out on the bottom side is displayed in Figure 5.16b. Multiple pellets are deformed, in all cases the matrix in between the pellets failed in tension.

The Tabletop SEM is used to investigate failure on micro scale. With the smaller impacts of 4.3J little fiber breakage was visible, however this was present with an impact of 13.2J. The hypothesis of adding a fiber with more strain-to-failure is to toughen the composite. In other words, the more brittle fibers break first while the more ductile fibers carry the remaining load. The fracture of glass fiber can be seen in Figure 5.17a, highlighted by the blue ovals. The image is taken from the impact-side of the specimen, at the top of the image some matrix areas of the outer surface are visible. The aramid fibers (dark grey coloured) did not fracture. Another observation is the sharp fractured surfaces of the glass fibers, indicating a brittle failure. The edge of the crater formed by the striker of the impact machine can be seen in Figure 5.17b. The bottom right of the image displays the top-side of the specimen, the blue oval highlights the broken glass fibers. The glass fiber is sheared off, whereas the Twaron fibers (yellow oval) bend and follow the form of the crater.

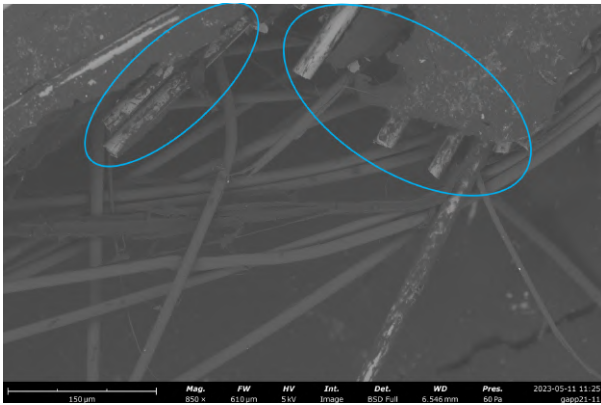


(a) Impact side specimen G/A/PP-21

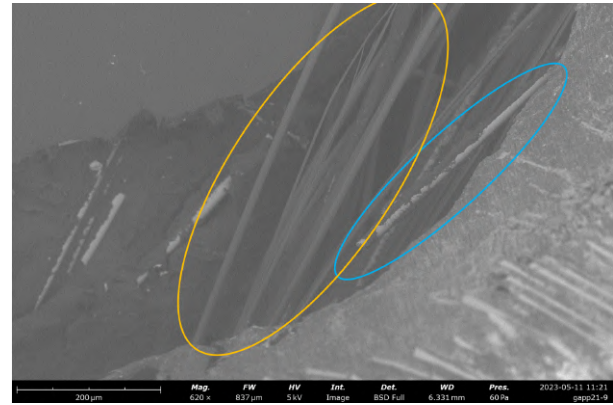


(b) Bottom side of G/A/PP-21 after impact test.

Figure 5.16: Impact specimen



(a) Impact side of specimen G/A/PP-21.



(b) Impact side of specimen G/A/PP-21.

Figure 5.17: SEM images of the impact-side of specimen G/A/PP-21

6 DEMONSTRATOR

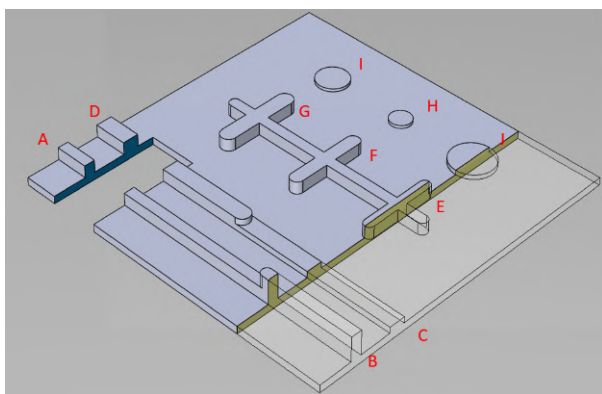
A composite product made with LFTP is only relevant if it is possible to achieve good levels of fiber distribution and reliable results in real-world use cases. A demonstrator part is designed to showcase the possibilities of LFTP. The features on the plate have different dimensions to see how these dimensions work in according with the dimensions of the pellets. The design is elaborated in Section 6.1, followed by the production process (6.2) and the results are presented in Section 6.3.

6.1 Demonstrator design

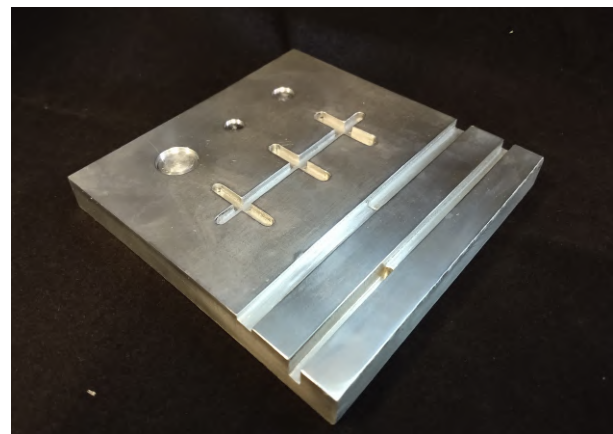
For Compression Molding features like stiffener ribs and local thicker section are interesting. With these features a normal flat part can be made much stiffer or have the ability to accommodate other hardware like bolts. The features of the die insert are listed in Table 6.1 and the Solidworks model with the labels is shown in Figure 6.1a. The production drawing can be found in Appendix D.

Features	Dimension	Label
Stiffener ribs	4x4 mm, 4x8 mm	A, B
	6x2 mm, 6x4 mm	C, D
Raster ribs	4x3 mm spine with 4,5,6 x3 mm crosses	E, F, G
Local round reinforcement	8, 10 x 1 mm	H, I
	16x1.5 mm	J

Table 6.1: Features demonstrator part



(a) Solidworks model of the plate with features and highlighted (blue, yellow) cross section areas



(b) Aluminium die insert

Figure 6.1: SOLIDWORKS model of the die insert and the actual insert after milling.

To achieve these features on a flat plate an insert is made for the normal 125x125 mm picture frame die. The negative of the features is milled in an aluminium plate. There are two options considering

the stacking order inside the picture frame die. Option 1 is that the aluminium insert is placed at the bottom (with the cavities facing upwards) and the pellets are randomly placed on top of the insert. The other option is that the pellets are placed inside the picture frame die, subsequently the aluminium insert is placed on top (cavities facing downwards). The advantage of the last method is that the pellet orientation is not (or less) influenced by the mold cavities. It is possible that pellets will fall inside the ribs and align over the longitudinal axis of the rib. On the other hand, with the aluminium insert on top, air can be trapped inside the features, resulting in voids or badly filled features.

The first method is used for pressing the plate. The downside of the possible alignment of pellets outweighs the possible worse filling with the second method.

An image of the opened die can be seen in Figure 6.2. Here one of the side walls is removed to see the stacking order properly: 1, 2 and 3 are respectively the bottom, side wall and top lid of the pressing die. At position 4 the spacer plates are located, those are polished to assure a good surface quality. The aluminium die is located at 5, the space in between the spacer plates and the die insert will be filled with pellets.

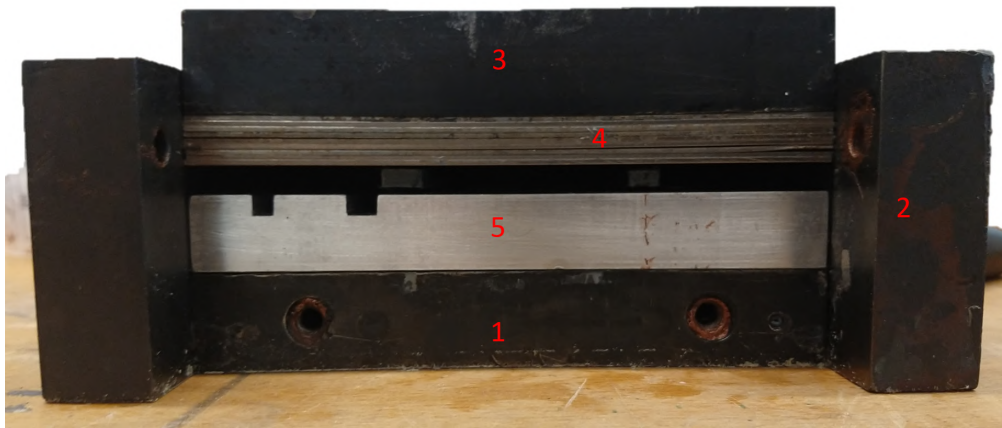


Figure 6.2: The side view of the pressing die including the insert. One of the side walls is removed to make the inside visible.

6.2 Compression molding

For the compression molding of the demonstrator part the same processing settings as are explained in Chapter 4.1 are being used. Rasheed [35] found that smaller flakes produced a more homogeneous composite with a lower void content and less non-impregnated regions, however in that research [0/90] woven flakes were used. The hypothesis is that despite the longer pellet lengths used in this test, the ability to mold the LFTP is better due to the UD fiber alignment. The pellets can deform easier in the 2-direction, or even split in multiple bundles during the compression molding process.

6.3 Results

After demoulding the part, the first optical assessment can be done on how well the features are filled. In this case all features are completely filled with a mixture of glass fiber and PP. The smallest reinforced circle (Feature I in Figure 6.1a) is matrix-rich. Larger features do have visible glass fiber bundles in them. The part has more curvature than the flat plates which are used for the test specimen. This can be caused by the stiffness differences of the features, also some damage was done by demoulding the part.

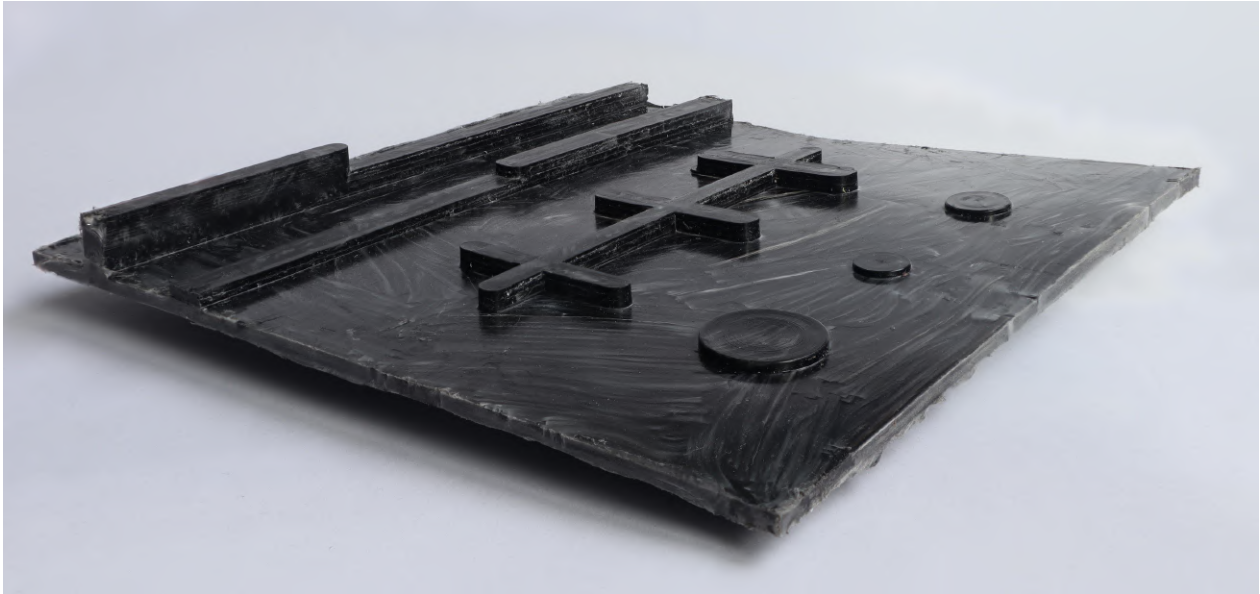


Figure 6.3: Demonstrator part 40 mm G/PP pellets.

On the normal photograph, see Figure 6.3, it can be seen that all the features are filled and no obvious voids/air pockets are created during the compression molding process. Next to that the glass fibers have moved into the ribs, even the shallow tall rib (feature B in Figure 6.1a) is not a matrix rich zone. To get a view on the presence of matrix rich zones, fiber position in the features and voids, the plate is cut, embedded and polished for optical microscopy. The micrographs are shown in the next figures. Four different sections are inspected, in Figure 6.1a these are highlighted. The blue section has the lower ribs, the yellow section is split into three samples: tall ribs, cross rib and round reinforcement. All four cross sections micrographs are displayed in Figure 6.6. The first analysis that is done is measuring the void content by image analysis, the results can be found in Table 6.2. Already visually it can be seen that the void content is higher within the stiffener features than in a flat plate. The measurements by the image analysis in the third column of Table 6.2 confirm this. There is not a direct correlation between the aspect ratio of the rib and the void percentage. At least two counter arguments can be given on that statement; namely only four cross sections are taken, so statistically not enough. Secondly the pellets can align in the die before the pressing starts, in this situation the rib is already (partly) filled and no voids can be created by poor flow in the ribs. In this situation the fibers align with the direction of the rib, which is beneficial considering the stiffness, this effect can be detected by checking the ribs on round fibers in the cross section. If the fibers are round the fibers are perpendicular with the cross section and so parallel with the rib. The alignment of pellets can be seen in Figure 6.4, especially in the enlarged crop the round fibers are clearly visible.

Feature	Width/height	Void content [%]
4x8 mm rib	0.5	6.3
4x4 mm rib	1	3.2
6x4 mm rib	1.5	8.5
6x2 mm rib	3	4.1
4x4 mm cross rib	6.25	6.2
16x1.5 mm round reinforcement	10.6	12.6 (big epoxy void, 6% more realistic)
Normal G/PP plate	-	1.4

Table 6.2: Void content features demonstrator



Figure 6.4: Pellet alignment inside the 4x8 mm rib

The geometry of the stiffener plays an important role in how well the feature is filled with reinforcement fibers. If the length of a particular feature is short in comparison to the length of the pellets, corners will be matrix-rich zones. This effect is visible in Figure 6.5, this is a close up of the right corner of the cross rib (see Figure 6.6c). Due to the sharp corner the fibers bend into the rib but do not flow into the outer corner, creating a M.R.Z. (Matrix-rich zone).

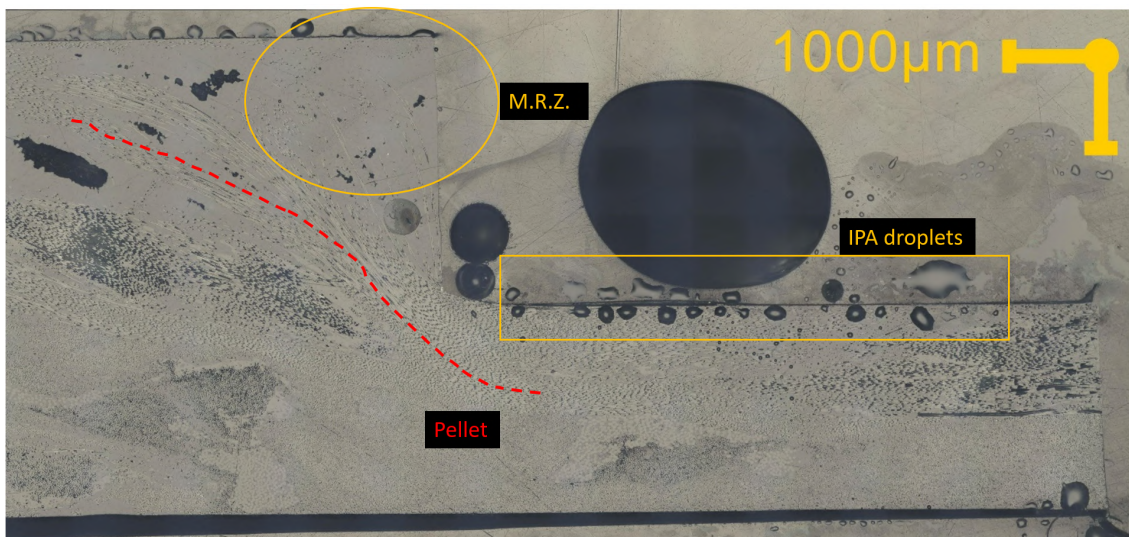
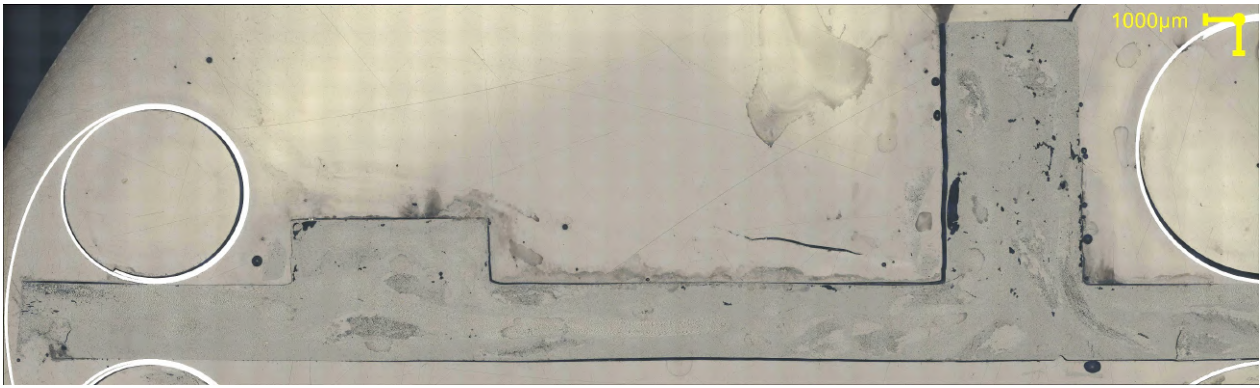


Figure 6.5: Close up of the cross rib (Figure 6.6c, right side) where pellet flow and matrix-rich regions are visible.

Concluding this chapter with answering the question if the LFTP are suitable for real-world use cases. Based on this relatively simple test the answer would be yes. However not without some recommendations.

- Entry radii are required to get a good flow of fibers into the stiffener features, otherwise Matrix-rich zone will be formed.
- Crossing ribs have proven not to be an issue considering void content.

- A relation between aspect ratio of the stiffener and void content was not found, however, if pellet alignment is not possible/occurring in the ribs, narrow tall ribs have the tendency create M.R.Z. (Matrix-rich zone) and/or more voids.
- Sink marks on the opposite side of the features are relatively rare. Those are prevented by the random pellet alignment, reducing M.R.Z. (Matrix-rich zone) above features.



(a) 6x2 mm and 2x8 mm ribs



(b) 4x4 mm and 6x4 mm ribs



(c) Cross rib 4x4 mm (feature E)



(d) Local round reinforcement 16x1.5 mm

Figure 6.6: Micrographs of the different features on the demonstrator

7 DISCUSSION

Multiple subjects of the thesis are discussed in this chapter. The discussion follows the same structure as the chapters, with the emphasis on the processing and mechanical properties of the (hybrid) LFTP.

We start the discussion with the topic **fiber commingling to a hybrid yarn**. The reason to hybridize the yarns, to enhance certain mechanical properties, is well-known and agreed upon. The road to the hybrid commingled yarn is not. In this research the hybrid yarn is formed from a pre-commingled G/PP yarn and a standalone aramid yarn. Experiments found that the materials in this form could work, however do not work in optimal form. Tests can be performed with three stand alone yarns. This can help to intermingle the reinforcement yarns better with each other. With a finer dispersion of the two reinforcement fibers a higher hybrid effect [8] can be achieved.

The **compression molding of the LFTP** resulted in a good quality composite plate. Although not measured, the warpage of the plates after cooling was almost non-existent. All plates were sufficiently flat to use for the specimen. Inspection via optical microscopy revealed a crack inside an aramid bundle, most probably due to the thermal loading and the different CTE of Twaron and PP. Unfortunately, a data sheet of the Comfil G/PP [26] commingled yarns is not available, so only an estimate of the CTE could be made. In a worst case situation the thermal strain caused by the difference in CTE of the PP and aramid can reach yielding levels of the matrix. The problem is not consistent in multiple specimens, so no further modification on the process are required to solve this.

Another point of interest is the **pellet alignment**. The repeatability of the fiber angles in the pressed plates is important for a robust production process. The results from the ImageJ analysis revealed that the pellet alignment is indeed not completely random. With a random alignment the histogram of the fiber directions should result in a horizontal line, in the measurements a peak in the range of 35-60 degrees (in relation to the horizontal axis, displayed in Figure 4.4) is measured. Boundary effects between the pellets and the pressing die can be cause of this., the length of the pellets is relatively long in relation to the dimensions of the pressing die. Tests with the same pellet length and a larger pressing die or a smaller pellet length should be performed to completely understand this topic.

Secondly on the theme of **pellet dimension** is the thickness of the pellets in relation to the thickness of the final product. Or phrased in other words, how many pellets are stacked in the thickness direction. The micrographs of the G/A/PP samples can be used to determine how many pellets are stacked upon each other, it is known that five aramid bundles are present in each pellet. Another image analysis procedure is made with ImageJ and Matlab (explained in Appendix B.4). The pellets are highlighted by the purple ovals in Figure 7.2. Five bundles with similar angles are assumed to be one pellet. Based on this micrograph up to four pellets are stacked over the thickness of the compression molded plates. However, on the left side of the image only two pellets are stacked and based on the color also with a similar angle, this can be a potential weak spot if the loading is perpendicular to those pellets.

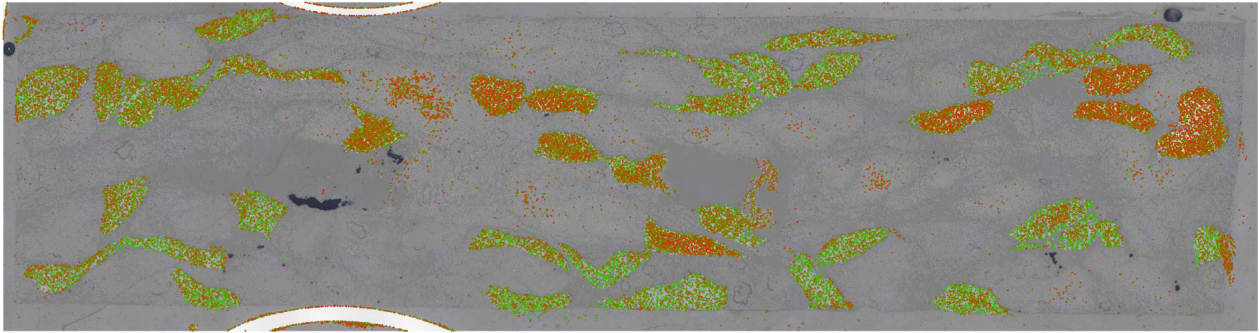


Figure 7.1: Aramid fiber directions made visible by color. Green is perpendicular to the image, red is parallel to the image.

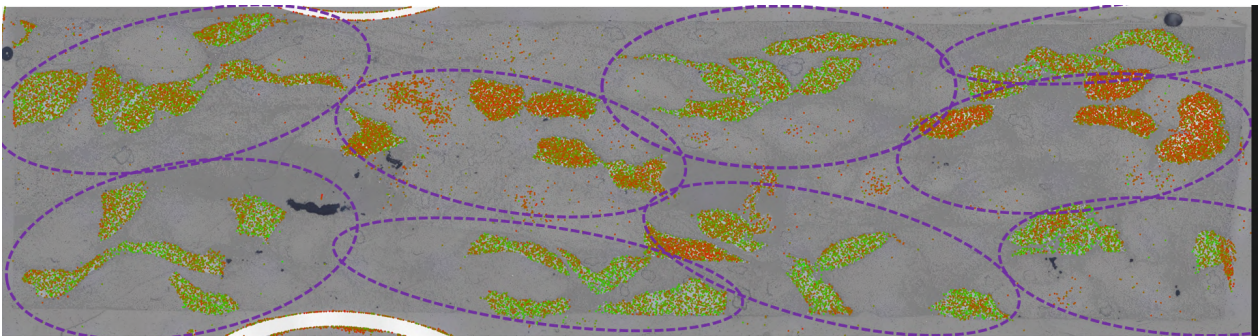


Figure 7.2: The same specimen with the pellets highlighted based on fiber angle.

The 4-PBT gave interesting results, both for the mechanical properties and for how a long fiber composite behaves and fails. Starting with the first topic of **mechanical performance**. A hybrid composite can be utilized to increase the overall stiffness by adding a stiffer, and in general a more expensive, fiber to create a balanced product that is stiff and cost effective. The results of the 4-PBT showed otherwise. The G/A/PP specimen did show a decrease of 26% in bending stiffness in comparison to the G/PP specimen. Although this is a large difference, the deviation within the specimen is large, in general the G/A/PP specimen perform less stiffness-wise. This is an interesting result, given that aramid fibers are added and thus increasing the V_f . Based on micro-mechanics this would increase the stiffness of the composites. The cause of lesser performance is most probably the poor fiber-matrix bonding of the aramid. Another key aspect of the aramid fibers are their anisotropic properties, whereas glass fiber is isotropic by itself. The stiffness of the aramid fibers in 2-direction is much lower, further decreasing the composite's stiffness if the aramid fibers are not at 0 (or close) degrees. Specimen RA1-1 and RA2-2 (Appendix C.1, Figure C.4) do show a significant higher stiffness values. Closer inspection of these two specimen revealed that the majority of the visible pellets have an angle of $0 - 10^\circ$ in relation to the length of the pellet, making them UD-like. To completely prove that the G/A/PP specimen have a higher stiffness when loaded in 1-direction, a set of UD-aligned G/A/PP specimen should be produced and tested.

The work utilized during the 4-PBT is 14% higher for the G/A/PP specimen, where the increased work is mainly achieved by a lower drop of force after the peak. With the addition of the aramid fibers a tougher composite is created with a less abrupt failure point.

SEM micrographs confirm the poor matrix bonding by showing clean aramid yarns in the fractured surface whereas the glass fibers are coated with the PP matrix and experience ductile matrix failure. Dry spots in the aramid bundles can be ruled out after checking the micrographs of the pressed G/A/PP samples (Appendix B.3), it can be seen that the matrix surrounds the aramid fibers.

Finally, the cracks discussed in Section 5.1 can act as a crack initiation, on top of that when the fibers and matrix are not bonded, the reinforcement fibers do not contribute to the overall stiffness if the loading is perpendicular to the crack.

Other research on recycled chopped fibers [36] found similar **failure modes** for long fiber random orientated composites. The specimen fail under tension on the bottom side where a large difference in stiffness is occurring due to changing fiber angles, which was also found in this research (Section 5.5). A topic that is not discussed yet is the **specimen size**. The pellet dimension is set at 40 mm with $\varnothing 3$ mm, after compression molding the width of a pellet is in the range of 10 mm. This can have a big influence on the stiffness across the specimen. Locally the width of the specimen can be filled with a single specimen, creating a relatively stiff or weak region. The big spread in test results of the 4-PBT underlines this phenomena. Furthermore, the impact tests, with a larger specimen/pellet dimension ratio, had a much narrower spread in results. It would be interesting to test the 4-PBT with wider specimen, aiming at a width of 3 times the pressed pellet width. This would mean a specimen size of 80x30x4 (L x W x T) mm instead of 80x10x4 mm.

The **impact tests** revealed the dynamic behaviour of the composite materials. The goal of the impact tests was to investigate the difference between the hybrid and non-hybrid composites, and these difference have been found. The goal of toughening the composite for out-of-plane impacts is achieved by adding the aramid fibers. Where the poor aramid-PP bonding is a bad thing for achieving a stiffer composite, it is a good way to achieve energy dissipation by debonding. The beneficial effect of fiber debonding, besides the energy dissipation, is that the fibers stay intact. Without fiber breakage more stiffness is kept in the structure. The fibers can still carry some load after a peak force is recorded, which was also measurable with the 4-PBT. The force-displacement graphs give a good comparison (Figure 5.9), the force with the G/A/PP specimen reaches a plateau where a sawtooth profile is formed. This behavior is desired for creating the so-called **pseudo-ductility** [21], which is normally not present in FRPC.

The impact zone of the impact test is $\varnothing 40$ mm, this mean that local stiff or less stiff areas do affect the test outcome to a lesser extent than during the 4-PBT. The data sets confirm this hypothesis, the force peaks are very consistent.

8 CONCLUSION AND RECOMMENDATIONS

This chapter aims to answer the research question *'How do hybrid fiber reinforcements affect the mechanical properties of composite parts made of long fiber thermoplastic pellets?'* By adding 8 % V_f Twaron fibers to the G/PP composite the failure strain is increased by up to 4.5%, the energy dissipation in bending by 14% and an impact is spread over a 19.5% longer time, thus reducing the peak load by 17.4%. On the other hand the stiffness is significant lower than the G/PP specimen by a significant 26.6%. The hybridization of G/PP with aramid results in a tougher composite and less brittle failure behaviour, with the downside of reduced stiffness.

We can now also answer the sub-questions:

How can a hybrid reinforcement thermoplastic yarn be manufactured consisting of two types of reinforcement fiber and a thermoplastic fiber? The most effective method to produce a combined yarn in a lab environment is via the commingling process. The designed commingling nozzle was working to an extent, however it is not advisable to use a pre-commingled G/PP yarn. In some sections the aramid yarn and the G/PP yarn are commingled well. Overall speaking the level of commingling is low.

What pultrusion parameters result in a good quality pultruded rod? Good is defined as a constant cross-section and well impregnated fibers. This question could be answered by try-and-error and knowledge of previous MSc assignments within the research chair. It turns out that pultrusion speed had little influence on the void content (100-250 mm/min tested), the most important factor to reduce voids is sufficient cooling and a good contact of the cooling block to the pultrusion die.

How do the mechanical properties of a LFTP part compare to other Fiber Reinforced Composites (FRC) production methods, produced with the same fiber/matrix materials? Verify by the Classical Laminate Theory or micromechanics. To answer this question, specimen with an UD pellet alignment have been produced. The results of the 4-PBT of these specimen do align very well with the expected value by the theory. The spread in stiffness and maximum stress in the specimen with a random pellet orientation was much wider. The mean of the results do agree the theory of Lavengood & Goettler [34] and are within the bandwidth calculated via the CLT.

Investigate the ability of the pellets to be pressed into a plate with a rib, to validate the pellets' real-world use case and processability. This sub-question is answered by producing the demonstrator part. It became clear that LFTP with a long fiber length are suitable for molding more complex shapes. Smaller features or sharp angles do have the tendency to become M.R.Z. (Matrix-rich zone), this can be reduced by adding more fillets at sharp corners. Jamming in the entrance region of the ribs was not found, neither dry areas due to matrix traveling to M.R.Z. was present. A possible explanation for this is the UD fibers in the pellet. The pellet can deform easily in the 2- and 3-direction during the compression molding cycle, where a woven ([0/90]) flake can be more restricted to deform in these directions.

8.1 Recommendations

Over the time of this research multiple points could be improved or the research extended. Those points are summarized in the following list.

- For long fiber composites made of flakes/pellets the specimen for mechanical testing should be sufficiently large to reduce local effects. As a rule, we propose the width of the specimen is three times the width of the pellet.
- Test UD aligned G/A/PP specimen in a 4-PBT to measure the stiffness in 1-direction. This can give an insight in the anisotropic properties of aramid and how the poor aramid-PP bonding influences the result for bending in 1-direction.
- Reduce the thickness of the pellets if the molded plates have a thickness of 3 – 4 mm. This will increase the number of pellets that can be stacked, further decreasing local effects in the material.
- The aramid/PP bonding is poor. This has advantages in energy dissipation and prevents fiber breakage. Tests with better seizing for aramid-PP should be performed to measure the influence on the stiffness and debonding.
- A combination of LFTP and continuous reinforced composites can be an interesting research field. With this idea recycled flakes/pellets can be combined with newly made fabrics.
- To get a better understanding of the flow of the pellets during the molding process a very thin metal wire can be embedding during the pultrusion process. By stopping the molding process halfway and de-molding the part a röntgen scan can be made where the metal wires are visible. Thus allowing for a better understanding of the flow of the fibers and matrix during the process.

REFERENCES

- [1] Wouter Grouve, "Composite principle image from slides Composites," in *Composite course slides 1*. Slides Composites Course, 2022.
- [2] Granta Edupack 2020, "Granta Edupack database," 2022.
- [3] P. Mallick, "Thermoplastics and thermoplastic–matrix composites for lightweight automotive structures," *Materials, Design and Manufacturing for Lightweight Vehicles*, pp. 187–228, 1 2021.
- [4] P. Malnati, "SMiLE - Fraunhofer ICT," 2019. [Online]. Available: https://www.ict.fraunhofer.de/en/press_media/press_releases/2019/2019-01-16.html
- [5] H. Mason, "Composite sidewall cover expands options for fire-safe rail components | CompositesWorld," 2023. [Online]. Available: <https://www.compositesworld.com/articles/composite-sidewall-cover-expands-options-for-fire-safe-rail-components>
- [6] A. Rajpurohit, V. Singery, S. Joannès, P. Sanial, and L. Laiarinandrasana, "Manufacturing and performance of hybrid fabric reinforcements and their composites," *ECCM 2018 - 18th European Conference on Composite Materials*, 2020.
- [7] Y. Swolfs, L. Gorbatikh, and I. Verpoest, "Fibre hybridisation in polymer composites: A review," *Composites Part A: Applied Science and Manufacturing*, vol. 67, pp. 181–200, 12 2014.
- [8] Y. Swolfs, R. M. McMeeking, I. Verpoest, and L. Gorbatikh, "The effect of fibre dispersion on initial failure strain and cluster development in unidirectional carbon/glass hybrid composites," *Composites Part A: Applied Science and Manufacturing*, vol. 69, pp. 279–287, 2015.
- [9] AGS Technology, "Plastics Profiler-Glass Fiber In Polypropylene." [Online]. Available: <https://agstechnology.com/newsletter/plastics-profiler-glass-reinforced-polypropylene/>
- [10] J. L. Thomason and M. A. Vlug, "Influence of fibre length and concentration on the properties of glass fibre-reinforced polypropylene: 4. Impact properties," *Composites Part A: Applied Science and Manufacturing*, vol. 28, no. 3, pp. 277–288, 1997.
- [11] J. L. Thomason, "The influence of fibre length and concentration on the properties of glass fibre reinforced polypropylene: 5. Injection moulded long and short fibre PP," *Composites Part A: Applied Science and Manufacturing*, vol. 33, no. 12, pp. 1641–1652, 12 2002.
- [12] —, "The influence of fibre length and concentration on the properties of glass fibre reinforced polypropylene: 7. Interface strength and fibre strain in injection moulded long fibre PP at high fibre content," *Composites Part A: Applied Science and Manufacturing*, vol. 38, no. 1, pp. 210–216, 1 2007.
- [13] PlastiComp and Inc, "Design Considerations for Successfully Using Long Fiber Thermoplastic Composites as Substitutes for Metals," *PlastiComp whitepaper*.

- [14] H. L. Cox, "The elasticity and strength of paper and other fibrous materials," *British Journal of Applied Physics*, vol. 3, no. 3, pp. 72–79, 1952.
- [15] ESA, "ESA - 3D printing CubeSat bodies for cheaper, faster missions," 2017. [Online]. Available: https://www.esa.int/Enabling_Support/Space_Engineering_Technology/3D_printing_CubeSat_bodies_for_cheaper_faster_missions
- [16] Saint-Gobain Vetrotex, "Twintex processing guideline ," 2005.
- [17] K. S. Pandya, C. Veeraj, and N. K. Naik, "Hybrid composites made of carbon and glass woven fabrics under quasi-static loading," *Materials and Design*, vol. 32, no. 7, pp. 4094–4099, 8 2011.
- [18] R. A. D. da Cunha, R. D. da Cunha, W. F. de Amorim Junior, A. M. da Silva Dias, and R. C. S. Freire Júnior, "Study of an Intraply/Yarn Composite Submitted to Low-Velocity Impact in the Presence of High Void Content," *Journal of Materials Engineering and Performance*, vol. 30, no. 10, pp. 7523–7531, 10 2021.
- [19] A. Wagih, T. A. Sebaey, A. Yudhanto, and G. Lubineau, "Post-impact flexural behavior of carbon-aramid/epoxy hybrid composites," *Composite Structures*, vol. 239, p. 112022, 5 2020.
- [20] Y. Shan and K. Liao, "Environmental fatigue behavior and life prediction of unidirectional glass–carbon/epoxy hybrid composites," *International Journal of Fatigue*, vol. 24, no. 8, pp. 847–859, 8 2002.
- [21] G. Czél and M. R. Wisnom, "Demonstration of pseudo-ductility in high performance glass/epoxy composites by hybridisation with thin-ply carbon prepreg," *Composites Part A: Applied Science and Manufacturing*, vol. 52, pp. 23–30, 2013.
- [22] R. Alagirusamy, V. Ogale, A. Vaidya, and P. M. Subbarao, "Effect of jet design on commingling of glass/nylon filaments," *Journal of Thermoplastic Composite Materials*, vol. 18, no. 3, pp. 255–268, 5 2005. [Online]. Available: <https://journals.sagepub.com/doi/pdf/10.1177/0892705705049555>
- [23] P. Kravaev, O. Stolyarov, G. Seide, and T. Gries, "Influence of process parameters on filament distribution and blending quality in commingled yarns used for thermoplastic composites," *Journal of Thermoplastic Composite Materials*, vol. 27, no. 3, pp. 350–363, 3 2014.
- [24] J. Schäfer, O. Stolyarov, R. Ali, C. Greb, G. Seide, and T. Gries, "Process–structure relationship of carbon/ polyphenylene sulfide commingled hybrid yarns used for thermoplastic composites," *Journal of Industrial Textiles*, vol. 45, no. 6, pp. 1661–1673, 5 2016.
- [25] Teijin, *Specsheet Twaron pdf*, 2022. [Online]. Available: www.teijinaramid.com/twaron
- [26] Comfil, "Comfil commingled yarns," 2022. [Online]. Available: <https://www.comfil.biz/yarns-rovings>
- [27] Timo Grootelaar, "THERMOPLASTIC PULTRUSION OF CONTINUOUS FIBER REINFORCED FILAMENT FOR FDM 3D-PRINTING," Ph.D. dissertation, Universiteit Twente, Enschede, 2022.
- [28] N. Aegerter, M. Volk, C. Maio, C. Schneeberger, and P. Ermanni, "Pultrusion of hybrid bicomponent fibers for 3D printing of continuous fiber reinforced thermoplastics," *Advanced Industrial and Engineering Polymer Research*, vol. 4, no. 4, pp. 224–234, 10 2021.
- [29] G. Jogur, D. Mourya, R. Alagirusamy, and A. Das, "Numerical simulation of airflow behaviour and nozzle geometry on commingling for thermoplastic composites," *Composites Part B: Engineering*, vol. 223, 10 2021.

- [30] J.-Y. Tinevez, "Directionality plugin for ImageJ," 2018. [Online]. Available: <https://imagej.net/plugins/directionality>
- [31] ISO and NEN, "ISO 14125-1998," *NENConnect*, 1998.
- [32] ISO, "ISO 6603-2 Plastics-Determination of puncture impact behaviour of rigid plastics," 2023. [Online]. Available: www.iso.org
- [33] S. Timoshenko and S. Woinowsky-Krieger, *Theory of Plates and Shells*, second edition ed. McGraw-Hill Book Company, 1989.
- [34] R. Lavengood and L. Goettler, "Stiffness of Non-Aligned Fiber Reinforced Composites," *Defense Technical Information Center*, 1971. [Online]. Available: <https://apps.dtic.mil/sti/citations/AD0886372>
- [35] M. I. A. Rasheed, "Compression molding of chopped woven thermoplastic composite flakes," Ph.D. dissertation, University of Twente, Enschede, The Netherlands, 7 2016. [Online]. Available: <https://research.utwente.nl/en/publications/compression-molding-of-chopped-woven-thermoplastic-composite-flak>
- [36] P. Kiss, W. Stadlbauer, C. Burgstaller, H. Stadler, S. Fehringer, F. Haeuserer, and V. M. Archodoulaki, "In-house recycling of carbon- and glass fibre-reinforced thermoplastic composite laminate waste into high-performance sheet materials," *Composites Part A: Applied Science and Manufacturing*, vol. 139, p. 106110, 12 2020.
- [37] G. Jogur, A. Das, R. Alagirusamy, and G. Jogur, "Development of Kevlar[®]/polypropylene towpregs through optimized commingling nozzle and processing parameters for thermoplastic composites," *Journal of Thermoplastic Composite Materials*, vol. 2022, no. 0, p. 089270572211234, 9 2022. [Online]. Available: <http://journals.sagepub.com/doi/10.1177/08927057221123487>

A COMMINGLING MACHINE

A.1 Machine information

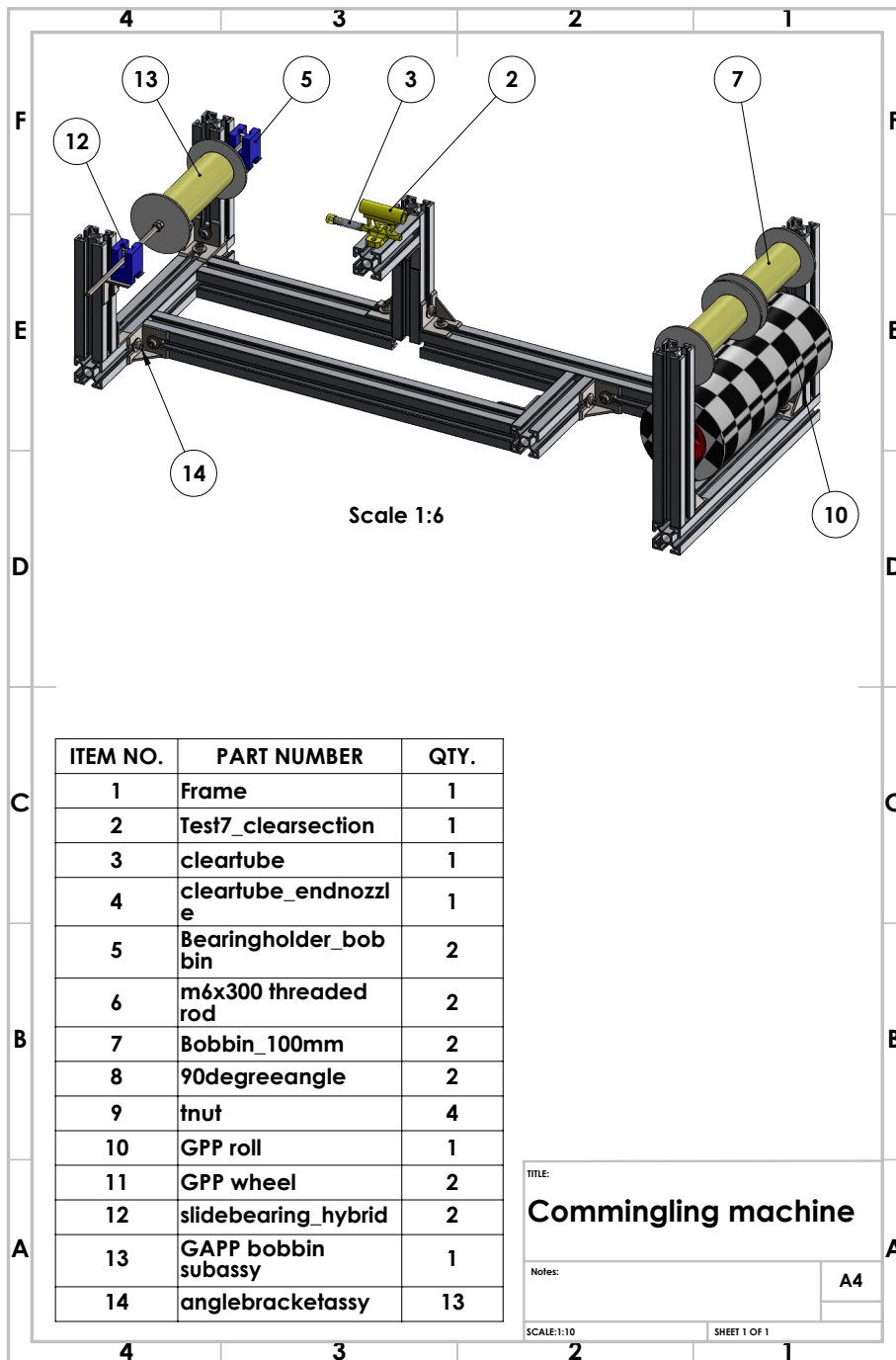


Figure A.1: Bill of Materials Commingling Machine

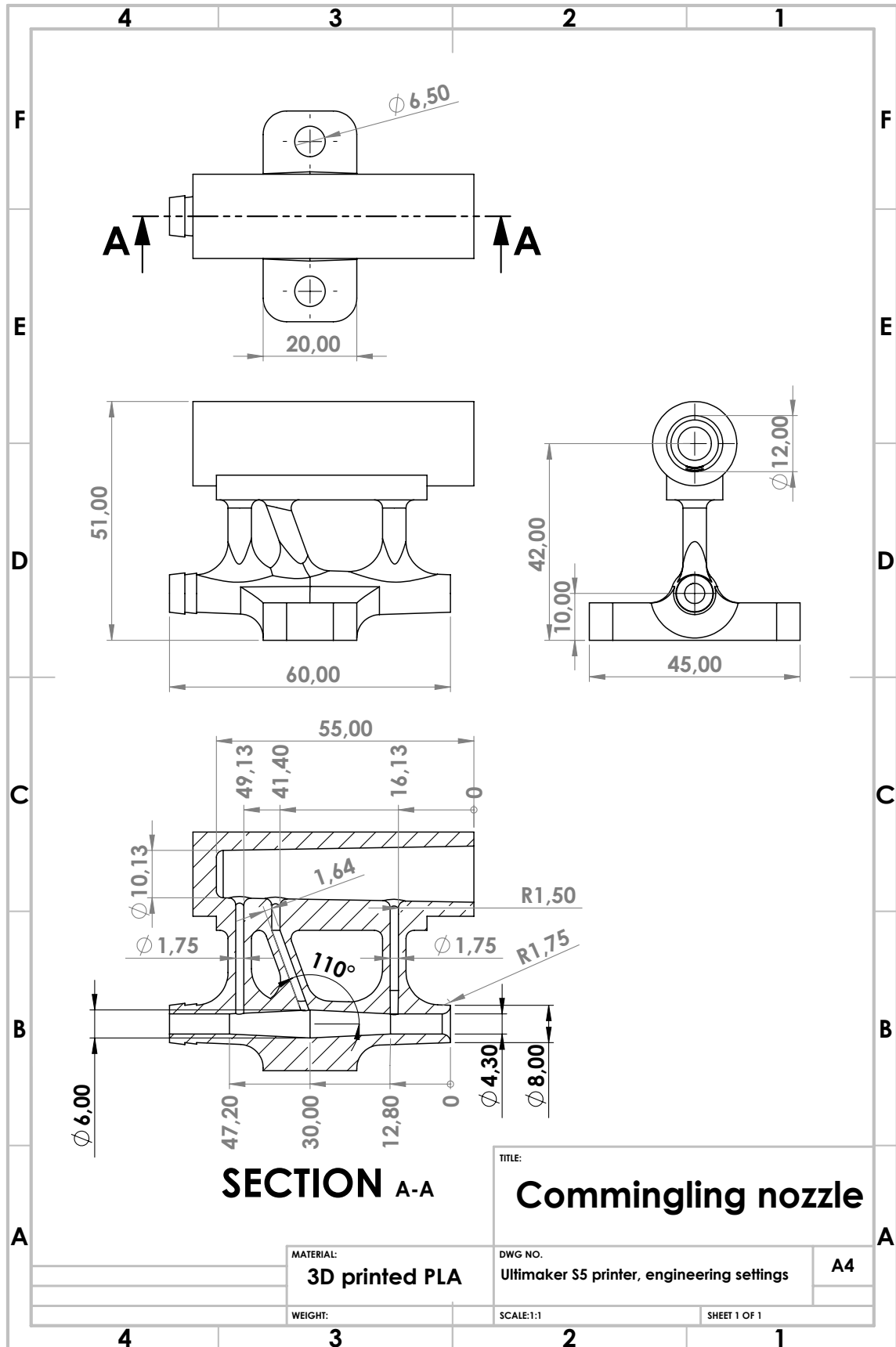


Figure A.2: Production drawing commingling nozzle

A.2 Nozzle analysis

Although the two 3D-printed nozzles made by a previous student do full fill the job to commingle two different yarns, the quality and design is only sufficient. In order to make a new improved design the working principle of the current nozzles are analysed with a CFD (Computational Fluid Dynamics) analysis in SOLIDWORKS.

The design requirements are listed via the MoSCoW method. M stand for Must have, without these features the design has failed. S is for Should have, features that greatly improve the design with some extra work/costs. C equals Could have, the nice to have features. Lastly W, Won't have. These things are out of the scope of the project. See Table A.1.

ID	Requirement	Specification	Importance	How checked?
M1	Minimum TEX capacity	At least 2600 TEX	M	Literature & testing
M2	Splitting/opening the yarn at entrance	Use an air channel perpendicular to the main channel	M	CFD analysis
M3	Producibility	Easy production of the nozzle for prototyping	M	3D printing with Fused Deposition Modeling (FDM).
S1	Air flows that mix the yarns	Use an air channel that creates swirls in the commingling chamber Enlarge the area where the yarns mingle together to increase the mobility of the yarns	S	CFD analysis
S2	Bigger commingling 'chamber'	The nozzle should be able to be mounted on a surface	S	Incorporate in the design
S3	Stability of the nozzle	The design should be able to release tension in the design to improve the commingling	S	Mount nozzle to surface
S4	Tension release on yarns	Add a transparent section in the nozzle	S	Add forward flow in the channel
C1	Look at the commingling process		C	Incorporate in the design

Table A.1: Requirements commingling nozzle design

A.2.1 CFD Analysis nozzles

The CFD analysis are performed in SOLIDWORKS 2022, with the SOLIDWORKS Flow Simulation package. The following project settings are used:

- Unit system: SI (m-kg-s)
- Internal analysis
- Physical features: Fluid flow, gravity

- Fluids: gasses -> air
- Flow type: Laminar and Turbulent, exclude high Mach number flow and humidity
- Default thermal conditions: adiabatic wall
- Temperature: 293.2 K, pressure 101325 Pa. All default settings

The boundary conditions consist of three separate conditions, since there are three in/outlets. The air inlet has a constant inlet velocity of 5 m/s. The other two boundaries are pressure openings, with environment pressure. Defined in the simulation project settings.

90 degree nozzle

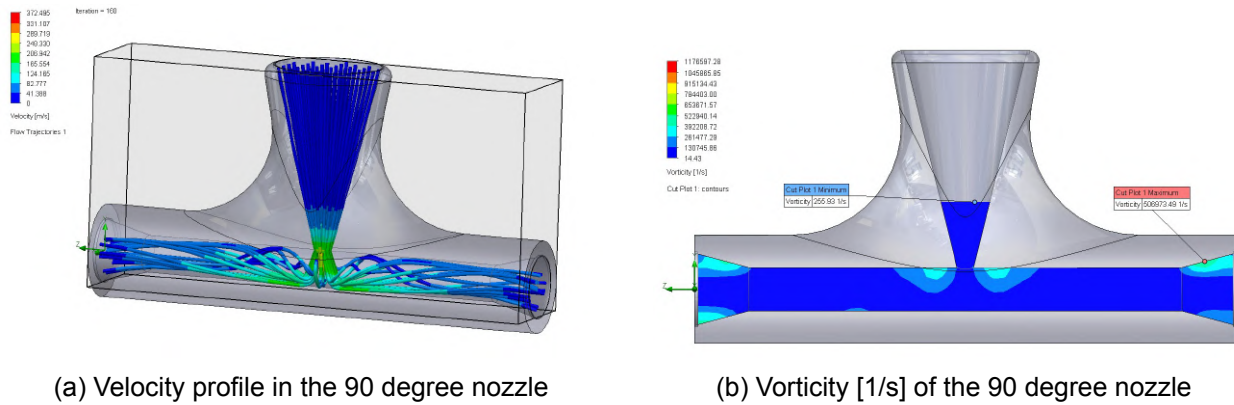


Figure A.3: 90 degree nozzle

90 + 45 degree nozzle

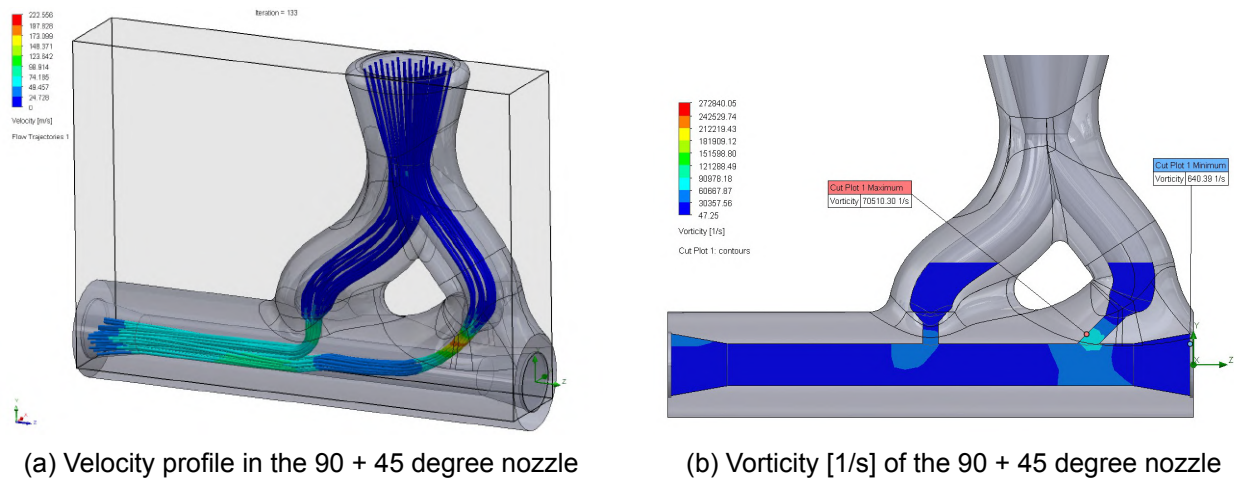


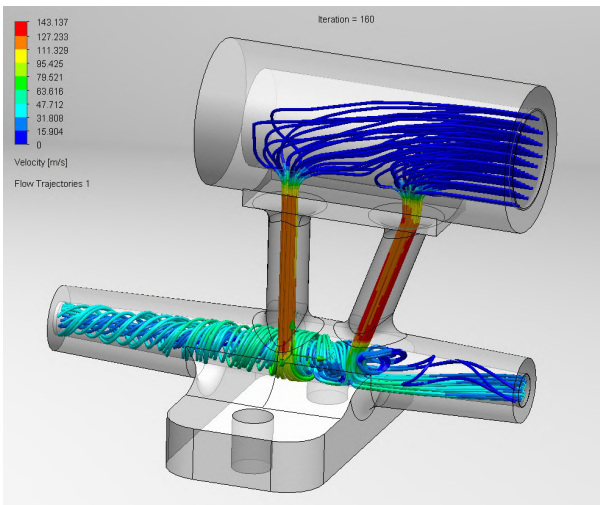
Figure A.4: 90 + 45 degree nozzle

A judgement on the current commingling nozzles can be made with the CFD analysis in combination with the test performed, seen in the images (A.3a-A.4b) above. A difference between the two nozzles that is directly visible, is that the nozzle with only a perpendicular air channel generates more turbulence than the two channel design. In Figure A.4a the velocity lines are quite laminar. The air stream from the 90 degree channel gets pushed by the 45 degree port, defeating the turbulence that is visible in Figure A.3a. This is in agreement with the vorticity plots. Vorticity is a measure of the rotation of a fluid element as it moves through the flow. With a higher vorticity the produced yarn will have a higher nip frequency and more stable nips [37]. Next to that the velocity of the air is different. In the one-channel design the air channel has a conical design, accelerating

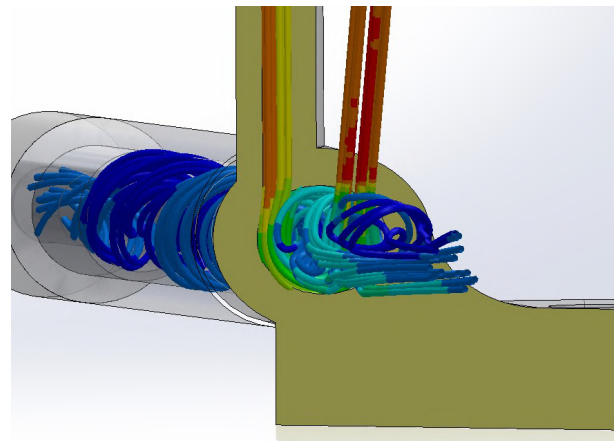
the air. Resulting is a higher velocity at the exit of the channel. In comparison to the two-channel design, where the Venturi effect is less pronounced.

Improved designs

As stated in the previous paragraph, creating air speed results in a more turbulent air stream. Next to that a so called swirl is incorporated in the design. A swirl is a rotating air stream around a central axis. This type of flow is created by moving the 90 degree air channel to the side, see Figure A.5b. Offsetting it to the edge of the commingling room. In this situation the air enters the commingling room by it's tangent. The second air channel is at 70 degrees, without offset to the sides. This channel is designed to open up the yarns and provide a (small) force vector in moving direction of the yarns. This releases some of the tension in the yarns, enabling better commingling. The release of tension recreates a similar effect as overfeeding, which increases the commingling level [37]. Also holes in the base to mount the nozzle to a steady platform.



(a) Improved design



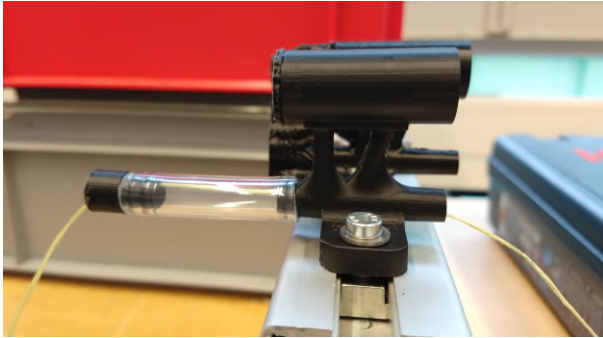
(b) Cross section (yellow), swirl generation visible by offset air channel

Figure A.5: Improved nozzle

Another requirement (ID C1, see Table A.1) was to include a clear section in the nozzle. This is look at the commingling process, within the nozzle. A quick test has been done with filming the process at the end of the nozzle. However this did not yield a nice result. Drawbacks on that setup were the non-ideal lighting conditions and the relative low frames per second (240). With this design the commingling process is at least visible. Tests have to determine if the process is too fast and not for the available camera equipment.

A.2.2 Test improved nozzle

In improved nozzle is 3D printed with an FDM machine (Ultimaker S5, PLA Tough black filament). The nozzle is tested with one yarn of 2000 TEX G/PP and one yarn Twaron 161 TEX. The results are in agreement with the flow simulations in SOLIDWORKS. The swirls do twist the yarns very well, however influence of the first air channel is (almost) completely vanished. In Figure A.6b it is clearly visible that the yarns are twisted together, instead of opened and commingled. This result is underpinned by a high speed video. The movement of the fibers is filmed through the clear section at 240 frames per second (10x slower). Albeit 10x slower, the movement of the fibers is still (too) fast. However the general motion can be observed, this is in line with the flow directories of Figure A.5a.



(a) Improved nozzle 3D printed mounted on fixture



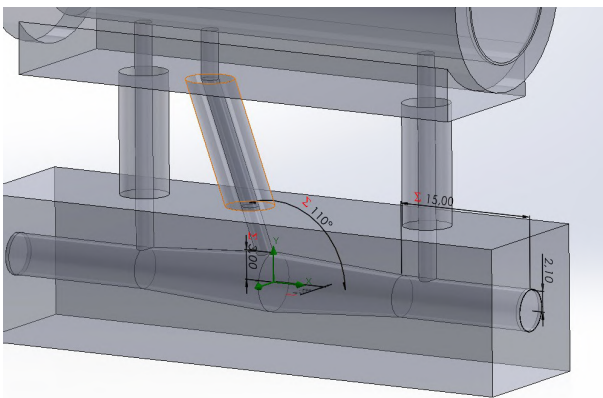
(b) Commingled yarn with improved nozzle

Figure A.6: Commingled yarn with improved nozzle

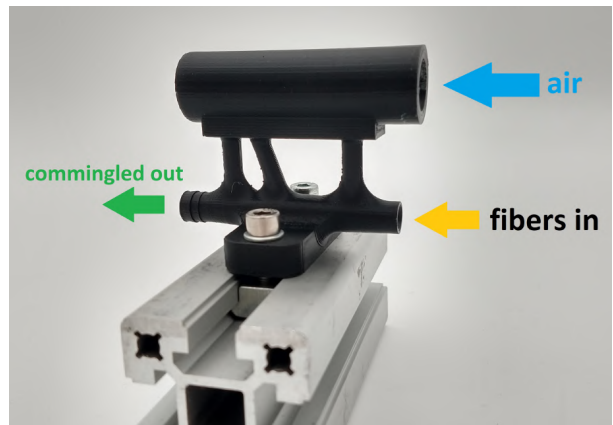
The bottom line of this design is that it is not optimal for commingling the yarns to a single yarn. However the movement of the yarns inside the nozzle is (visually) similar to the flow directories of the CFD analysis. With this information a new iteration can be designed.

A.3 Parametric optimization process

With the knowledge from the CFD analysis of the original commingling nozzles and the test of the first improvement a parametric optimization study is made in Solidworks. The parameters are diameter of the air channels, air channel angle, 2 or 3 channels and the length of the entry tube to the 'commingling room' and the diameter of the commingling room. With those variables 24 scenarios are made in a so-called 'What if Analysis'. The output of this study is an optimal scenario based on the goals. The goals are defined as the TKE (Turbulent Kinetic Energy) and output velocity of the air channels. The optimized shape is further modelled to a 3D-printable model and displayed in Figure A.7b.



(a) Parametric CFD optimization model



(b) Final version commingling nozzle

Figure A.7: Improved nozzle

B MICROSCOPY IMAGES

The aim of the microscopy images is to examine the produced composites for defects and fiber distribution. The image analysis is performed in MATLAB, functions from the Image Processing Toolbox are being used.

The image analysis process is as follows:

- Load the desired image from (any) folder.
- Apply a crop to reduce the image size (if necessary).
- Draw an ellipse that covers the cross section of the sample. It is important to match the shape as close as possible. The area of this ellipse will be used in the calculations later on.
- The script takes over, the image will be converted to a RGB image.
- With the function 'imsegkmeans' all the colors will be clustered into six (variable) colors. The outcome of this is 6 so called masks. These masks are plotted as an overlay on the original image of the cross section, highlighting certain sections. The mask is a matrix with the size of the image, on the pixel position of that specific colormask the value is one. Otherwise the value is zero.

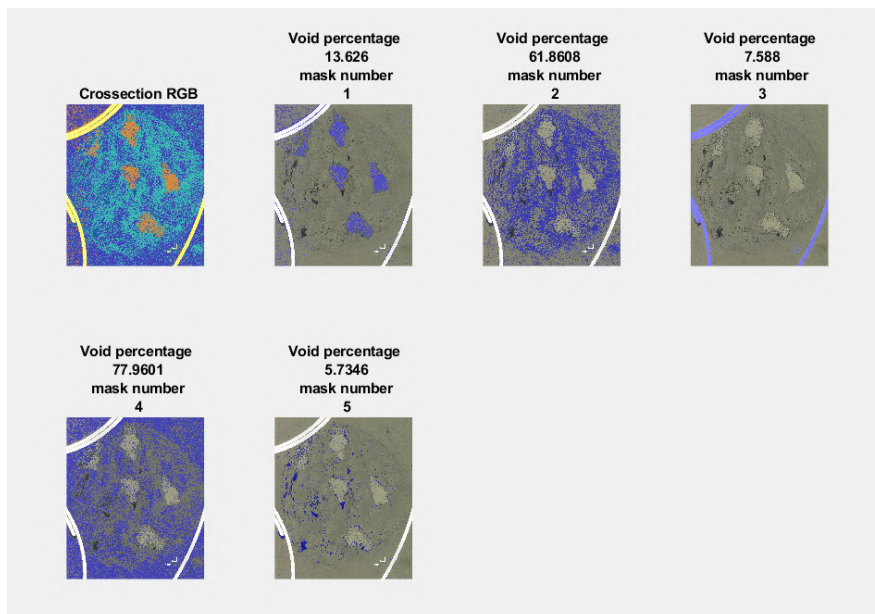


Figure B.1: Color masks in the Matlab program

- To complete the image, the user has to enter which mask is the correct mask for the voids (and aramid fibers if present).
- A figure is created with the original cross section, one with the voids highlighted. And in the case of a G/A/PP sample, a figure with the aramid highlighted.
- Finally the void and aramid content [%] is calculated. This is done by counting the pixels of the color mask and calculating the fraction with the number of pixels of the ellipse mask.

B.1 Glass Polypropylene samples

Void analysis of cross section
sample1_1.jpg

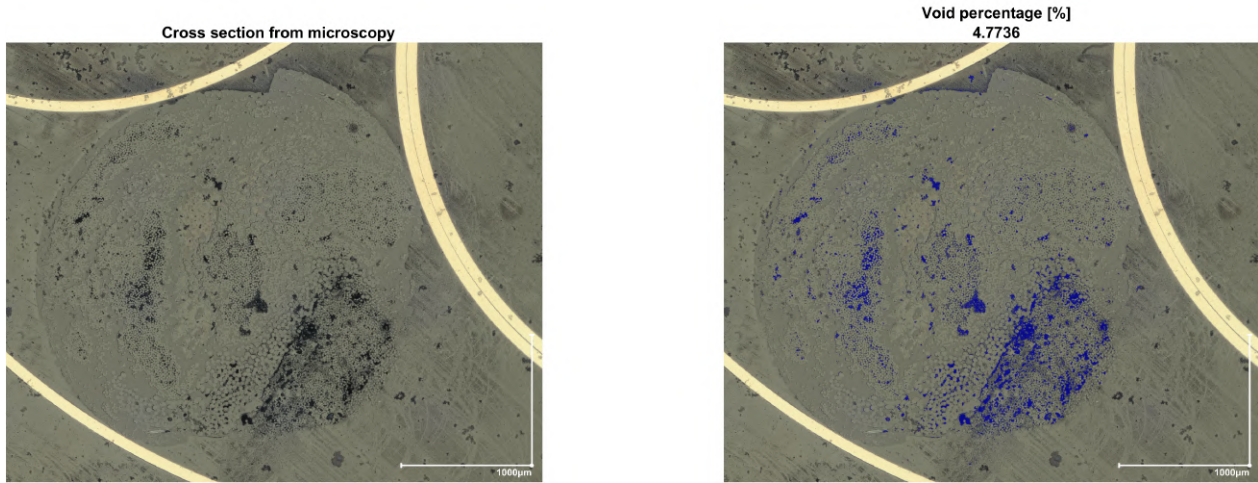


Figure B.2: GPP 1st produced meter, 1st sample

Void analysis of cross section
sample1_2.jpg

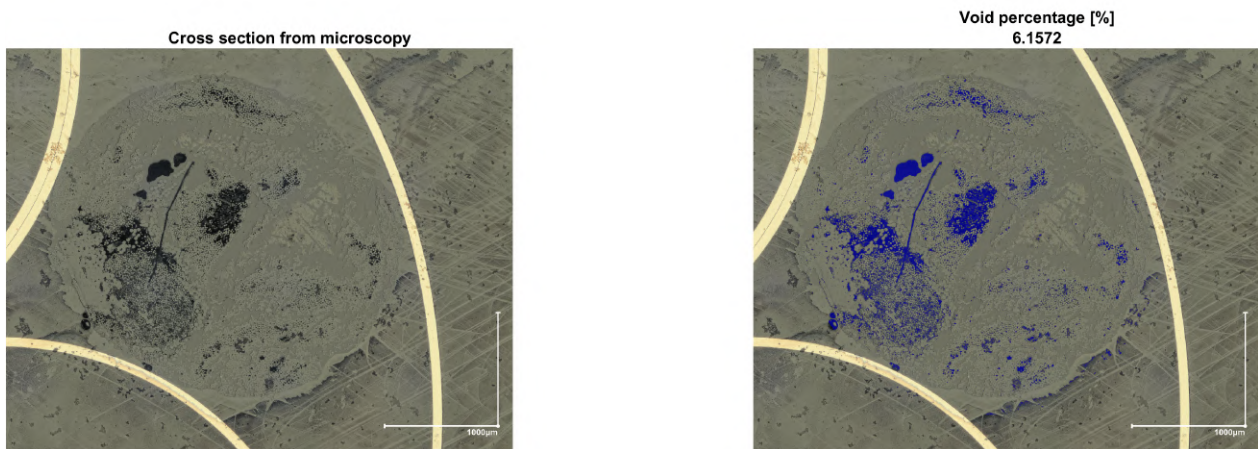


Figure B.3: GPP 1st produced meter, 2nd sample

Void analysis of cross section
sample3_1.jpg

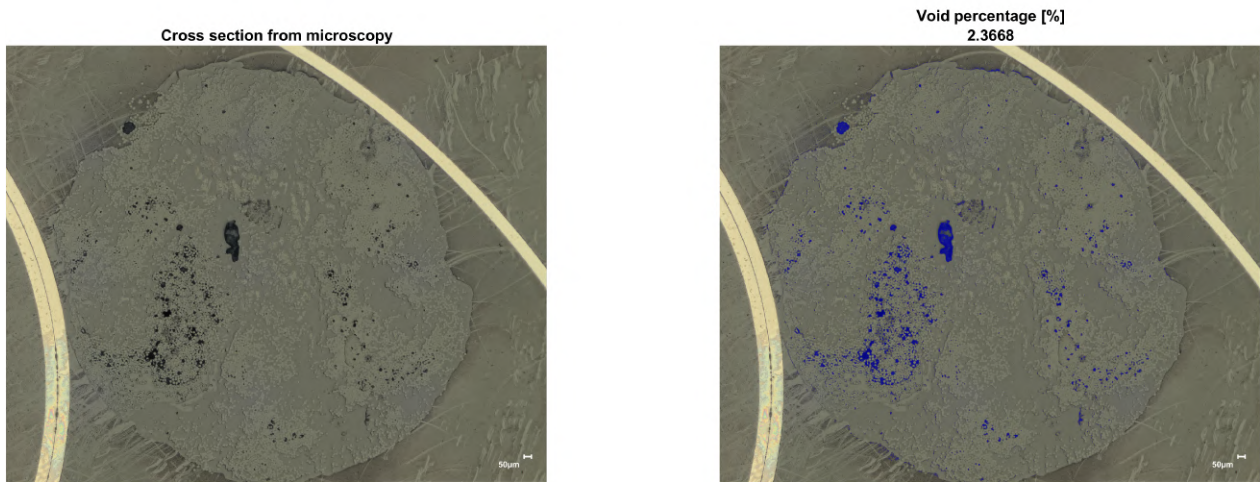


Figure B.4: GPP 3rd produced meter, 1st sample

Void analysis of cross section
sample3_2.jpg

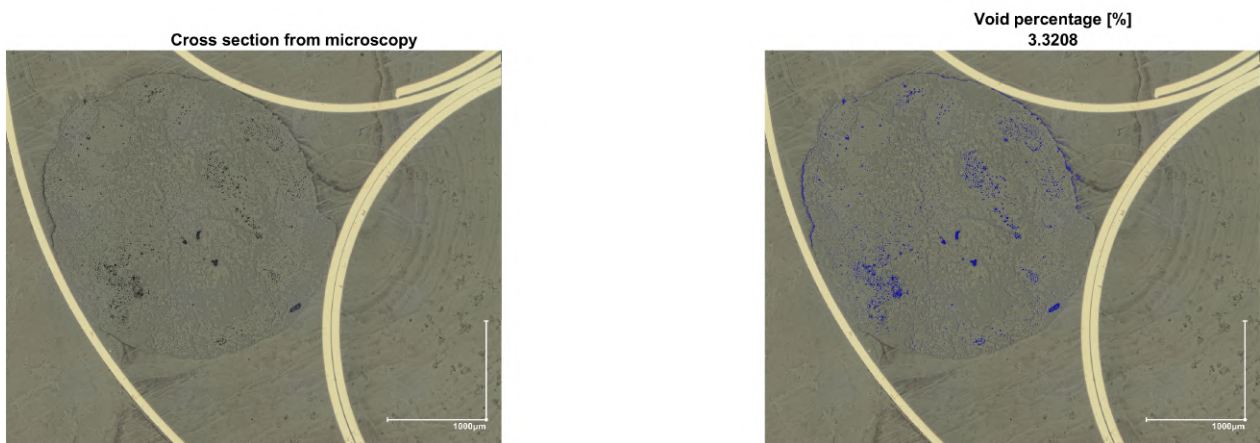


Figure B.5: GPP 3rd produced meter, 2nd sample

Void analysis of cross section
sample14_1.jpg

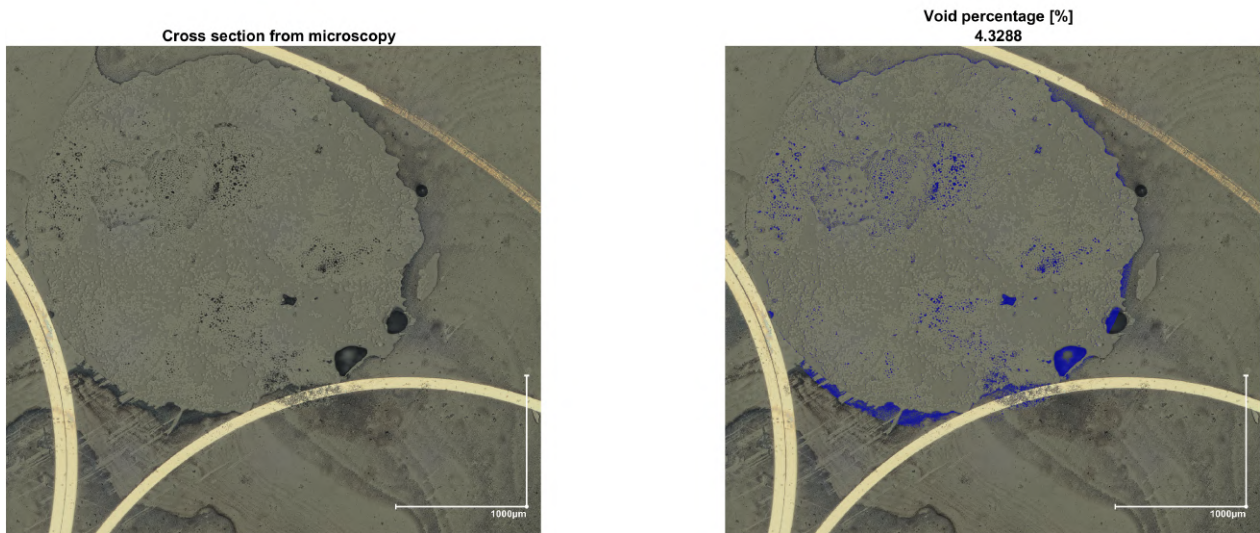


Figure B.6: GPP 14th produced meter, 1st sample

Void analysis of cross section
sample14_2.jpg

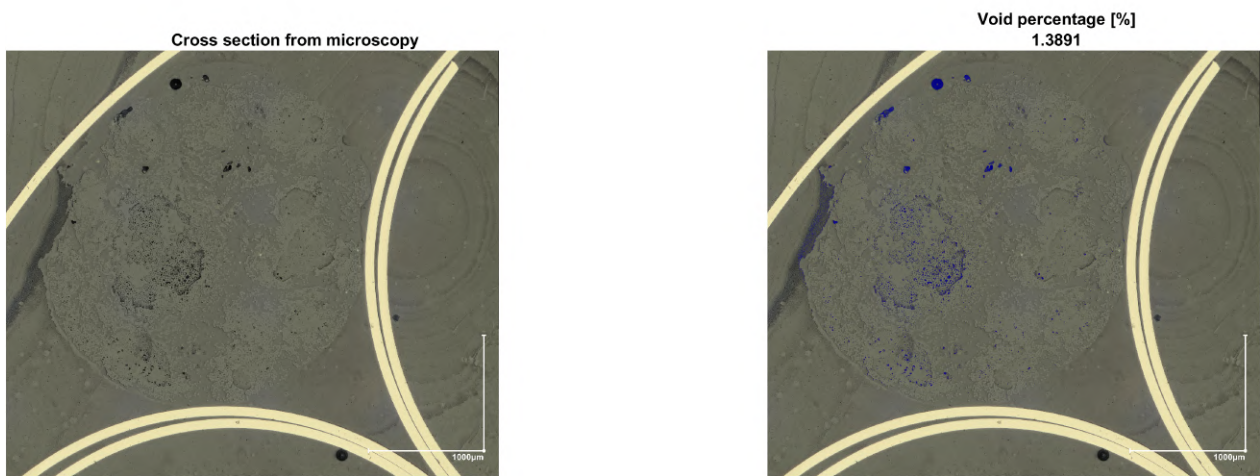


Figure B.7: GPP 14th produced meter, 2nd sample

B.2 Glass Aramid Polypropylene samples

Void analysis of cross section
GAPPSample2_1.jpg

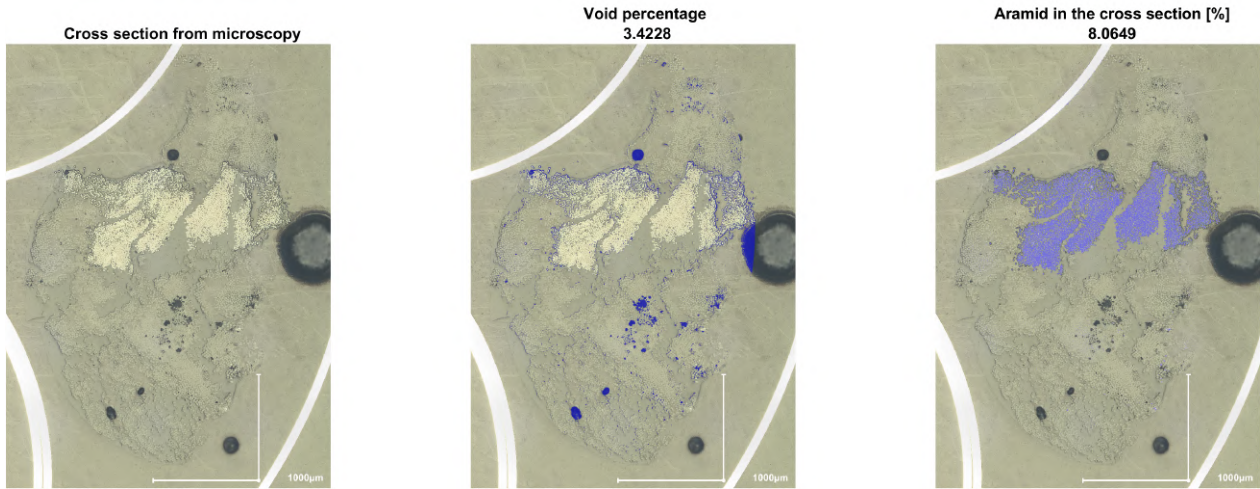


Figure B.8: GAPP 2nd produced meter, 1st sample

Void analysis of cross section [%]
GAPPSample2_2.jpg

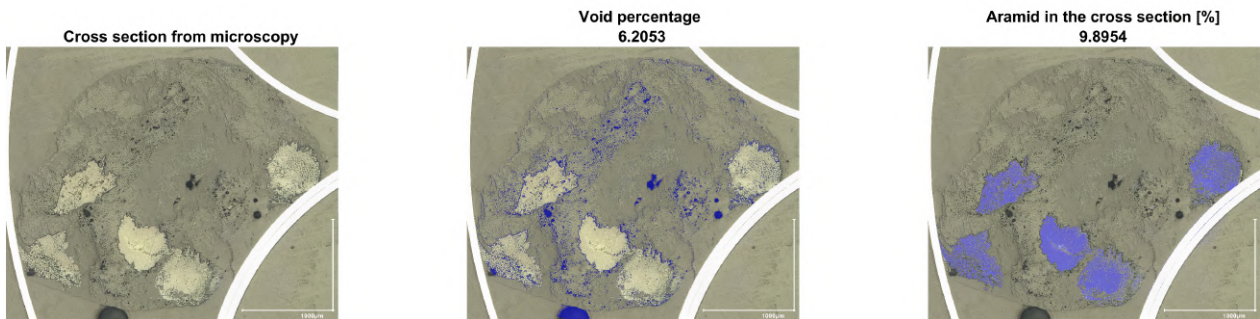


Figure B.9: GAPP 2nd produced meter, 2nd sample

Void analysis of cross section
GAPPSample2_3.jpg

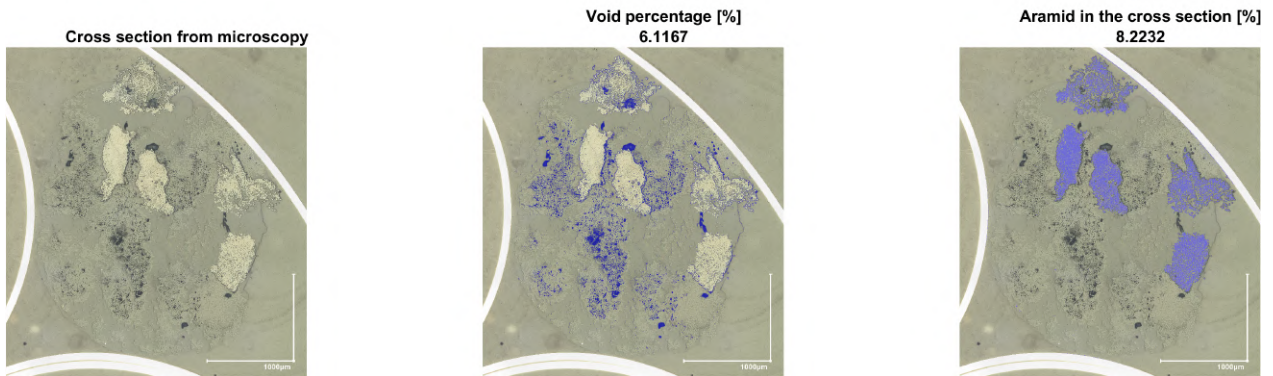


Figure B.10: GAPP 2nd produced meter, 3rd sample

Void analysis of cross section
GAPPSample4_1.jpg

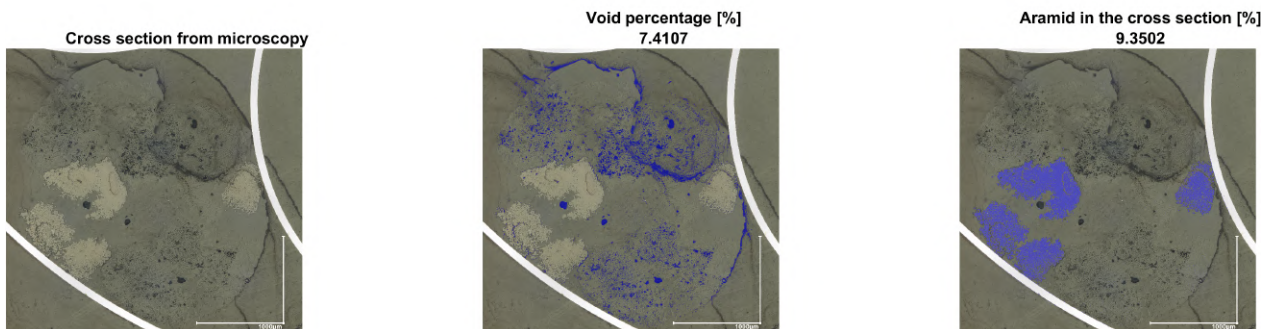


Figure B.11: GAPP 4th produced meter, 1st sample

Void analysis of cross section
GAPPSample4_3.jpg

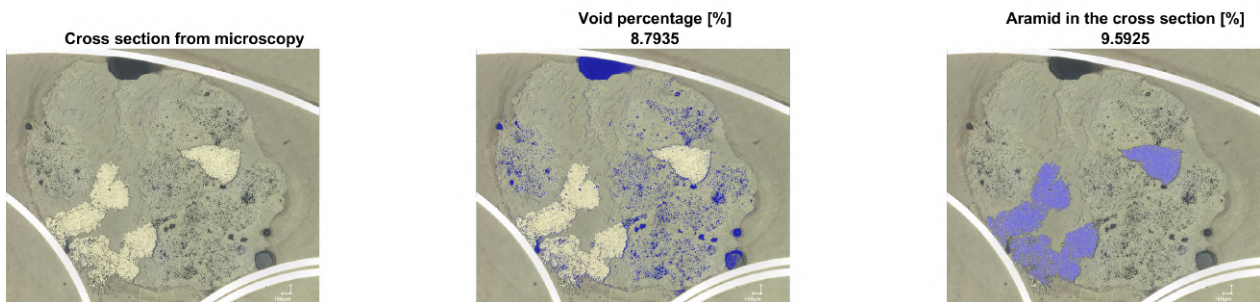


Figure B.12: GAPP 4th produced meter, 3rd sample

Void analysis of cross section
GAPPSample16_1.jpg

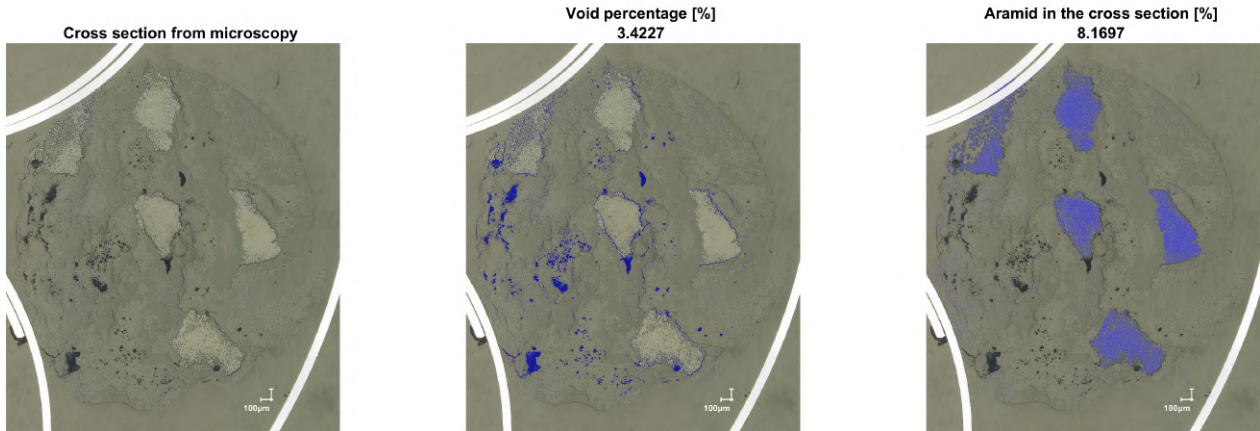


Figure B.13: GAPP 16nd produced meter, 1st sample

Void analysis of cross section
GAPPSample16_2.jpg

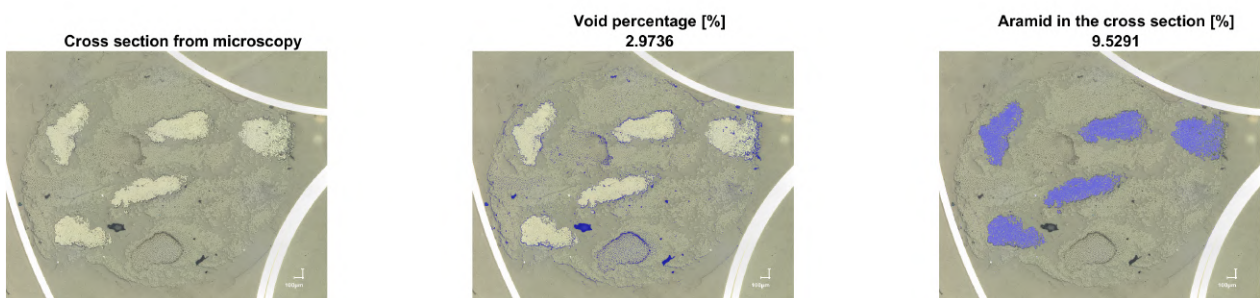


Figure B.14: GAPP 16th produced meter, 2nd sample

Void analysis of cross section
GAPPSample16_3.jpg

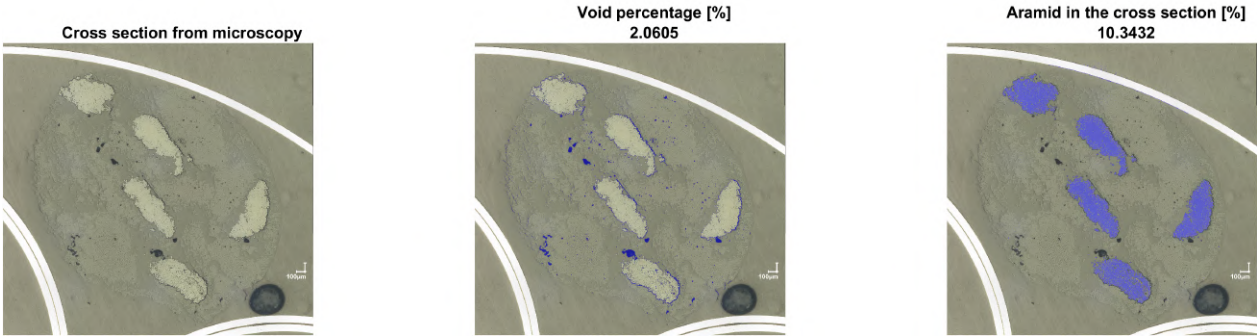


Figure B.15: GAPP 16th produced meter, 3rd sample

B.3 Samples compression molded composites

Analysis of cross section
Vf aligned plate 1 direction

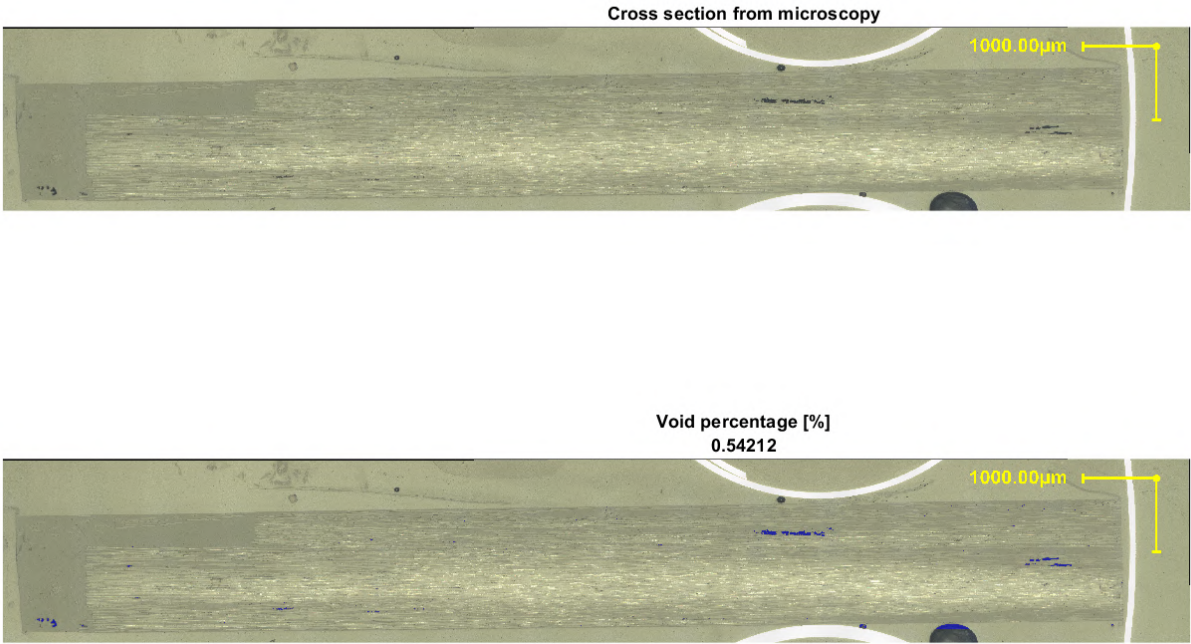


Figure B.16: Sample with aligned G/PP pellets, 1-direction

Analysis of cross section
Vf aligned plate 2 direction

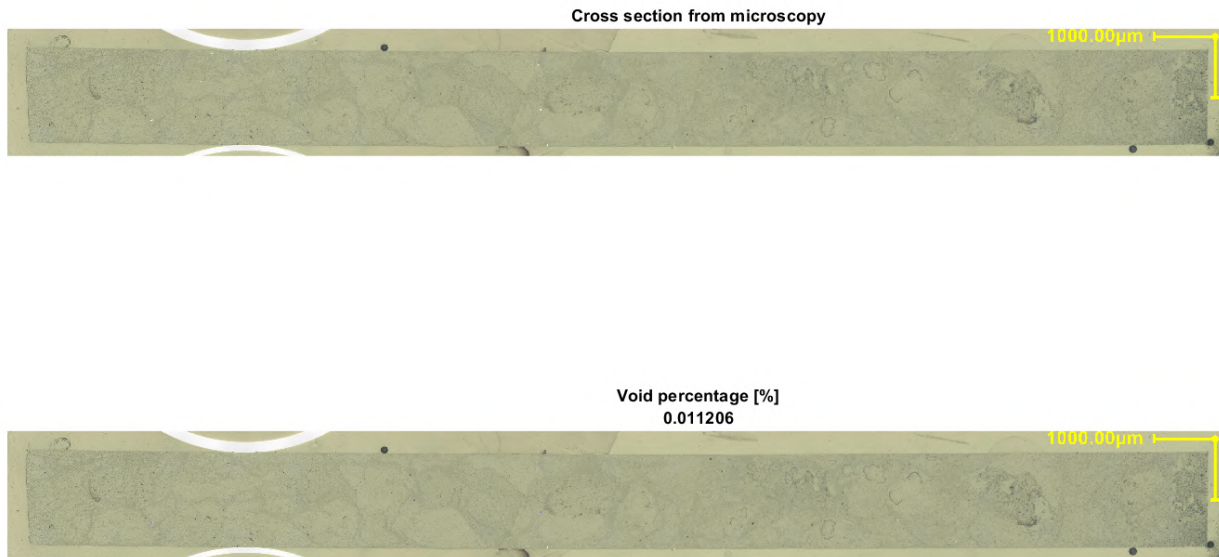


Figure B.17: Sample with aligned G/PP pellets, 2-direction

Analysis of cross section
Vf random R1GPP

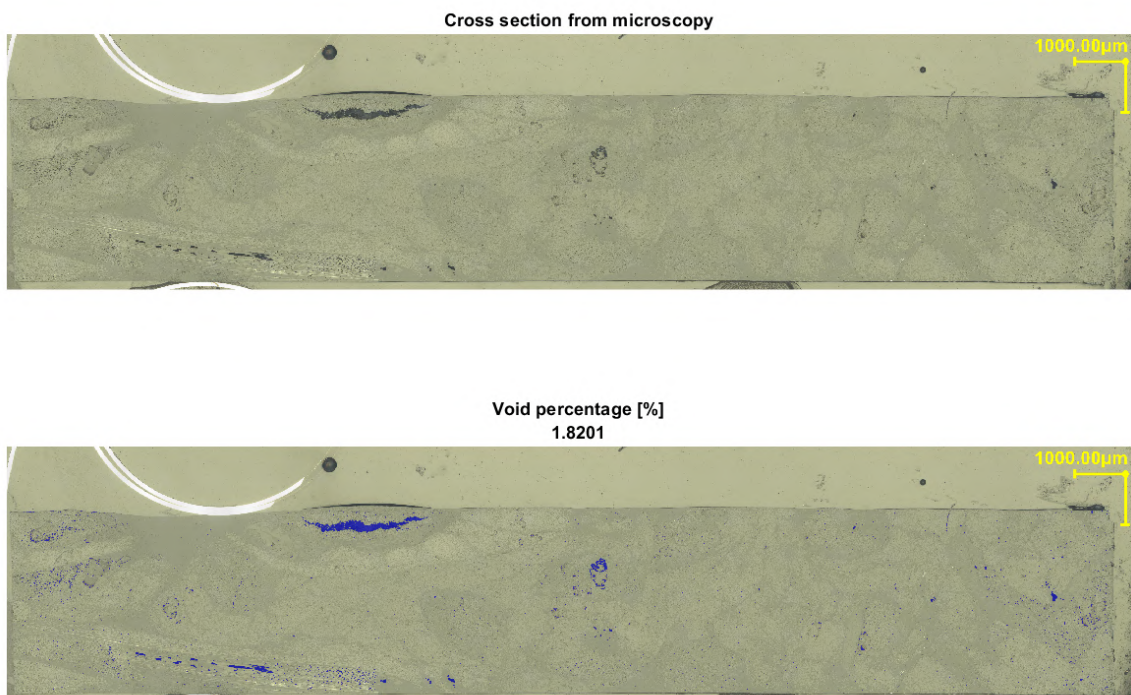


Figure B.18: Sample 2 with random G/PP pellets batch 1

Analysis of cross section
Vf random GPP batch 2
Cross section from microscopy



Void percentage [%]
0.75349

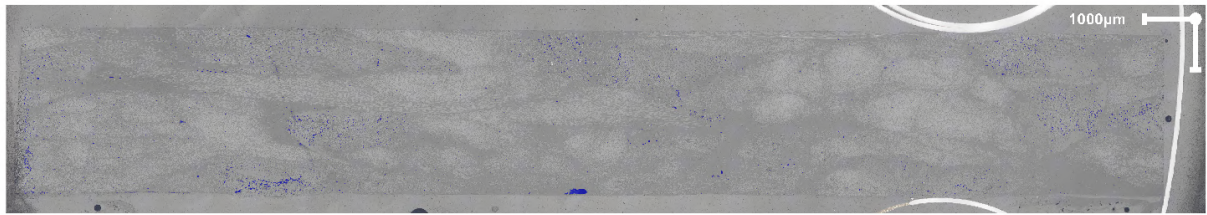
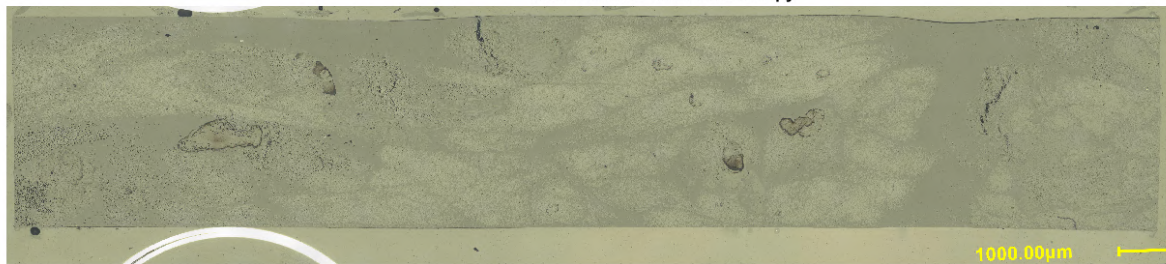


Figure B.19: Sample with random G/PP pellets batch 2

Analysis of cross section
Vf random GPP 2

Cross section from microscopy



Void percentage [%]
1.9019

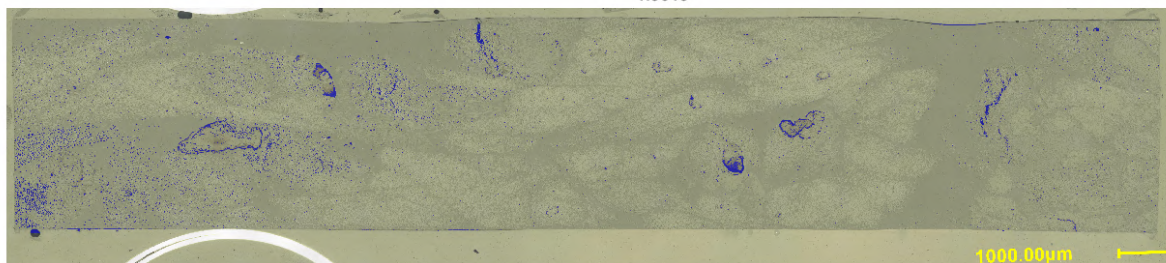
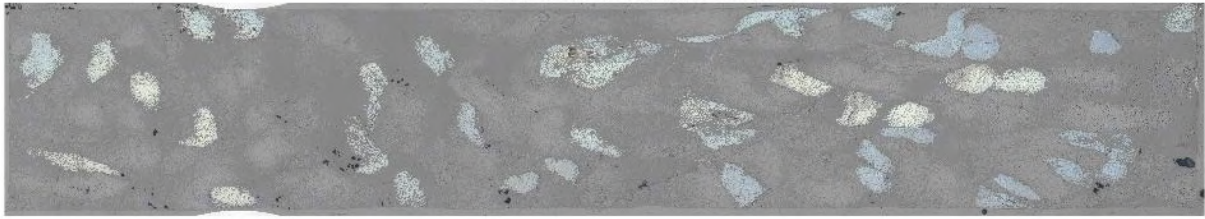


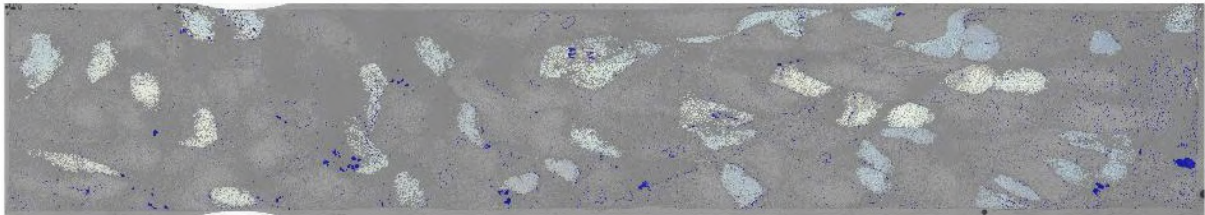
Figure B.20: Sample with random G/PP pellets batch 2

Analysis of cross section
GAPP1random

Cross section from microscopy



Void percentage [%]
1.4222



Aramid in the cross section [%]
11.0229

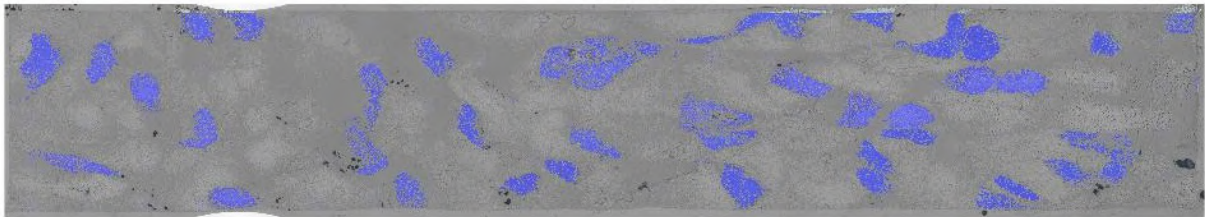


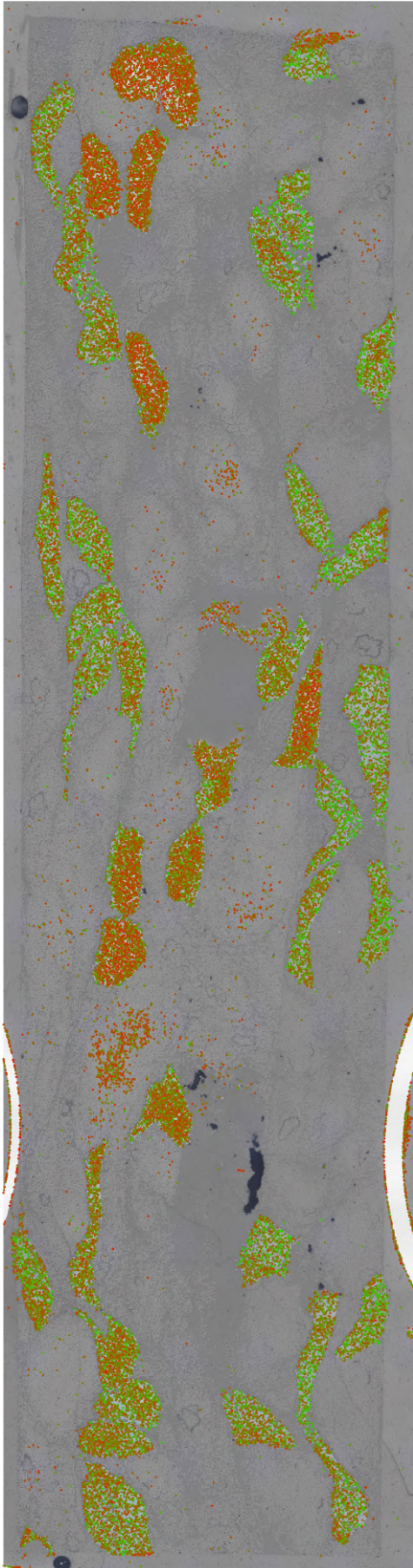
Figure B.21: Sample with random G/A/PP pellets batch 1

The mean void content of the of the samples with a random pellet alignment is 1.47%. There is some over-estimation due to voids created by the cutting or polishing process and some polishing residue that has a similar color tint. An assumption can be made that the real void content is more in the region of 1.2%. The void content in the aligned specimen is much lower. This was expected, the random orientated pellets require a larger flow during the process, hence more room for air to be trapped within the composite.

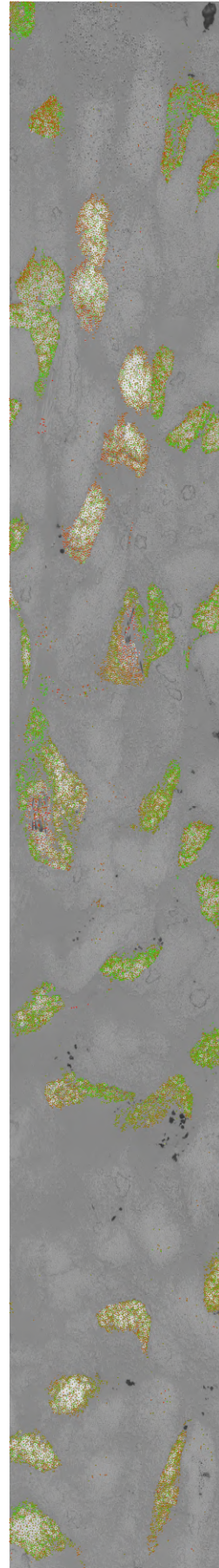
B.4 Fiber angle analysis

The fiber angles in the compression molded composites are evaluated with ImageJ and Matlab. the analysis is executed via the following steps:

- Open the desired micrograph in ImageJ, take a crop if there are distracting elements outside the ROI.
- Convert the image to an 8-bit image, use the 'Threshold function' to select the aramid fibers in the micrograph.
- This step is only required if the fibers are packed closely together and touching each other. Convert to a binary image, use the 'Watershed separation function' to separate any fibers that are touching.
- Use the 'Analyze Particles' function, select 'Show ellipse' to judge the result.
- The output is an .csv file with all the found ellipses. The coordinates, major minor axis, angle and area are given.
- Switch to Matlab, load the micrograph and .csv file.
- In Matlab the data set is filtered by minimum area (variable) to get rid of noise.
- The original micrograph is plotted with colored dots on the found ellipses. Green is perpendicular to the micrograph (out-of-plane) and red is parallel to the micrograph.



(a) Specimen GA2 with the image analysis



(b) Specimen GA1 (cropped) with the image analysis

Figure B.22: Micrograph of compression molded plates with fiber angles

C TEST SPECIMEN

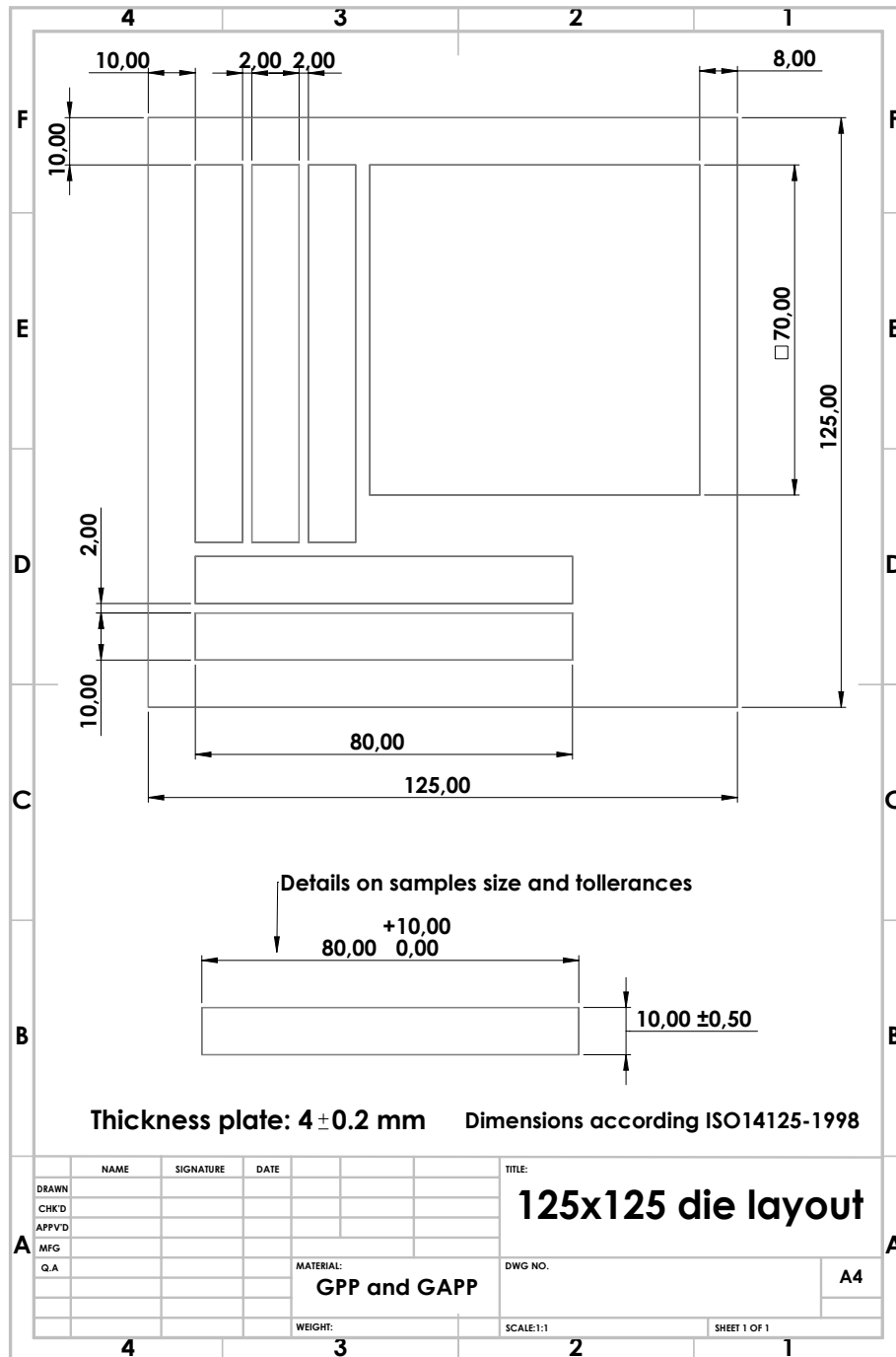


Figure C.1: Four point bending test specimen drawings

C.1 Test report 4 point bending test

This section of the Appendix includes the test information of the 4 point bending tests and measurement results. In the table all the test information is given as well as a graph with all the force-displacement curves.

Date testing:	23-1-2023
Test name:	Random 40 mm pellets and aligned pellets
Specimen name random:	RG1-x R : RG: random glass RA: random Glass/Aramid, 1: plate number, x: specimen number.
Specimen name aligned:	AG1-x.n : aligned, 1: plate number, x: fiber direction (1 or 2), n: specimen number.
Test information random pellets specimen	
Norm taken as guideline:	ISO 14125_1998
Material:	Glass-Polypropylene pellets 40 mm
Material class:	Class I for the random pellet configuration
Specimen thickness:	4 mm (random)
Specimen preparation method:	Compression moulded pellets to a flat plate. Cut by a water-cooled diamond saw to size.
Test conditions:	Standard lab conditions
Number of specimen:	6 beams, taken from x and y direction of the plate.
Machine used:	Zwick i-line Z5.0
Outer span length:	66 mm
Inner span length:	22 mm
Speed of testing:	2 mm/min
Fixtures:	Steel tubes on roller bearings. Fixture radius: 5 mm, indenter radius: 4 mm.
Test information aligned pellets specimen	
Norm taken as guideline:	ISO 14125_1998
Material:	Glass-Polypropylene pellets 40 mm
Material class:	Class III for unidirectional composites
Specimen thickness:	1.8 mm (aligned)
Specimen preparation method:	Compression moulded pellets to a flat plate. Cut by a water-cooled diamond saw to size.
Test conditions:	Standard lab conditions
Number of specimen:	5 beams, taken from x and y direction of the plate.
Machine used:	Zwick i-line Z5.0
Outer span length:	45 mm
Inner span length:	22 mm
Speed of testing:	1 mm/min
Fixtures:	Steel tubes on roller bearings. Fixture radius: 5 mm, indenter radius: 4 mm.

Table C.1: Test information 4-point bending tests

Specimen	Efflex	u at max load	sigmax max load	u first peak	Sigmaflex first peak	Strain first peak	Energy under curve	Energy up to 1st peak	% peak of total	average J total	Average J 1st peak
RG1-1	8307.651	4.82	88.743	3.93	85.762	0.674	0.850	0.417	0.49	0.625	0.313
RG1-2	8176.353	4.03	97.139	4.03	97.139	0.792	0.646	0.478	0.74		
RG1-3	8169.347	4.27	87.877	4.27	87.877	0.768	0.663	0.498	0.75		
RG1-4	10233.098	7.65	93.136	2.30	64.798	0.454	0.989	0.182	0.18		
RG1-5	11497.872	1.22	54.678	1.22	54.678	0.511	0.375	0.076	0.20		
RG1-6	14917.714	1.95	101.522	1.95	101.522	0.859	0.225	0.225	1.00		
AG1-1.1	36738.512	2.49	398.589	2.20	357.512	2.377	1.012	0.598	0.59	0.663	0.366
AG1-1.2	32865.195	2.95	441.855	2.44	375.393	2.946	1.525	0.806	0.53		
AG1-2.2	3941.335	1.65	24.596	1.65	24.596	0.208	0.047	0.040	0.84		
AG1-2.3	5526.652	1.33	26.797	1.07	24.358	0.163	0.070	0.020	0.29		
RG2-1	0.000	0.00	0.000	0.00	0.000	0.000	0.000	0.000	0.00	0.45	0.35
RG2-2	14637.664	6.01	213.391	5.84	210.713	1.298	3.022	1.261	0.42		
RG2-3	5958.162	5.79	48.037	1.81	40.679	0.316	0.585	0.078	0.13		
RG2-4	8126.736	8.57	123.652	3.98	99.750	0.661	1.677	0.394	0.23		
RG2-5	4292.058	2.30	26.143	1.88	26.027	0.204	0.087	0.054	0.62		
RA1-1	19794.154	5.50	235.782	5.05	232.048	1.781	2.394	1.466	0.61	1.665	0.758
RA1-2	7433.167	5.04	95.139	4.34	93.487	0.922	1.333	0.609	0.46		
RA1-3	7820.563	7.11	97.738	4.53	90.310	0.788	1.246	0.560	0.45		
RA1-4	4245.365	7.34	68.154	5.11	64.399	0.637	1.296	0.490	0.38		
RA1-5	8235.496	6.84	137.727	4.71	119.121	0.940	2.056	0.663	0.32		
RA2-1	4645.432	8.81	84.856	5.43	72.674	0.788	1.551	0.593	0.38	1.663	0.642
RA2-2	13907.974	6.13	198.957	4.26	185.699	1.805	2.465	1.105	0.45		
RA2-3	6952.414	6.27	124.090	5.15	122.505	1.269	1.513	0.915	0.60		
RA2-4	5603.368	5.78	57.757	3.69	52.547	0.445	0.819	0.254	0.31		
RA2-5	11199.774	5.24	130.543	2.74	111.353	0.931	1.965	0.343	0.17		
RG3-1	8152.171	5.01	106.423	4.75	106.423	0.785	0.641	0.595	0.93	1.462	0.672
RG3-2	7132.363	10.00	70.483	4.14	59.272	0.435	1.053	0.301	0.29		
RG3-3	14991.099	6.89	244.432	5.40	239.532	1.651	2.083	1.420	0.68		
RG3-4	15671.247	3.93	134.781	3.39	132.961	0.880	0.588	0.464	0.79		
RG3-5	14993.834	7.12	187.640	4.48	184.349	1.548	2.078	1.044	0.50		
RG3-6	12744.702	10.00	146.174	2.10	88.677	0.718	2.327	0.208	0.09		

Figure C.2: Overview of the results per specimen

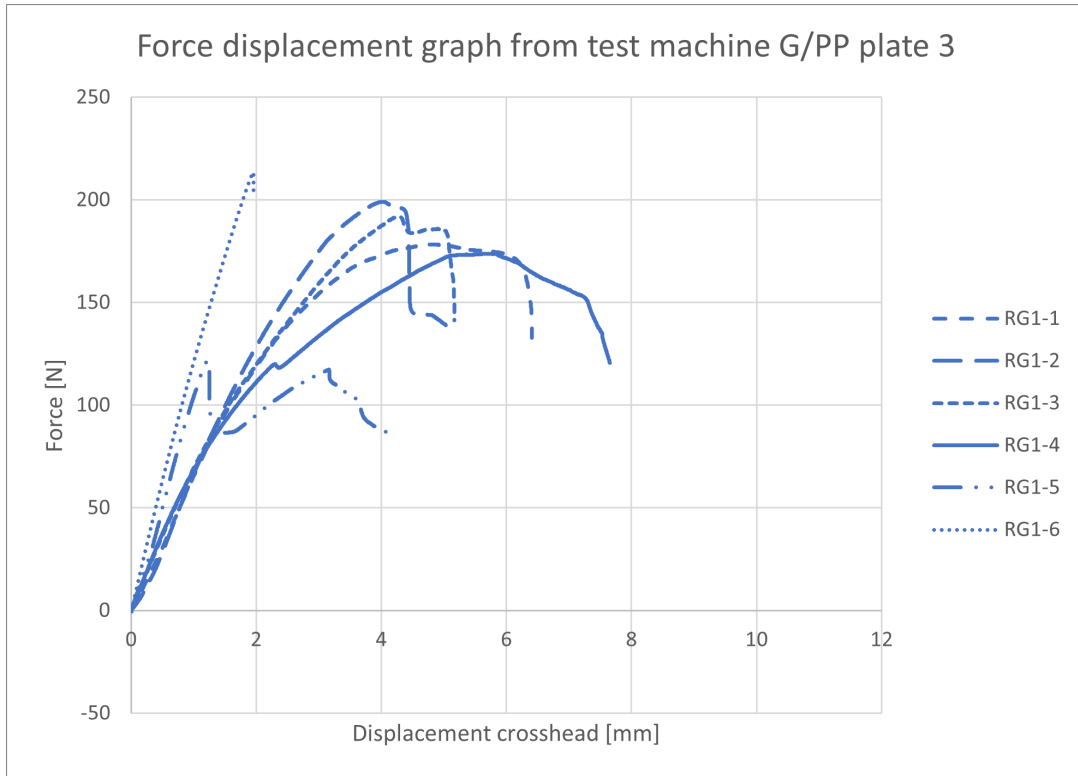


Figure C.3: Test data 4-PBT of G/PP plate 3

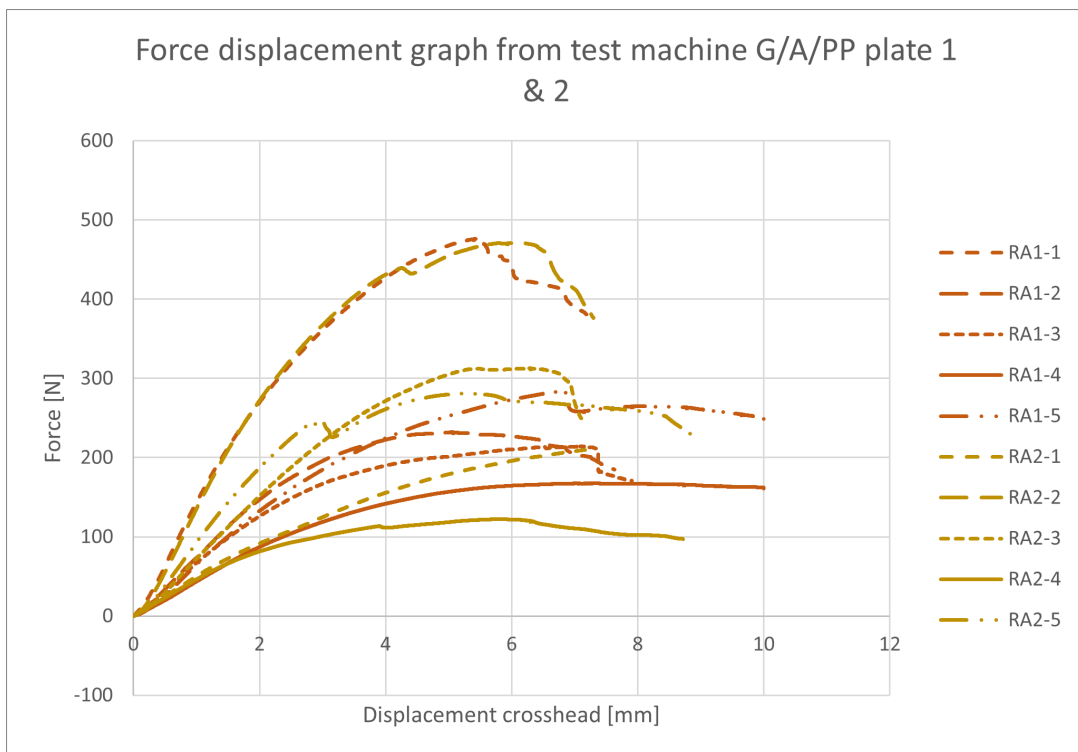


Figure C.4: Test data 4-PBT of G/A/PP plate 1 and 2

D DEMONSTRATOR PART

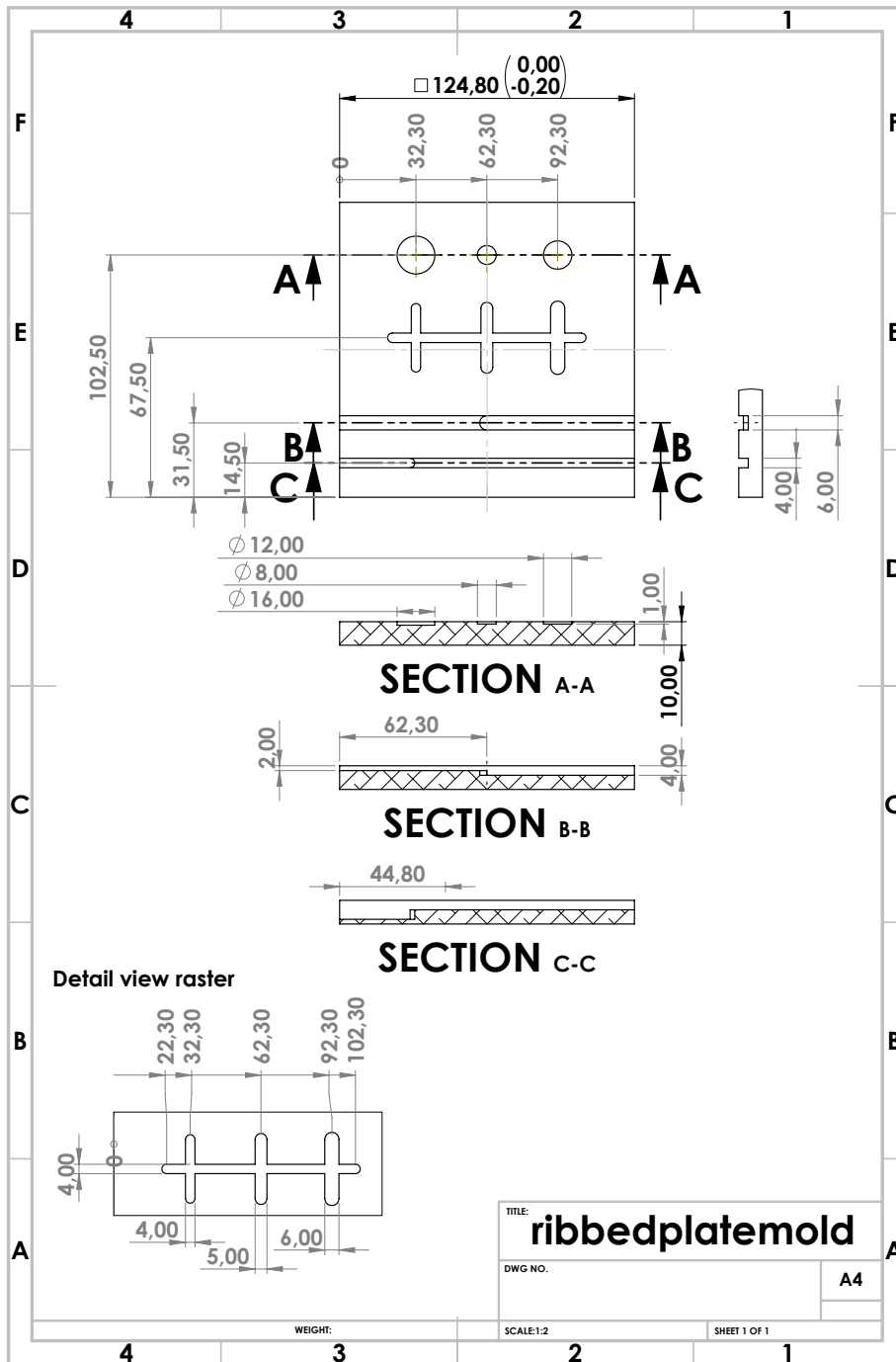


Figure D.1: Production drawing mold insert

E PLAGIARISM REPORT



Similarity Report ID: oid:6294:151753365

PAPER NAME

Arthur Haverkort - Thesis_June 2023.pdf

AUTHOR

Arthur Haverkort

WORD COUNT

18539 Words

CHARACTER COUNT

89741 Characters

PAGE COUNT

81 Pages

FILE SIZE

2.6MB

SUBMISSION DATE

Jun 22, 2023 2:59 PM GMT+2

REPORT DATE

Jun 22, 2023 3:01 PM GMT+2

● 5% Overall Similarity

The combined total of all matches, including overlapping sources, for each database.

- 4% Internet database
- 3% Publications database
- Crossref database
- Crossref Posted Content database
- 1% Submitted Works database

● Excluded from Similarity Report

- Small Matches (Less than 10 words)

● 5% Overall Similarity

Top sources found in the following databases:

- 4% Internet database
- 3% Publications database
- Crossref database
- Crossref Posted Content database
- 1% Submitted Works database

TOP SOURCES

The sources with the highest number of matches within the submission. Overlapping sources will not be displayed.

1	downloads.hindawi.com	Internet	<1%
2	inderscience.com	Internet	<1%
3	Mathieu Imbert, Philipp Hahn, Markus Jung, Frank Balle, Michael May. ...	Crossref	<1%
4	core.ac.uk	Internet	<1%
5	Jose Lira Braga Neto, Ricardo Alex Dantas da Cunha, Talita Galvão Tar...	Crossref	<1%
6	lirias.kuleuven.be	Internet	<1%
7	hal.archives-ouvertes.fr	Internet	<1%
8	utwente on 2023-01-17	Submitted works	<1%

9	dergipark.org.tr	Internet	<1%
10	ethz.ch	Internet	<1%
11	ia800600.us.archive.org	Internet	<1%
12	ijser.org	Internet	<1%
13	hindawi.com	Internet	<1%
14	Cephas Yaw Attahu. "Composite laminates made of unidirectional carb...	Crossref	<1%
15	e-pub.uni-weimar.de	Internet	<1%
16	Zhiyang Zhao, Renbo Song, Changhong Cai, Ke Guo. "Pipe comb-tooth ...	Crossref	<1%
17	labra.weso.es	Internet	<1%
18	essay.utwente.nl	Internet	<1%
19	Harichandra Chandekar, Vikas V. Chaudhari, Sachin Waigaonkar. "Theo...	Crossref	<1%
20	utwente on 2019-11-08	Submitted works	<1%

21	Ganesh Jogur, Apurba Das, Ramasamy Alagirusamy. " Development of ...	<1%
	Crossref	
22	hdl.handle.net	<1%
	Internet	
23	ore.exeter.ac.uk	<1%
	Internet	
24	siem.sandipfoundation.org	<1%
	Internet	
25	grin.com	<1%
	Internet	
26	www2.mathematik.tu-darmstadt.de	<1%
	Internet	
27	digitalrepository.unm.edu	<1%
	Internet	
28	edge.rit.edu	<1%
	Internet	
29	folk.ntnu.no	<1%
	Internet	
30	iosrjournals.org	<1%
	Internet	
31	rappporter.ffi.no	<1%
	Internet	
32	Bin Yang, Jinhua Leng, Bobing He, Heng Liu, Yu Zhang, Zhaohua Duan. ...	<1%
	Crossref	

33	Biswas, Sandhyarani, Amar Patnaik, and Ritesh Kaundal. "Effect of Red..."	<1%
	Crossref	
34	Textile Materials for Lightweight Constructions, 2016.	<1%
	Crossref	
35	openaccess.city.ac.uk	<1%
	Internet	
36	spiral.imperial.ac.uk	<1%
	Internet	
37	studentsrepo.um.edu.my	<1%
	Internet	
38	escholar.manchester.ac.uk	<1%
	Internet	